Chapter 5

Regional Gravity Field Modeling: Theory and Practical Results

Heiner Denker

H. Denker (✉)
Institut für Erdmessung (IfE), Leibniz Universität Hannover (LUH),
Schneiderberg 50, 30167 Hannover, Germany
E-mail: denker@ife.uni-hannover.de

Revised version (Nov. 13, 2012) of
Denker, H., Regional gravity field modeling: Theory and practical results. Chapter 5 in G. Xu (ed.), *Sciences of Geodesy – II*, pp 185–291, Springer-Verlag Berlin Heidelberg 2013.
DOI: 10.1007/978-3-642-28000-9_5.

This page is intentionally blank.

Regional Gravity Field Modeling: Theory and Practical Results

Contents

This page is intentionally blank.

1 Introduction

Geodesy, with its three core areas positioning and reference systems, Earth rotation determination, and gravity field modeling, is striving for a relative accuracy of at least 10^{-9} for all relevant quantities, and to a great extent this goal has already been reached (10^{-9} corresponds to about 6 mm relative to the Earth's radius and 10^{-8} m s^{-2} = 1 μGal in terms of gravity). Regarding gravity field modeling, the highest accuracy demands are from geodesy, especially GNSS (Global Navigation Satellite System) positioning, oceanography, and geophysics. In this context, the geoid and quasigeoid are of major interest; e.g., these quantities are required for the transformation between the purely geometric GNSS (ellipsoidal) heights and gravity field related heights as well as for the modeling of the (mean) dynamic ocean topography (DOT), requiring accuracies at the level of about 1 cm or even below. In this way, the importance of geoid and quasigeoid modeling has increased considerably – also for economic reasons – and as early as 1982 Torge (1982) postulated a "renaissance of the geoid."

Over the past decades, significant progress has been achieved in the collection of high-resolution gravity and terrain data, computing and modeling techniques, as well as the operational availability of satellite data from several altimetry and gravity field missions. Of special interest are the results from the CHAMP (CHAllenging Minisatellite Payload, active from 2000 to 2010), GRACE (Gravity Recovery And Climate Experiment, operational since 2002), and GOCE (Gravity field and steady-state Ocean Circulation Explorer, launched in 2009) missions; while the CHAMP and GRACE missions already delivered the long wavelength geoid with an accuracy of about 1 cm up to a resolution (half wavelength) of 650 km and 200 km, respectively, the GOCE mission is targeting at an accuracy of 1–2 cm for the geoid and 1 mGal for gravity, both at a resolution of approximately 100 km. In addition, the GRACE mission allows the determination of the long wavelength geoid (up to about 350 km resolution) with an accuracy of 1 mm on a monthly basis, from which time variations of the geoid can be deduced. However, due to the required satellite altitudes of at least a few 100 km (below this level, satellite orbits become unstable due to air drag, etc.), the pure satellite gravity field solutions alone can only provide long wavelength gravity field models associated with an omission error (gravity field components not included in the model) of several decimeters regarding the geoid. Consequently, even in the future, only a combination of the satellite gravity fields with high-resolution terrestrial (mainly gravity and terrain) data can provide the complete geoid spectrum (all wavelengths) with an accuracy of 1 cm or even better. In this context, the satellite and terrestrial data ideally complement each other, with the satellite data providing accurately the long wavelength gravity field structures, while the terrestrial data sets, with potential weaknesses in the large-scale accuracy and coverage, mainly contribute the short wavelength features.

Altogether, there is considerable interest in high-resolution regional gravity field modeling, i.e., on a provincial to national and continental scale (several 1000 km),

especially with regard to the geoid and quasigeoid. At present, the combination of terrestrial data sets with up-to-date satellite gravity field models allows the calculation of geoid and quasigeoid models with accuracies of a few centimeters, provided that high-resolution and high-quality terrestrial and satellite data are utilized; furthermore, in view of the GOCE mission, the accuracy may be improved to the level of about 1 cm in the near future, being close to the general accuracy goal of 10^{-9} in geodesy.

This chapter specifically refers to the experiences gained at the Institut für Erdmessung (IfE), Leibniz Universität Hannover (LUH), Germany, within the field of gravity field modeling, especially the calculation of the geoid and quasigeoid. IfE has a long tradition in local and regional geoid and quasigeoid determinations, starting even before the (GNSS) Global Positioning System (GPS) era, when at the beginning of the 1970s a test network was set up in the Harz mountains in Northern Germany, this being the classic geoid research area of Helmert (Torge 1977). Then, with the advent of the GPS, studies on geoid and quasigeoid modeling with centimeter accuracy were intensified, and in a small test area near Hannover, Germany, it could be shown for the first time that an agreement between gravimetric and GPS/leveling results at the centimeter level is in fact possible (Denker and Wenzel 1987). These computations were subsequently extended to larger regions, covering Lower Saxony, Germany (Denker 1988), and the whole of Germany (Denker 1989). Based on these experiences, IfE proposed to perform corresponding computations for the whole of Europe, and this task has been supported by the International Association of Geodesy (IAG) since 1990; IfE served as the computing center within the IAG Geoid Sub-Commission for Europe from 1990 to 2003, from 2003 (when the new IAG structure was implemented) to 2011 the work was supported in the form of an IAG Commission 2 Project "CP2.1 – European Gravity and Geoid Project (EGGP)," and since 2011 this task has continued as IAG Sub-Commission 2.4a "Gravity and Geoid in Europe." Major results of this IAG enterprise are the high-resolution European geoid and quasigeoid models EGG1997 (Denker and Torge 1998) and EGG2007/2008 (see Sect. 4).

After providing the motivation for preparing this chapter, the necessary fundamentals of physical geodesy are described in Sect. 2, including reference systems, basic gravity field properties, the geoid and height systems, the normal gravity field, as well as some remarks about temporal gravity field variations, tidal systems, and atmospheric effects. The intention of this section is to provide all the basics needed for high-precision gravity field modeling with as few approximations as possible. Section 3 describes the methodology of gravity field modeling, where the disturbing potential is the primary quantity of interest. The emphasis is on the spatial gravity field description related to quantities defined at the Earth's surface, such as the disturbing potential as well as the height and gravity anomalies, which require no assumptions about the Earth's interior gravity field (in contrast to the geoid). After giving an overview on geodetic boundary value problems, the linearization of the boundary conditions (observation equations) is discussed, aiming at the rigorous implementation of a high-degree geopotential model as a

reference field. Then the spherical and constant radius approximations are introduced, leading to the classical Poisson, Hotine, Stokes, and other integral formulas. Afterwards, the solution of Molodensky's boundary value problem (related to the Earth's surface) and Stokes's boundary value problem (related to the geoid) are outlined. In addition, the spectral combination technique, least-squares collocation, and astronomical leveling are mentioned. Although most of these modeling techniques can be utilized globally, they are primarily used at regional (provincial to national and continental) scale in connection with the remove–compute–restore (RCR) technique and topographic reductions as well as a global geopotential model, which is described at the end of Sect. 3. Finally, Sect. 4 gives some practical results related to the European geoid and quasigeoid calculations carried out at IfE, starting with a discussion of the data requirements, then an outline of the European gravity and geoid project and the collected gravity and terrain data sets is given, followed by an overview on the development and evaluation of the European Gravimetric (Quasi)Geoid model EGG2008.

2 Fundamentals of Physical Geodesy

2.1 Reference Systems

The definition and realization of reference systems has become a major part of geodesy. Length, mass, and time are basic quantities used in geodesy, the units being meter (m), kilogram (kg), and second (s), respectively, as defined through the International System of Units (SI), see BIPM (2006). Furthermore, fundamental constants (e.g., the gravitational constant) are regularly updated and recommended by the Committee on Data for Science and Technology (CODATA); the latest set of constants originates from 2006 (Mohr et al. 2008).

For the modeling of the Earth's gravity field, global and local reference systems are needed. In this context, a terrestrial reference system (TRS), also denoted as Earth-fixed (global) reference system, is of vital importance. A TRS is a spatial reference system co-rotating with the Earth in its diurnal motion in space, in which points at the solid Earth's surface undergo only small variations with time (e.g., due to geophysical effects related to tectonics or tides). With regard to the terminology, it is fundamental to distinguish between a "reference system," which is based on theoretical considerations or conventions, and its realization, the "reference frame," to which users have access. The International Earth Rotation and Reference Systems Service (IERS) is in charge of defining, realizing and promoting the International Terrestrial and Celestial Reference System (ITRS and ICRS, respectively), including the necessary transformations; the use of these reference systems is recommended by the International Astronomical Union (IAU) and the International Union of Geodesy and Geophysics (IUGG).

The ITRS origin is at the center of mass of the whole Earth including oceans and atmosphere (geocenter), the unit of length is the meter (SI), the orientation is equatorial and initially given by the Bureau International de l'Heure (BIH) terrestrial system at epoch 1984.0, and the time evolution of the orientation is ensured by using a no-net-rotation condition with regard to the horizontal tectonic motions over the whole Earth. Accordingly, the Z-axis is directed towards the IERS reference pole (i.e., the mean terrestrial North Pole), the axes X and Y span the equatorial plane, with the X-axis being defined by the IERS reference meridian (Greenwich), such that the coordinate triplet X,Y,Z forms a right-handed Cartesian system. The instantaneous North Pole (more precisely, the Celestial Intermediate Pole, CIP, which is defined conventionally by the IERS precession and nutation models) deviates from the IERS reference pole by the effect of polar motion (described by rectangular coordinates x_P,y_P). The ITRS is materialized by the International Terrestrial Reference Frame (ITRF), consisting of the three-dimensional positions and velocities of stations observed by space geodetic techniques, where the positions are regularized in the sense that high-frequency time variations (mainly geophysical ones) are removed by conventional corrections. The most recent realization of the ITRS is the ITRF2008 with the reference epoch 2005.0. The accuracy of the geocentric positions (X,Y,Z) is at the level of 1 cm or better. For further details including Earth orientation parameters (EOPs) and transformations see IERS (2010), Kovalevsky and Seidelmann (2004), and Angermann et al. (2012). A corresponding terrestrial reference system (TRS) is the World Geodetic System 1984 (WGS84) which is intended to be as closely coincident as possible with the ITRS; it is maintained by the National Geospatial-Intelligence Agency (NGA), U.S.A., for use with the NAVSTAR Global Positioning System (GPS). The latest realization of WGS84 (i.e., the terrestrial reference frame, TRF) is denoted as "Reference Frame G1150;" it agrees with the ITRF at the level of 1 cm. Moreover, the WGS84 definitions also include the parameters of a level ellipsoid (see Sect. 2.5); for further details see NIMA (1997 and 2002).

Customarily, owing to the Earth's general shape (approximately spherical with a slight flattening at the poles), ellipsoidal geographic coordinates (ellipsoidal latitude, longitude, and height, φ, λ, h, also known as geodetic coordinates), based on an ellipsoid of revolution (ellipse rotating about its minor (polar) axis), are employed in many geodetic applications; regarding the ITRF solutions; IERS (2010) recommends the Geodetic Reference System 1980 (GRS80) ellipsoid (for further details see Sect. 2.5). In addition, spherical coordinates (polar distance or spherical colatitude, spherical longitude, radius, θ, λ, r; the spherical and ellipsoidal longitudes are identical) are of great significance in gravity field modeling. After introducing a reference ellipsoid (e.g., by the geometrical parameters a = semimajor axis and e = first eccentricity), the following relation holds:

$$\mathbf{X} = \begin{pmatrix} X \\ Y \\ Z \end{pmatrix} = \begin{pmatrix} (N+h)\cos\varphi\cos\lambda \\ (N+h)\cos\varphi\sin\lambda \\ ((1-e^2)N+h)\sin\varphi \end{pmatrix} = \begin{pmatrix} r\sin\theta\cos\lambda \\ r\sin\theta\sin\lambda \\ r\cos\theta \end{pmatrix} . \qquad (1)$$

N is the prime vertical radius of curvature of the reference ellipsoid, which can be computed as

$$N = \frac{a}{\sqrt{1 - e^2 \sin^2 \varphi}} \quad . \tag{2}$$

The inversion of the system (1) is straightforward for the spherical case and can be carried out iteratively for the ellipsoidal case (Torge 2001); in addition, formula (1) can be used to transform ellipsoidal into spherical coordinates (e.g., needed in connection with spherical harmonic expansions; see Sects. 2.2 and 3.3) and vice versa.

In this context, it should be noted that historically many ellipsoidal systems and the associated Cartesian systems (i.e., national reference frames) were non-geocentric. This is mainly due to the orientation of the classical geodetic networks by astronomical observations, which provide only direction information, but no direct access to the geocenter. In this case, the non-geocentric X_{ng}, Y_{ng}, Z_{ng} system can be transformed to the X, Y, Z system by a three-dimensional similarity transformation (Torge 2001):

$$\mathbf{X} = \mathbf{X}_0 + (1+m)\,\mathbf{R}(\varepsilon_{X_{ng}}, \varepsilon_{Y_{ng}}, \varepsilon_{Z_{ng}})\,\mathbf{X}_{ng} \tag{3}$$

with

$$\mathbf{X}_0 = \begin{pmatrix} X_0 \\ Y_0 \\ Z_0 \end{pmatrix}, \quad \mathbf{R}(\varepsilon_{X_{ng}}, \varepsilon_{Y_{ng}}, \varepsilon_{Z_{ng}}) = \begin{pmatrix} 1 & \varepsilon_{Z_{ng}} & -\varepsilon_{Y_{ng}} \\ -\varepsilon_{Z_{ng}} & 1 & \varepsilon_{X_{ng}} \\ \varepsilon_{Y_{ng}} & -\varepsilon_{X_{ng}} & 1 \end{pmatrix}, \tag{4}$$

where $\mathbf{X}_0$ is a translation vector with the coordinates of the origin of the X_{ng}, Y_{ng}, Z_{ng} system with respect to the geocenter, m is a (small) scale correction, $\mathbf{R}$ is a rotation matrix with three (small) Eulerian angles, and $\mathbf{X}_{ng}$ is the coordinate vector in the non-geocentric system. It should be noted that the transformation model (3) is a linearized formula which is sufficient due to the small size of the rotation angles; furthermore, the sign conventions are according to Torge (2001). The geodetic datum describes the orientation of any geodetic system with respect to the global geocentric system (seven transformation parameters of (3)) and also includes the parameters of the reference ellipsoid employed. Numerous examples of national (non-geocentric) geodetic datums can be found in NIMA (1997) and Torge (2001); the translation parameters can reach several hundreds of meters, the scale corrections may be in the order of 10^{-5}, the rotation angles are usually quite small at the level of 1 arc second or below (due to the orientation by astronomical observations), and miscellaneous reference ellipsoids were employed for national geodetic surveys, carried out since the nineteenth century.

After introducing ellipsoidal coordinates in the vectors $\mathbf{X}$ and $\mathbf{X}_{ng}$ in (3), while also allowing a change of ellipsoid parameters, the following transformation formula is obtained for the ellipsoidal heights:

$$h = h_{ng} + \cos\varphi\cos\lambda\, X_0 + \cos\varphi\sin\lambda\, Y_0 + \sin\varphi\, Z_0 - \Delta a + a\sin^2\varphi\,\Delta f \quad , \qquad (5)$$

with the ellipsoidal heights h and h_{ng} in the geocentric and non-geocentric system, respectively, and the changes in the ellipsoid parameters $\Delta a = a - a_{ng}$ (semimajor axis) and $\Delta f = f - f_{ng}$ (flattening). The above formula is based on spherical approximations (terms of the order of the flattening $o(f)$ are neglected), where the rotation angles have no effect. The translation parameters (X_0, Y_0, Z_0) can be converted into changes in the ellipsoidal coordinates of a fundamental station, and hence be interpreted as height shift and tilts in north–south and east–west direction of the respective ellipsoid surfaces. Formula (5) is applied, e.g., for the transformation of geoid and quasigeoid heights. Corresponding formulas for the transformation of latitudes and longitudes ($\varphi_{ng}, \lambda_{ng} \rightarrow \varphi, \lambda$) can be found in Torge (2001); in addition, more precise transformation formulas without the usual spherical approximations are given in Heck (2003). Finally, it is assumed in the following that all coordinates refer directly (e.g., through the application of space geodetic techniques) or have been converted (from national geodetic datums) consistently to an IERS reference frame (e.g., ITRF2008, epoch 2005.0).

Because most geodetic and astronomical observations refer to the Earth's gravity field by orientating observation instruments along the local vertical (through levels or plummets), local coordinate systems related to the Earth's gravity field are introduced. These local astronomical (Cartesian) systems have their origin at the observation point P, the z-axis points toward the zenith (tangent of the plumb line, outer normal of the level surface), while the x-axis (north) and y-axis (east) span the horizontal plane, which is tangential to the level surface at P. The local astronomical system (x, y, z) is left-handed. As the direction of the plumb line (local vertical) with respect to the global geocentric system is given by the astronomical latitude Φ and longitude Λ (see Fig. 1), the coordinate vector $\mathbf{x}$ in the local astronomical system can be transformed into a coordinate difference vector $\mathbf{\Delta X}$ in the global geocentric system by

$$\mathbf{\Delta X} = \mathbf{A}_\mathbf{x}\,\mathbf{x} \qquad (6)$$

with

$$\mathbf{A}_\mathbf{x} = \mathbf{A}_\mathbf{x}(\Phi,\Lambda) = \begin{pmatrix} -\sin\Phi\cos\Lambda & -\sin\Lambda & \cos\Phi\cos\Lambda \\ -\sin\Phi\sin\Lambda & \cos\Lambda & \cos\Phi\sin\Lambda \\ \cos\Phi & 0 & \sin\Phi \end{pmatrix} . \qquad (7)$$

The transformation matrix $\mathbf{A}_\mathbf{x}$ is orthogonal, thus

$$\mathbf{A}_\mathbf{x}^{-1} = \mathbf{A}_\mathbf{x}^{T} \quad . \qquad (8)$$

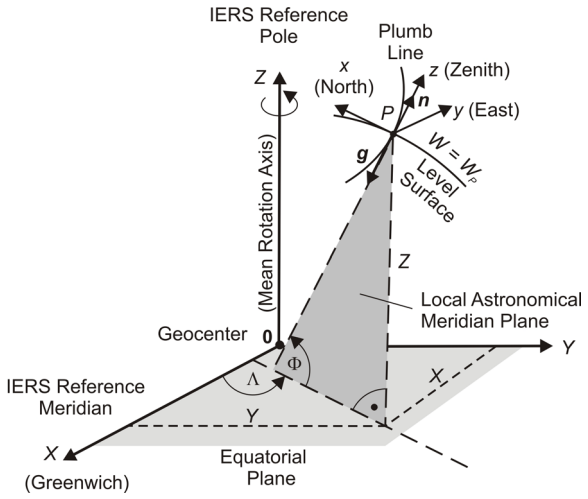

Fig. 1 Earth-fixed global geocentric and local astronomical system

Accordingly, local ellipsoidal and spherical (Cartesian) coordinate systems can be introduced as needed, for example in connection with the rigorous calculation of parameters related to the actual, normal, or anomalous gravity field (see Sects. 2.3, 2.5, and 3.2). Regarding the local ellipsoidal system (x^e, y^e, z^e), the z^e-axis points toward the ellipsoidal zenith (ellipsoidal normal), with the x^e-axis (north) and y^e-axis (east) being perpendicular to it. On the other hand, in the local spherical system (x^s, y^s, z^s), the z^s-axis points radially outwards (along the geocentric radius vector), with the axes x^s, y^s (north and east) again being perpendicular to it (see Fig. 2). Analogous to (6), the transformation to the global system is given by

$$\mathbf{\Delta X} = \mathbf{A}_{\mathbf{x^e}}\,\mathbf{x^e} \quad , \qquad \mathbf{A}_{\mathbf{x^e}} = \mathbf{A}_{\mathbf{x^e}}(\varphi, \lambda) \quad , \tag{9}$$

$$\mathbf{\Delta X} = \mathbf{A}_{\mathbf{x^s}}\,\mathbf{x^s} \quad , \qquad \mathbf{A}_{\mathbf{x^s}} = \mathbf{A}_{\mathbf{x^s}}(90° - \theta, \lambda) \quad . \tag{10}$$

The above transformation matrices $\mathbf{A}_{\mathbf{x^e}}$ and $\mathbf{A}_{\mathbf{x^s}}$ are defined according to (7); the only difference is that the parameters Φ, Λ are replaced by φ, λ and $90° - \theta, \lambda$, respectively. The transformation matrices also relate to the coordinate basis vectors of the corresponding Cartesian coordinate systems, e.g., if $\mathbf{e_X}, \mathbf{e_Y}, \mathbf{e_Z}$ are unit vectors along the coordinate axes X, Y, Z, and $\mathbf{e}_{\mathbf{x^s}}, \mathbf{e}_{\mathbf{y^s}}, \mathbf{e}_{\mathbf{z^s}}$ are the corresponding vectors along the axes x^s, y^s, z^s, the following relation holds (see also Wenzel 1985):

$$\begin{pmatrix} \mathbf{e_X} \\ \mathbf{e_Y} \\ \mathbf{e_Z} \end{pmatrix} = \mathbf{A}_{\mathbf{x^s}} \begin{pmatrix} \mathbf{e}_{\mathbf{x^s}} \\ \mathbf{e}_{\mathbf{y^s}} \\ \mathbf{e}_{\mathbf{z^s}} \end{pmatrix} = \begin{pmatrix} -\cos\theta\cos\lambda & -\sin\lambda & \sin\theta\cos\lambda \\ -\cos\theta\sin\lambda & \cos\lambda & \sin\theta\sin\lambda \\ \sin\theta & 0 & \cos\theta \end{pmatrix} \begin{pmatrix} \mathbf{e}_{\mathbf{x^s}} \\ \mathbf{e}_{\mathbf{y^s}} \\ \mathbf{e}_{\mathbf{z^s}} \end{pmatrix} \quad . \tag{11}$$

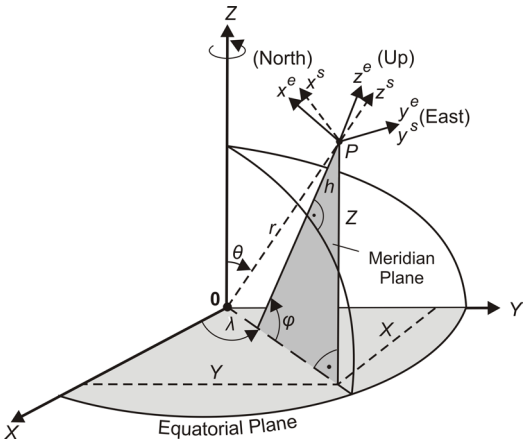

Fig. 2 Global ellipsoidal, local ellipsoidal, and local spherical system

Moreover, the transformation formulas can also be combined to transform coordinates and basis vectors from one local system to another.

2.2 Newton's Law of Gravitation and Potential

According to Newton's law of gravitation, two point masses m_1 and m_2 attract each other with gravitational (attractive) force which is directly proportional to the product of their masses and inversely proportional to the square of the distance l between them. The gravitational force is directed from either point mass to the other and applies equally to one mass as the other. The vector form of Newton's law is given by

$$\mathbf{F_b} = -G\frac{m_1 m_2}{l^2}\,\frac{\mathbf{l}}{l} \quad , \tag{12}$$

where $\mathbf{l}/l$ is a unit vector pointing from m_1 to m_2, $\mathbf{F_b}$ is the gravitational force vector attached to m_2 and pointing to m_1, and G is known as Newton's gravitational constant. G can be determined by experiment and the current best value (recommended by CODATA, 2006; Mohr et al. 2008) is

$$G = (6.67428 \pm 0.00067) \times 10^{-11} \ \mathrm{m^3\,kg^{-1}\,s^{-2}} \quad . \tag{13}$$

The SI unit of force is $\mathrm{m\,kg\,s^{-2}}$ with the special name "newton" and symbol "N," – see BIPM (2006). In this context, gravitation is exclusively based on Newton's classical formulation; for a discussion of some aspects related to Einstein's theory of general relativity consult Kovalevsky and Seidelmann (2004), IERS (2010), Jekeli (2009), or Müller et al. (2008).

A gravitational acceleration (also termed gravitation) can be ascribed to the gravitational force $\mathbf{F_b}$, which represents the acceleration that one mass undergoes due to the gravitational attraction of the other. From (12) it follows, for the attracted point P (after dropping the indices),

$$\mathbf{b} = -G\frac{m}{l^2}\,\frac{\mathbf{l}}{l} \quad , \tag{14}$$

where m is the attracting mass, $\mathbf{l} = \mathbf{r}-\mathbf{r'}$, with $\mathbf{r}$ and $\mathbf{r'}$ being the position vectors of the attracted point P and the source point P', respectively. By the law of superposition, the gravitational acceleration of an extended body like the Earth can be computed as the vector sum of the accelerations generated by the individual point masses (or mass elements), yielding

$$\mathbf{b} = \mathbf{b}(\mathbf{r}) = -G\iiint\limits_{\text{Earth}} \frac{\mathbf{r}-\mathbf{r}'}{\left|\mathbf{r}-\mathbf{r}'\right|^3}\,dm = -G\iiint\limits_{\text{Earth}} \frac{\mathbf{r}-\mathbf{r}'}{\left|\mathbf{r}-\mathbf{r}'\right|^3}\,\rho\,dv \quad , \quad \rho = \rho(\mathbf{r}') \quad , \tag{15}$$

where dm is the differential mass element, ρ is the volume density (unit kg m^{-3}), and dv is the volume element. The SI unit of acceleration is m s^{-2} (BIPM 2006). However, the non-SI unit gal is still used frequently in geodesy and geophysics, and it is also listed in BIPM (2006) under "non-SI units accepted for use with the SI, Table 9" (name of unit: gal; symbol of unit: Gal):

$$\begin{aligned} &1\ \text{Gal} = 1\ \text{cm s}^{-2} = 0.01\ \text{m s}^{-2}, \quad 1\ \text{kGal} = 10\ \text{m s}^{-2}, \\ &1\ \text{mGal} = 10^{-5}\ \text{m s}^{-2}, \quad 1\ \mu\text{Gal} = 10^{-8}\text{m s}^{-2}\ . \end{aligned} \tag{16}$$

The gravitational acceleration vectors $\mathbf{b}$ form a conservative vector field, also known as potential field. A conservative vector field is a vector field which is the gradient of a scalar potential function. It has the important property that line integrals from one point to another are path independent, and, conversely, path independence is equivalent to the vector field being conservative. Conservative vector fields are also irrotational or non-vortical, meaning that (in three dimensions) they have vanishing curl; the converse of this property (i.e., fields with vanishing curl are conservative) is also true if the domain is simply connected (Kellog 1953).

The gravitational acceleration vector $\mathbf{b}$ can be represented as the gradient of the gravitational potential V:

$$\mathbf{b} = \text{grad}\,V \quad . \tag{17}$$

The gradient vector has the properties that it points in the direction of greatest change of the potential function V, its magnitude equals the rate of change with respect to the distance in this direction, and it is everywhere normal to a surface of constant potential V. Furthermore, the directional derivative of V with respect to the distance in a particular direction (specified by a vector $\mathbf{d}$) is the projection of grad$V$ onto that direction.

For a point mass m, see (14), the gravitational potential is given by

$$V = \frac{Gm}{l} \quad , \qquad \text{with} \quad \lim_{l \to \infty} V = 0 \quad , \tag{18}$$

and correspondingly for the Earth, see (15), the potential is obtained by

$$V = V(\mathbf{r}) = G \iiint_{\text{Earth}} \frac{dm}{l} = G \iiint_{\text{Earth}} \frac{\rho \, dv}{l} \quad , \qquad \text{with} \quad \lim_{l \to \infty} V = 0 \quad , \tag{19}$$

where in both cases the latter condition implies that the potential is regular at infinity. It can easily be shown that the acceleration vectors in (14) and (15) result from (18) and (19) by applying the gradient operator, respectively. In this context, it should be noted that the potential V is defined with a positive sign in geodesy, in contrast to physics, where it is usually defined with opposite sign (conceptually closer to potential energy; Jekeli 2009).

According to potential theory, the gravitational effect of concentric homogeneous mass shells is equal to the effect of the entire mass being concentrated at the center of mass of the object. This property is useful for approximating the effect of celestial bodies at larger distances or the computation of atmospheric effects (see Sect. 2.6). On the other hand, this relates to the inverse problem of potential theory; the inverse problem (determination of the masses from the potential), in contrast to the direct problem (determination of the potential from the masses), has no unique solution, because, in general, there are infinitely many mass distributions possible, which are in accordance with a given exterior potential function.

The gravitational potential at a point P indicates the work done by gravitation in order to move the unit mass from infinity ($V = 0$) to P (Sigl 1985, Torge 2001). The unit of the potential is $\mathrm{m^2\,s^{-2}}$. If the density structure and geometry of the entire Earth were known, (19) would permit the calculation of the gravitational potential and its functionals. In reality, of course, this information is not available with sufficient accuracy, e.g., densities are known with only two or three significant digits, and global Earth models merely consider radial density structures. Therefore, the determination of the exterior potential field can be solved only by measurements performed at or above the Earth's surface (boundary value problems; see Sects. 3.1–3.5); for a comprehensive presentation of this and further specialized topics of potential theory (e.g., existence and uniqueness theorems, or the classical integral theorems of Gauss, Green, and Stokes, which are of great importance in physical geodesy), reference should be made to the textbooks of Kellogg (1953), MacMillan (1958), and Sigl (1985); furthermore, a concise overview is given in Jekeli (2009).

The gravitational (volume) potential V according to (19) and its first derivatives are continuous and bounded everywhere; this holds even in the case that the evaluation point P is on the bounding surface or inside the mass distributions (case $l = 0$, weak singularity; see Jekeli 2009, Torge 2001). The second derivatives of V satisfy

under certain conditions on the mass density ρ (so-called Hölder conditions; see Kellogg 1953, Heck 1997) the following partial differential equation, known as Poisson's equation:

$$\Delta V = \frac{\partial^2 V}{\partial x^2} + \frac{\partial^2 V}{\partial y^2} + \frac{\partial^2 V}{\partial z^2} = V_{xx} + V_{yy} + V_{zz} = -4\pi G\rho \ , \tag{20}$$

where Δ is the Laplace operator, and x, y, z are coordinates in any Cartesian system. Consequently, the second derivatives of V exhibit discontinuities where abrupt changes of the mass density ρ occur. A special case of the above equation applies for those regions where the density vanishes (i.e., in free space); then Poisson's equation turns into the Laplace equation:

$$\Delta V = 0 \ . \tag{21}$$

The Laplace operator Δ may also be defined as the divergence of a gradient field, i.e.,

$$\Delta V = \operatorname{div}(\operatorname{grad} V) \ . \tag{22}$$

As the divergence operator represents the (gravitational) flux generated per unit volume at each point of the field, (22) emphasizes that the sources of the gravitational field are the masses, i.e., the divergence of the field is zero in free space and non-zero inside the masses. A vector field with constant zero divergence is also called solenoidal (or incompressible).

The solutions of the Laplace equation are known as harmonic functions, which are important in many fields of mathematics and physics, such as potential fields related to gravitation, electrostatics, magnetics, etc. For instance, every Newtonian potential is a harmonic function in free space, and conversely, every harmonic function can be represented as a Newtonian potential of a mass distribution (Jekeli 2009). Formally, (21) represents a partial differential equation of second order for V, which holds in the exterior space of the Earth (the atmosphere, etc., are neglected for the moment). Like any differential equation, a complete solution is obtained only with the application of boundary conditions (conditions which the solution must satisfy at the boundary of the region, i.e., the Earth's surface; Jekeli 2009).

Laplace's equation (21) can be solved by introducing an appropriate coordinate system. In geodesy, the solution based on spherical polar coordinates (θ, λ, r) is of great significance. A solution of $\Delta V = 0$, rewritten in spherical coordinates, can be found by the method of separation of variables, where the solution of V is postulated as $V(\theta, \lambda, r) = f(\theta)\, g(\lambda)\, h(r)$. The general solution can be written as

$$V(\theta,\lambda,r) = \frac{GM}{a} \sum_{n=0}^{\infty} \left(\frac{a}{r}\right)^{n+1} \sum_{m=0}^{n} \left(C_{nm} \cos m\lambda + S_{nm} \sin m\lambda\right) P_{nm}(\cos\theta) \ , \tag{23}$$

where n,m are integers denoted as degree and order of the expansion, GM is the geocentric gravitational constant (gravitational constant G times the mass of the

Earth *M*), *a* is in the first instance an arbitrary constant, but is typically set equal to the semimajor axis of a reference ellipsoid, $P_{nm}(\cos\theta)$ are the associated Legendre functions of the first kind, and C_{nm}, S_{nm} are the spherical harmonic coefficients (also denoted as Stokes's constants). In particular in satellite geodesy, sometimes the following conventions are used:

$$\begin{aligned} &J_{nm} = -C_{nm}\,, \quad K_{nm} = -S_{nm}\,, && \text{for} \quad n \neq 0 \ \text{ or } \ m \neq 0\,, \\ &J_{00} = C_{00} = 1\,, && \text{for} \quad n = 0 \ \text{ and } \ m = 0\,. \end{aligned} \tag{24}$$

For the case $m = 0$, the index m is usually dropped, leading to the coefficients J_n and the Legendre polynomials $P_n(\cos\theta)$.

The (unitless) spherical harmonic coefficients C_{nm}, S_{nm} represent mass integrals, as the spherical harmonic expansion (23) is just another way of expressing the volume integral over the Earth's masses in (19). Furthermore, the low degree coefficients have a simple physical interpretation. The coefficient $C_{00} = 1$ leads to the zero degree term *GM/r* of the gravitational potential, which represents the effect of a point mass, or equivalently a radially layered spherical Earth. The degree one terms are associated with the coordinates of the Earth's center of mass; they are forced to zero if the coordinate system is geocentric. The terms of degree two are connected with the moments and products of inertia (see Torge 2001). Regarding the magnitude of the harmonic coefficients, C_{20} ($J_2 = -C_{20}$ is also known as the dynamical form factor, characterizing the Earth's flattening) is more than three orders of magnitude smaller than the central term, and the remaining coefficients contribute again at least two to three orders of magnitude less than C_{20}, indicating that the bulk of the potential can be described by an ellipsoidal model.

For numerical reasons, it is convenient to introduce the so-called fully normalized associated Legendre functions and corresponding spherical harmonic coefficients:

$$\begin{aligned} &\overline{P}_{nm}(\cos\theta) = F_{nm}\, P_{nm}(\cos\theta)\,, \qquad \begin{Bmatrix} \overline{C}_{nm} \\ \overline{S}_{nm} \end{Bmatrix} = \frac{1}{F_{nm}} \begin{Bmatrix} C_{nm} \\ S_{nm} \end{Bmatrix}, \\ &F_{nm} = \sqrt{k(2n+1)\frac{(n-m)!}{(n+m)!}} \quad \text{with} \quad k = \begin{cases} 1 & \text{for } m = 0 \\ 2 & \text{for } m \neq 0 \end{cases}. \end{aligned} \tag{25}$$

With (25), the spherical harmonic expansion (23) can be written compactly as

$$V(\theta,\lambda,r) = \sum_{n=0}^{\infty} \left(\frac{a}{r}\right)^{n+1} \sum_{m=-n}^{n} \overline{V}_{nm}\, \overline{Y}_{nm}(\theta,\lambda)\ , \tag{26}$$

with

$$\overline{Y}_{nm}(\theta,\lambda)=\overline{P}_{n|m|}(\cos\theta)\begin{cases}\cos m\lambda & \text{for } m\geq 0\\ \sin|m|\lambda & \text{for } m<0\end{cases},\quad \overline{V}_{nm}=\frac{GM}{a}\begin{cases}\overline{C}_{nm} & \text{for } m\geq 0\\ \overline{S}_{nm} & \text{for } m<0\end{cases}. \tag{27}$$

The functions $r^{-(n+1)}\overline{Y}_{nm}(\theta,\lambda)$ in (26) are called solid spherical harmonics, while $\overline{Y}_{nm}(\theta,\lambda)$ are called Laplace's surface spherical harmonics, fulfilling the orthogonality relations

$$\frac{1}{4\pi}\iint_{\sigma}\overline{Y}_{nm}(\theta,\lambda)\overline{Y}_{n'm'}(\theta,\lambda)\,d\sigma=\begin{cases}1 & \text{for } n=n' \text{ and } m=m'\\ 0 & \text{otherwise}\end{cases}, \tag{28}$$

where σ is the unit sphere, and $d\sigma$ is the corresponding surface element. In this context, the spherical harmonic expansion may also be regarded as a complete system of orthogonal basis functions (eigenfunctions), with the coefficients being the corresponding eigenvalues, which can be interpreted as the spectrum on the sphere (Jekeli 2009).

The infinite spherical harmonic series (23), or equivalently (26), converges uniformly for all $r > R_c$, where R_c is the radius of the sphere that encloses all terrestrial masses (the so-called Brillouin sphere), while the convergence below this sphere down to the Earth's surface (i.e., in free space) has been a subject of controversy in the literature and is still not fully solved. However, due to the theorem of Runge-Krarup, any regular harmonic function can be approximated arbitrarily well by a spherical harmonic series in the mass-free space, and hence convergence of the series can be assumed there for all practical applications, including truncated spherical harmonic series. For further details on this topic, see, e.g., Moritz (1980) or Jekeli (1983, 2009). Besides the spherical harmonic series expansion, which is of outstanding importance in geodesy, other solutions of the Laplace equation (21) also exist for specific coordinate types. Of some relevance are the ellipsoidal harmonics, which are based on elliptical coordinates (β, λ, u; β = reduced latitude; λ = ellipsoidal longitude; u = semiminor axis of a confocal ellipsoid; see Heiskanen and Moritz 1967). Ellipsoidal harmonics are used, e.g., in connection with the (ellipsoidal) normal gravity field (Heiskanen and Moritz 1967) or for intermediate results within the development of high-degree global geopotential models (Pavlis et al. 2008); the elliptical coordinates, β, λ, u, should not be confused with the ellipsoidal geographic coordinates, φ, λ, h, which do not admit a separation of variables solution of the Laplace equation (Grafarend 1988, Jekeli 2009).

2.3 The Earth's Gravity Field

A body rotating with the Earth experiences the resultant of the gravitational force, $\mathbf{F}_b$, and the centrifugal force, $\mathbf{F}_c$, due to the Earth's rotation, while an artificial satellite, not rotating with the Earth, is affected only by gravitation. Regarding the centrifugal force, $\mathbf{F}_c$, again an acceleration (acting on a unit mass) can be ascribed

to it, which is directed outwards and perpendicular to the rotation axis. Based on the Earth-fixed reference system (X, Y, Z; see Sect. 2.1), the centrifugal acceleration is given by

$$\mathbf{z} = \mathbf{z}(\mathbf{p}) = \omega^2 \mathbf{p} \ , \qquad \mathbf{p}^{\mathrm{T}} = \begin{pmatrix} X & Y & 0 \end{pmatrix} \ , \qquad p = |\mathbf{p}| = \sqrt{X^2 + Y^2} \ , \tag{29}$$

where ω is the angular velocity, and $\mathbf{p}$ is the distance vector from the rotation axis (Z), with $\mathbf{p}$ and $\mathbf{z}$ having the same direction.

The centrifugal acceleration vectors $\mathbf{z}$ also form a conservative vector field and hence can be represented as the gradient of a potential function Z. With

$$\mathbf{z} = \operatorname{grad} Z \ , \tag{30}$$

the centrifugal potential Z becomes

$$Z = Z(p) = \frac{\omega^2}{2} p^2 \ . \tag{31}$$

Applying the Laplace operator on Z yields

$$\Delta Z = 2\,\omega^2 \ , \tag{32}$$

i.e., the centrifugal potential Z is not harmonic, as opposed to V.

The gravity acceleration (or gravity) vector $\mathbf{g}$ is the resultant of the gravitation $\mathbf{b}$ and the centrifugal acceleration $\mathbf{z}$:

$$\mathbf{g} = \mathbf{b} + \mathbf{z} \ . \tag{33}$$

The force of gravity $\mathbf{F_g}$ is obtained by multiplying $\mathbf{g}$ by the mass m of the attracted object, i.e., $\mathbf{F_g} = m\,\mathbf{g}$. The direction of $\mathbf{g}$ is the direction of the plumb line (vertical), the magnitude g is called the gravity intensity (or often just gravity; see Torge 2001). In this context, time variations are not considered here, assuming that they are taken into account by appropriate reductions (see Sect. 2.6).

Finally, with

$$\mathbf{g} = \operatorname{grad} W = \mathbf{b} + \mathbf{z} = \operatorname{grad} V + \operatorname{grad} Z \ , \tag{34}$$

the gravity potential W of the Earth is given by

$$W = W(\mathbf{r}) = V + Z = G \iiint_{\text{Earth}} \frac{dm}{l} + \frac{\omega^2}{2} p^2 \ . \tag{35}$$

From (20) and (32), the generalized Poisson equation is obtained:

$$\Delta W = -4\pi G\rho + 2\,\omega^2 \ , \tag{36}$$

which reduces to the generalized Laplace equation in free space:

$$\Delta W = 2\,\omega^2 \quad . \tag{37}$$

The gravity vector **g** and accordingly the gradient operator can be expressed in various coordinate systems. Regarding the global Cartesian Earth-fixed coordinate system X, Y, Z, the following representations are common:

$$\mathbf{g} = \operatorname{grad} W = \begin{pmatrix} \frac{\partial W}{\partial X} \\ \frac{\partial W}{\partial Y} \\ \frac{\partial W}{\partial Z} \end{pmatrix} = \begin{pmatrix} W_X \\ W_Y \\ W_Z \end{pmatrix} = \left[\mathbf{W_X}\right] = W_X \mathbf{e_X} + W_Y \mathbf{e_Y} + W_Z \mathbf{e_Z} \ , \tag{38}$$

where the gradient vector is first defined as a column vector, and second written by means of the unit vectors $\mathbf{e_X}$, $\mathbf{e_Y}$, $\mathbf{e_Z}$, pointing along the coordinate axes X, Y, Z, respectively. In the case where spherical coordinates θ, λ, r are employed (e.g., in connection with a spherical harmonic expansion of the gravitational potential V), it is convenient to represent **g** with respect to the local spherical system (x^s, y^s, z^s; see Sect. 2.1):

$$\mathbf{g} = \operatorname{grad} W = \begin{pmatrix} \frac{\partial W}{\partial x^s} \\ \frac{\partial W}{\partial y^s} \\ \frac{\partial W}{\partial z^s} \end{pmatrix} = \begin{pmatrix} W_{x^s} \\ W_{y^s} \\ W_{z^s} \end{pmatrix} = \left[\mathbf{W_{x^s}}\right] = W_{x^s} \mathbf{e_{x^s}} + W_{y^s} \mathbf{e_{y^s}} + W_{z^s} \mathbf{e_{z^s}} \ , \tag{39}$$

where $\mathbf{e_{x^s}}, \mathbf{e_{y^s}}, \mathbf{e_{z^s}}$ are again unit vectors pointing along the local coordinate axes x^s, y^s, z^s, respectively. The derivatives of W with respect to the local spherical system can be obtained by using the chain rule for differentiation (Tscherning 1976a, b), e.g.,

$$\frac{\partial}{\partial x^s} = \frac{\partial \theta}{\partial x^s}\frac{\partial}{\partial \theta} + \frac{\partial \lambda}{\partial x^s}\frac{\partial}{\partial \lambda} + \frac{\partial r}{\partial x^s}\frac{\partial}{\partial r} \quad , \text{ and } \quad \frac{\partial}{\partial y^s}, \frac{\partial}{\partial z^s} \text{ accordingly,} \tag{40}$$

which, given (1) and (10), leads to

$$\left[\mathbf{W_{x^s}}\right] = \begin{pmatrix} -\frac{1}{r}W_\theta & \frac{1}{r\sin\theta}W_\lambda & W_r \end{pmatrix}^{\mathbf{T}} \quad , \tag{41}$$

with W_θ being the derivative with respect to θ, etc. Then with (10) or (11), the transformation to the Earth-fixed system yields

$$\left[\mathbf{W_X}\right] = \mathbf{A_{x^s}} \left[\mathbf{W_{x^s}}\right] . \tag{42}$$

On the other hand, in the Earth-fixed system, the components of the gravity vector **g** can also be expressed by the astronomical latitude and longitude Φ, Λ (plumb line parameters; see Fig. 1):

$$\mathbf{g} = -g\mathbf{n} = -g \begin{pmatrix} \cos\Phi\cos\Lambda \\ \cos\Phi\sin\Lambda \\ \sin\Phi \end{pmatrix} , \tag{43}$$

which together with (38) yields

$$\begin{aligned} &\sin\Phi = -\frac{1}{g}W_Z \ , && \cos\Phi = \frac{1}{g}\sqrt{W_X^2 + W_Y^2} \ , \\ &\sin\Lambda = -\frac{W_Y}{g\cos\Phi} = -\frac{W_Y}{\sqrt{W_X^2 + W_Y^2}} \ , && \cos\Lambda = -\frac{W_X}{g\cos\Phi} = -\frac{W_X}{\sqrt{W_X^2 + W_Y^2}} \ , \\ &g = \sqrt{W_X^2 + W_Y^2 + W_Z^2} \ . \end{aligned} \tag{44}$$

Φ, Λ, and $W(X, Y, Z)$ form the so-called natural coordinates (Torge 2001). A surface of constant gravity potential W is designated as equipotential, level, or geopotential surface, and the gravity vector **g** is everywhere normal to it.

Following the line of thought used for deriving (41), the second derivatives of the gravity potential W with respect to the local spherical system are given by (Moritz 1971; Tscherning 1976a)

$$\begin{aligned} \left[\mathbf{W}_{\mathbf{x}^s\mathbf{x}^s}\right] = \operatorname{grad}\mathbf{g} = \operatorname{grad}(\operatorname{grad} W) &= \begin{pmatrix} W_{x^s x^s} & W_{x^s y^s} & W_{x^s z^s} \\ W_{y^s x^s} & W_{y^s y^s} & W_{y^s z^s} \\ W_{z^s x^s} & W_{z^s y^s} & W_{z^s z^s} \end{pmatrix} \\ &= \begin{pmatrix} \underline{\frac{1}{r}W_r + \frac{1}{r^2}W_{\theta\theta}} & \frac{1}{r^2\sin\theta}(\cot\theta\, W_\lambda - W_{\theta\lambda}) & \frac{1}{r^2}W_\theta - \frac{1}{r}W_{\theta r} \\ \cdots & \underline{\frac{\cot\theta}{r^2}W_\theta + \frac{1}{r}W_r + \frac{1}{r^2\sin^2\theta}W_{\lambda\lambda}} & \frac{1}{r\sin\theta}(-\frac{1}{r}W_\lambda + W_{\lambda r}) \\ \cdots & \cdots & \underline{W_{rr}} \end{pmatrix} \end{aligned} , \tag{45}$$

where, e.g., $W_{\theta\theta}$ is the second derivative with respect to θ, etc. The corresponding matrix with respect to the Earth-fixed system (X, Y, Z) is given by

$$\left[\mathbf{W}_{\mathbf{XX}}\right] = \mathbf{A}_{\mathbf{x}^s}\left[\mathbf{W}_{\mathbf{x}^s\mathbf{x}^s}\right](\mathbf{A}_{\mathbf{x}^s})^{\mathbf{T}} \ . \tag{46}$$

The matrix of the second derivatives of W, e.g., in the form (45) or (46), is also denoted as gravity gradient tensor, Eötvös tensor, or Marussi tensor; it can be expressed by means of curvature parameters, which completely describe the geome-

try (curvature) of the level surfaces and the plumb lines (Marussi 1985). The gravity gradient tensor includes only five independent elements; the matrix is symmetric (because of curl $\mathbf{g} = \text{curl grad } W = 0$, i.e., $W_{xy} = W_{yx}$, etc.) and the trace must fulfil the conditions (36) or (37), respectively.

The approach of computing, in the first instance the (first and second) derivatives with respect to the local spherical system, followed by a transformation to the Earth-fixed system, involves no approximations (Wenzel 1985) and is particularly suitable in connection with spherical harmonic expansions, e.g., the high-degree geopotential model EGM2008 (Pavlis et al. 2008). It should also be noted that (41) and (42) for the first derivatives as well as (45) and (46) for the second derivatives can be utilized accordingly for each of the components of W, i.e., V and Z; moreover, they may be used in connection with the disturbing potential and its functionals (see Sect. 3.2). With regard to the presently active satellite mission GOCE (ESA 1999, Rummel et al. 2011), the second derivatives of V are of special interest. Finally, the results in the Earth-fixed system can be further transformed to any other Cartesian system of interest.

At this point it is emphasized that the primary goal of physical geodesy is the determination of the gravity potential W as a function of position; if $W(\mathbf{r})$ were known, then all parameters of interest could be derived from it, including the gravity vector $\mathbf{g}$ (direction parameters, Φ, Λ, and magnitude, g, see (44)), the curvature of the level surfaces and plumb lines (depending on the second derivatives of W, e.g., (46)), as well as the form of the equipotential surfaces (by solving the equation $W(X, Y, Z) = \text{const.}$). However, as mentioned above, the gravity potential W cannot be computed directly based on (35) due to the insufficient knowledge about the density structure of the entire Earth; instead, the determination of the exterior potential field must be solved by measurements performed at or above the Earth's surface (see Sect. 3).

2.4 The Geoid and Heights

The geoid is of great importance in geodesy, oceanography, geophysics, and other Earth sciences, serving as a reference surface for heights over the continents as well as for the dynamic ocean topography (DOT). The geoid was introduced by C.F. Gauss as an equipotential surface of the Earth's gravity field, coinciding with the mean sea level (MSL) of the idealized oceans (i.e., homogeneous water masses at rest, subject only to the time-invariable force of gravity; see Torge 2001). The basis of this definition, i.e., the geoid being a selected equipotential surface of the Earth's gravity field (with $W = W_0$), is of fundamental importance and is still useful today. Given the gravity potential value W_0, the equation of the geoid is

$$W = W(\mathbf{r}) = W_0 \quad . \tag{47}$$

As discussed in the previous section, the geoid is a closed and continuous surface, even inside the Earth; however, inside the masses, the curvature of the geoid may

exhibit discontinuities where abrupt density changes occur. The vertical distance between the geoid and a given reference ellipsoid is denoted as the geoid height or geoid undulation.

The geoid is conceptionally chosen to approximate (in some mathematical sense) the mean ocean surface (Rapp 1995). However, mean sea level (MSL), derived by averaging the instantaneous sea surface over a sufficiently long time span (e.g., at least 1 year), may also vary over longer time spans (for instance, due to the global secular sea level rise of about 1–2 mm/year, observed over the past 100 years; Torge 2001), and furthermore it does not coincide with a level surface due to the forcing of the oceans by winds, atmospheric pressure, and buoyancy (as a result of density differences associated with corresponding temperature and salinity differences) in combination with gravity and the Earth's rotation. The deviation of MSL from a best fitting equipotential surface (geoid) is denoted as the (mean) dynamic ocean topography (DOT). The DOT reaches maximum values of about ±2 m (Rapp and Balasubramania 1992; Bosch and Savcenko 2010) and is of vital importance for oceanographers, as it allows the derivation of the absolute circulation of the oceans (Wunsch and Gaposchkin 1980; Condi and Wunsch 2004).

Accordingly, a refined definition of the geoid is needed, which could be based on a (global) minimum condition with regard to the deviation of MSL from a best fitting level surface, and which should also consider that MSL is not constant in time. In principle, two options exist: either the geoid definition has to refer to a certain epoch of MSL, or a time-dependent geoid linked to the respective MSL could be introduced. However, corresponding to the general geodetic practice of reducing time-variable quantities to a quasi-static state (see also Sect. 2.6), mainly the first option is feasible (e.g., for employing the geoid as a height reference surface). Nevertheless, the gravity potential of a best fitting level surface of MSL at a given point in time may be expressed by the (static) geoid potential W_0 (associated with a certain reference epoch) and a linear change with time in first approximation (e.g., completely corresponding to the ITRF station positions and velocities). Finally, a refined geoid definition must also include specifications regarding the treatment of the notable permanent tide effects (see Sect. 2.6). For further details on the definition and realization of the geoid as well as the W_0 aspect see Heck (2004) and Heck and Rummel (1990).

The numerical value for the geoid potential W_0 can in principle be deduced from the MSL spatial positions with respect to the (global) Earth-fixed reference system and a geopotential model such as EGM2008 (Pavlis et al. 2008), possibly supplemented by an oceanographic or geodetic model of the mean dynamic ocean topography; the (absolute) gravity potential W is derived for the MSL (or MSL minus MDOT) points from the geopotential model ($W = V + Z$; (26) and (31), presupposing that V is regular at infinity), and finally some averaging procedure is applied to reduce random effects. The MSL positions can be taken from satellite altimetry (available within the latitude band ±86°; see Andersen et al. 2010), providing directly the sea surface height (SSH), or from tide gauge and GNSS (Global Navigation Satellite System) observations (see Fig. 3). The first approach based on satel-

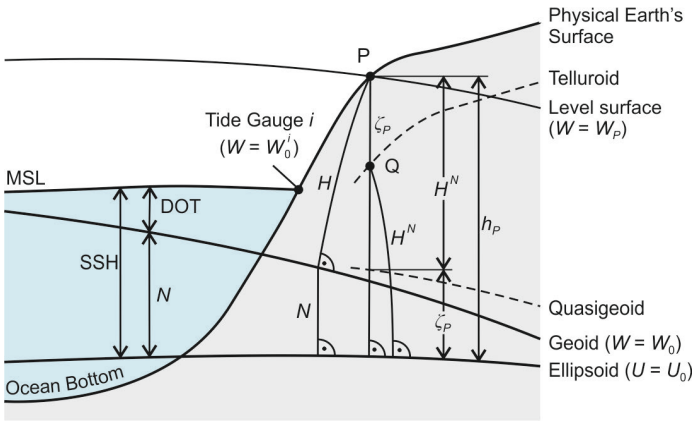

Fig. 3 Geoid, quasigeoid, heights, continental topography, mean sea level (MSL), and dynamic ocean topography (DOT)

lite altimetry gives access to almost the entire ocean domain and was applied by Bursa et al. (2002), while the latter approach is restricted to the existing tide gauge stations at the coasts. Furthermore, it is noted that a numerical value for W_0 (based on the satellite altimetry approach; Bursa et al. 2002) is provided in the IERS conventions (IERS 2010):

$$W_0 = 62{,}636{,}856.0\ \mathrm{m^2 s^{-2}} \quad . \tag{48}$$

However, Sanchez (2008) published W_0 values, differing by about 2–3 $\mathrm{m^2\,s^{-2}}$ from the above value (corresponds to a vertical distance of about 2–3 dm).

After defining the geoid by a (conventional) value W_0, it is still necessary to realize it, i.e., to find the position of the geoid in space, or equivalently to find for a given point P at the Earth's surface the vertical distance between P and the geoid, which corresponds to determining the potential difference $W_0 – W_P$ (see Fig. 3). The most promising procedure is to use GNSS stations or networks together with a global geopotential model (e.g., EGM2008), ideally supplemented by local gravity observations; based on the ITRF positions for the GNSS sites, the corresponding (absolute) gravity potential (W_P) can be computed (from the global model, possibly plus local gravity data), yielding then the potential difference $W_0 – W_P$ and hence the position of the geoid. Another option for realizing the geoid is to use tide gauge stations (or connected leveling stations) together with a DOT model (see Fig. 3). Naturally, several stations should be employed in either approach to average out random effects.

The definition of a world height system and the W_0 topic have been discussed for more than 25 years; within the International Association of Geodesy (IAG), this subject has been treated recently within the Inter-Commission Project 1.2, Vertical Reference Frames (Ihde 2009) and is now continued within the GGOS (Global

Geodetic Observing System) project. Corresponding to the IERS approach, most likely, there will be an ideal "vertical reference system" (VRS) with corresponding conventions (including a conventional W_0 value), and a realization, the "vertical reference frame" (VRF). In this context, Heck (2004) emphasizes that the absolute gravity potential (including W_0) is dependent on the assumption of regularity at infinity, see (19) and (31), and that the numerical value of the absolute potential W_0 is not needed at all in practice, as only potential differences are relevant for the determination and connection of vertical reference systems. Further details on the concepts for a world height system and the unification of national systems can be found, e.g., in Rapp (1983a, 1995), Rummel and Teunissen (1988), Heck and Rummel (1990), Rapp and Balasubramania (1992), Heck (2004), Ihde and Sanchez (2005), and Ihde (2009).

Historically, height systems (vertical datums) were related to mean sea level (MSL) through one or more tide gauge stations (the introduction of more than one tide gauge may lead to additional network distortions). Therefore, due to the existence of the dynamic ocean topography (DOT), these systems have different reference surfaces ($W = W_0^i$), implying inconsistencies up to a level of about ±2 m; examples of this kind can be found in Rapp and Balasubramania (1992) and Ihde and Sanchez (2005). The existing height systems are almost exclusively based on geometric leveling (also called spirit leveling). Geometric leveling is a quasi-differential technique, providing height differences δn (backsight minus foresight reading) with respect to the local astronomical system (see Fig. 1). Over longer distances, the non-parallelism of the level surfaces cannot be neglected, as it results in a path dependence of the results. This problem can be overcome by introducing potential differences, which are path independent because the gravity field is conservative (see Sects. 2.2 and 2.3). With

$$dW = \frac{\partial W}{\partial x}dx + \frac{\partial W}{\partial y}dy + \frac{\partial W}{\partial z}dz = \operatorname{grad} W \,\mathbf{ds} = \mathbf{g}\,\mathbf{ds} = -g\,dn\,, \tag{49}$$

dn being the distance along the outer normal of the level surface (zenith), the geopotential number C is defined as

$$C = W_0 - W_P = -\int_{P_0}^{P} dW = \int_{P_0}^{P} g\,dn\,, \tag{50}$$

where P_0 is an arbitrary point on the geoid (height reference surface) and P is a point on the Earth's surface. Thus, in addition to the leveling results (dn), gravity observations (g) are also needed along the path between P_0 and P (with regard to the required spacing and accuracy of the gravity points, see Torge 2001). Historically, the geopotential numbers were referred to local reference surfaces (W_0^i), but henceforth no distinction is made between W_0^i (local reference surface) and W_0 (geoid).

The geopotential numbers are ideal quantities for describing the direction of water flow, i.e., water flows from points with higher geopotential numbers C to points with lower values. However, the geopotential numbers have the unit $m^2\ s^{-2}$ (or $10\ m^2\ s^{-2} = 1$ kGal m = 1 gpu), and are thus somewhat inconvenient in disciplines like civil engineering, etc. Therefore, a conversion to metric heights is desirable, which can be achieved by dividing the C values by an appropriate gravity value. Widely used are the orthometric heights (e.g., U.S.A., Canada, Austria, and Switzerland) and normal heights (e.g., Germany, and many other European countries), which also play an important role in gravity field modeling due to the strong height dependence of various gravity field quantities (Sect. 3).

The orthometric height H is defined as the distance between the surface point P and the geoid, measured along the curved plumb line (see Fig. 3), which explains the common understanding as "height above sea level" (Torge 2001). The orthometric height can be derived from (50) by expanding the right side by H and integrating along the plumb line from the geoid to the surface point P:

$$H = \frac{C}{\overline{g}} \quad , \quad \overline{g} = \frac{1}{H}\int_0^H g\, dH \quad , \tag{51}$$

where $\overline{g}$ is the mean gravity along the plumb line (inside the Earth). As $\overline{g}$ cannot be observed directly (besides some stations with borehole gravity data; Strange 1982), hypotheses about the interior gravity field are necessary, which is one of the main drawbacks of the orthometric heights. Assuming a constant density of the topographic masses ($2670\ kg\ m^{-3}$) as well as a flat topography (so-called Poincaré-Prey reduction) leads to

$$\overline{g}_{[ms^{-2}]} = g_{P\,[ms^{-2}]} + 0.424\times10^{-6}\, H_{[m]} \, , \tag{52}$$

where g_P is the gravity value at the surface point P. The heights based on the mean gravity estimate (52) are denoted as Helmert-orthometric heights H^H (they are used, e.g., for the North American Vertical Datum, NAVD88; Zilkoski et al. 1995). For a discussion on refined procedures for the computation of $\overline{g}$, see Marti and Schlatter (2001), Flury and Rummel (2009), or Sjöberg (2010). Lastly, it is noted that points with equal orthometric heights are normally associated with slightly different level surfaces, which is due to the non-parallelism of the level surfaces.

In order to avoid the hypotheses about the Earth's interior gravity field, the normal heights H^N were introduced by Molodensky (e.g., Molodenskii et al. 1962). The normal height is defined as

$$H^N = \frac{C}{\overline{\gamma}} \quad , \quad \overline{\gamma} = \frac{1}{H^N}\int_0^{H^N} \gamma\, dH^N \quad , \tag{53}$$

where $\bar{\gamma}$ is a mean normal gravity value along the normal plumb line, and γ is the magnitude of the normal gravity vector (for further details see next section). Consequently, the normal height H^N is measured along the slightly curved normal plumb line (Heiskanen and Moritz 1967, Torge 2001); it is in the first instance defined as the elevation of the telluroid above the ellipsoid, but can also be considered as the elevation of the surface point P above the quasigeoid (for details see Sect. 3.2 and Fig. 3). The quasigeoid is not a level surface and has no physical interpretation. Hence, the concept of the normal height and quasigeoid is less illustrative than that of the orthometric height and geoid, respectively, but it has the significant advantage that it is exclusively based on quantities of the Earth's exterior gravity field, avoiding any hypotheses about the interior field. Furthermore, it is noted that Heck (2003) defines the normal height in a conceptually different way as the ellipsoidal height (measured along the straight ellipsoidal normal) of the telluroid; in this case, (53) has to be adapted by computing the corresponding mean normal gravity value along the ellipsoidal normal, using the normal gravity component in the direction of the ellipsoidal normal instead of the absolute value of normal gravity itself. However, due the small length difference between the ellipsoidal normal and the normal plumb line (see below), the concept from Heck (2003) and the classical formulation can be considered as equivalent for all practical applications.

Another option is the so-called dynamic height H^{dyn}, which is defined as

$$H^{dyn} = \frac{C}{\gamma_0^{45}} \ , \tag{54}$$

where γ_0^{45} is a constant normal gravity value, usually at the ellipsoid surface at 45° latitude. As the dynamic heights differ from the geopotential numbers only by a constant factor, points with the same H^{dyn} are located on the same level surface. As the dynamic heights have no geometric interpretation, and because the corrections to the raw leveling are quite large, they are not very widely used in practice.

Historically, when no gravity values were available for the computation of the geopotential numbers C, normal gravity values were used in some cases, resulting in the so-called normal-orthometric heights H^{NO} (e.g., still in use in Australia, Featherstone et al. 2011, or employed formerly in Germany, Heck 2003); these heights can be regarded as an approximation to the normal heights (Wolf 1974), but have the significant disadvantage of being path-dependent, in contrast to the above defined heights H, H^N, and H^{dyn}. Therefore, the H^{NO} are unsuitable for a modern height system.

It is also worth mentioning that the raw leveling results along lines (Δn) can be converted directly into corresponding height differences (ΔH, ΔH^N, ΔH^{dyn}) by the orthometric, normal, and dynamic corrections, respectively (Torge 2001, Heck 2003). Moreover, although the precision of geometric leveling is rather high (standard deviation for a 1-km traverse about 0.2–1.0 mm), it is important to keep

in mind, that geometric leveling is a differential technique and hence susceptible to systematic errors; examples are the differences between the second and third geodetic leveling in Great Britain (about 0.2 m in north–south direction over about 1000 km distance; Kelsey 1972), corresponding differences between the old and new leveling in France (about 0.25 m from the Mediterranean Sea to the North Sea, also mainly in north–south direction, distance about 900 km; Rebischung et al. 2008), as well as inconsistencies of more than 1 m across Canada and the U.S.A. (differences between different levelings and with respect to an accurate geoid; Véronneau et al. 2006 and Smith et al. 2010). Regarding Canada and the U.S.A., this led to the decision to abandon geometric leveling completely and to use GNSS techniques together with a so-called "geoid based vertical datum," which shall be introduced by 2013 (Canada) and 2021 (U.S.A.), respectively (Smith et al. 2010).

In recent years, some authors (e.g., Steinberg and Papo 1998; Kumar 2005) became proponents of purely (geometric) ellipsoidal height systems, which neglect the effect of gravity. However, these are considered as unsuitable for any application involving fluid flow, among others (Vaníček 1998). However, the approach of using the GNSS technique and a geoid based vertical datum, as initiated in Canada and the U.S.A., appears to be a good alternative to avoid the time-consuming and expensive geometric leveling, especially in view of the now possible geoid and quasigeoid accuracies (see Sect. 4).

The geoid and quasigeoid serve as the zero height surfaces (vertical datum) for the orthometric and normal heights, respectively. With regard to the ellipsoidal heights h (from GNSS observations), the following relation holds:

$$h = H + N = H^N + \zeta \,, \tag{55}$$

where N is the geoid height or geoid undulation, and ζ is the quasigeoid height or height anomaly (see also Fig. 3). The above equation neglects that in the strict sense the relevant quantities are measured along slightly different lines in space. The ellipsoidal height (h) of a point in space is measured along the straight ellipsoidal normal, while the corresponding normal height (H^N) is measured along the slightly curved normal plumb line (see Fig. 3); the length difference between both paths can be estimated from the curvature of the normal plumb line, yielding less than 10^{-7} m for a point 10 km above the ellipsoid, which can be safely neglected. For the orthometric heights, the corresponding length difference can be roughly estimated by means of the deflection of the vertical (the angle between the actual plumb line and the ellipsoidal normal; see Fig. 3), resulting in an effect of about 0.4 mm for a station height of 10 km and an extreme deflection of the vertical of 1'. Hence, (55) is accurate at the millimeter level for all practical cases; another possibility would be to work with the corresponding potentials instead of the heights.

A transformation between the orthometric and normal heights, or geoid and quasigeoid heights, is possible by combining (51), (53), and (55), giving

$$H^N - H = N - \zeta = \frac{\overline{g} - \overline{\gamma}}{\overline{\gamma}} H = \frac{\overline{g} - \overline{\gamma}}{\overline{g}} H^N \approx \frac{\Delta g_B}{\overline{\gamma}} H \,. \tag{56}$$

The difference H^N–H or N–ζ is mainly depending on the station height as well as $\overline{g} - \overline{\gamma}$, which is approximately the (simple) Bouguer anomaly Δg_B (Heiskanen and Moritz 1967; Torge 2001). In this context, it is noted that the Bouguer approximation in (56) is virtually exact in connection with the Helmert-orthometric heights (Forsberg and Tscherning 1997). The magnitude of the difference H^N–H or N–ζ can reach several centimeters to about 1 dm in low mountain ranges, about 3–5 dm (or even more) in the high mountains such as the European Alps or Rocky Mountains, and about 3 m in the Himalayan Mountains (Rapp 1997; Marti and Schlatter 2001; Tenzer et al. 2005; Flury and Rummel 2009). On the oceans, the geoid and quasigeoid practically coincide (Torge 2001), as the effect of the DOT is only marginal.

Finally, regarding the orthometric heights, the various procedures in use for the computation of the mean gravity value $\overline{g}$ (e.g., (52) or more sophisticated methods) may lead to substantially different results (e.g., Marti and Schlatter 2001; Flury and Rummel 2009); therefore, it is essential to ensure that the heights H and the corresponding geoid undulations N are consistent such that (55) is satisfied.

2.5 The Normal Gravity Field

The normal gravity field is introduced as an approximation of the Earth's gravity field. On the one hand it should provide a reasonably good agreement with the real field, since it is used for the linearization of the observation equations, and on the other hand it should be simple to compute, as well as useful for other disciplines (Torge 2001). Based on these considerations, the level ellipsoid (or so-called Somigliana-Pizetti normal field) is almost exclusively used; another argument may also be the utilization of an ellipsoid for station coordinates (see Sect. 2.1). However, today, with the availability of very accurate satellite gravity field models (e.g., from the GRACE and GOCE missions), it is also worth considering the employment of a complete spherical harmonic expansion up to some maximum degree n_{max}.

Corresponding to the gravity potential W, the normal gravity potential U is introduced as the sum of the normal gravitational potential V^N and the normal centrifugal potential Z^N:

$$U = V^N + Z^N \,. \tag{57}$$

The associated normal gravity vector is given by

$$\boldsymbol{\gamma} = \operatorname{grad} U \,. \tag{58}$$

The direction of $\boldsymbol{\gamma}$ is the direction of the normal plumb line, the magnitude γ is the normal gravity (intensity).

The normal gravity field of the level ellipsoid solely depends on four parameters. These can be two parameters describing the size and shape of the ellipsoid (for example, the semimajor axis, a_N, and flattening, f_N), the Earth's rotation rate, ω_N, and the total mass of the Earth, M_N. Numerical values for such parameters are recommended from time to time by the IUGG, IAG, etc. The latest set of constants was recommended by the IUGG and IAG in 1979 at the XVIIth General Assembly of the IUGG in Canberra (e.g., Moritz 2000), known as the Geodetic Reference System 1980 (GRS80), with the four defining parameters being a_N, J_2^N, ω_N, and GM_N. An updated (current best) set of parameters is also provided in IERS (2010). Besides GRS80, the WGS84 level ellipsoid is frequently used (NIMA 1997). It is defined by the geometrical parameters a_N and f_N and the physical parameters GM_N and ω_N; apart from the significantly different GM_N values of GRS80 and WGS84, the a_N and ω_N parameters are identical, while the flattening parameters show only marginal differences (corresponding to 3×10^{-5} m with respect to the semiminor axis).

All parameters related to the normal gravity field of the level ellipsoid can be computed by closed formulas based on ellipsoidal harmonics (Heiskanen and Moritz 1967). However, the normal gravitational potential of the level ellipsoid can also be expanded in a rapidly converging spherical harmonic series; due to the symmetry with respect to the rotational axis as well as the equator, only the even zonal coefficients are non-zero, and an expansion up to degree 10 is fully sufficient. The spherical harmonic series approach, proposed by Tscherning (1976a), is well suited for the computation of U and its first and second derivatives, gives accurate results everywhere in space (including satellite positions), is easy to use in connection with high-degree Earth gravity field models such as EGM2008, and can also be generalized to more complicated normal gravity fields, e.g., based on a complete spherical harmonic gravitational model up to some degree n_{max}.

Considering a complete spherical harmonic expansion of the normal gravitational potential (up to degree n_{max}) as well as the centrifugal potential (with $p = r\sin\theta$) according to (26) and (31), respectively, yields

$$U(\theta,\lambda,r) = V^N + Z^N = \sum_{n=0}^{n_{max}} \left(\frac{a_N}{r}\right)^{n+1} \sum_{m=-n}^{n} \overline{V}_{nm}^N \overline{Y}_{nm}(\theta,\lambda) + \frac{\omega_N^2}{2} \mathrm{r}^2 \sin^2\theta \quad , \tag{59}$$

with

$$\overline{V}_{nm}^N = \frac{GM_N}{a_N} \begin{cases} \overline{C}_{nm}^N & \text{for } m \geq 0 \\ \overline{S}_{nm}^N & \text{for } m < 0 \end{cases} . \tag{60}$$

The first and second derivatives of U with respect to the spherical coordinates θ, λ, r can be derived easily from the above equation (require the derivatives of the

associated Legendre functions), which can then be used to compute the derivatives with respect to the local spherical system (x^s, y^s, z^s) in analogy to (41) and (45). Regarding the normal gravity vector, the transformation to the Earth-fixed system yields

$$\boldsymbol{\gamma} = \left[\mathbf{U}_{\mathbf{X}}\right] = \mathbf{A}_{\mathbf{xs}}\left[\mathbf{U}_{\mathbf{xs}}\right] = -\gamma \begin{pmatrix} \cos\varphi^{\gamma}\cos\lambda^{\gamma} \\ \cos\varphi^{\gamma}\sin\lambda^{\gamma} \\ \sin\varphi^{\gamma} \end{pmatrix}, \tag{61}$$

where $\varphi^{\gamma}, \lambda^{\gamma}$, describing the direction of the normal gravity vector (in correspondence with (43)), as well as γ can be computed by applying (44) accordingly. This procedure is exact, involves no approximations, and works everywhere in space. In the case of the level ellipsoid, φ^{γ}, λ^{γ}, are identical with the normal latitude and longitude, φ^N, λ^N, with $\lambda = \lambda^N$ (the normal plumb line of the level ellipsoid is only slightly curved in the meridian plane).

The first and second derivatives of U can be expressed as well with respect to a local coordinate system oriented at the normal gravity vector. Corresponding to the local ellipsoidal system (see Sect. 2.1), a Cartesian system (x^{γ}, y^{γ}, z^{γ}) is introduced, where the z^{γ}-axis points in the opposite direction to that of $\boldsymbol{\gamma}$, and the axes x^{γ}, y^{γ} are pointing north and east, respectively. The local system (x^{γ}, y^{γ}, z^{γ}) and the local ellipsoidal system (x^e, y^e, z^e) deviate by the curvature of the normal plumb line. In the local system (x^{γ}, y^{γ}, z^{γ}), the horizontal components (x^{γ}, y^{γ}) of the normal gravity vector are zero and the vertical component (z^{γ}) is equal to the negative value of γ. With the transformation matrix $\mathbf{A}_{\mathbf{x}\gamma} = \mathbf{A}_{\mathbf{x}\gamma}(\varphi^{\gamma}, \lambda^{\gamma})$, defined analog to (7), the second derivatives of U with respect to the local system (x^{γ}, y^{γ}, z^{γ}) are given by (Tscherning 1976a)

$$\left[\mathbf{U}_{\mathbf{x}^{\gamma}\mathbf{x}^{\gamma}}\right] = (\mathbf{A}_{\mathbf{x}\gamma})^{\mathrm{T}}\,\mathbf{A}_{\mathbf{x}^{\mathbf{s}}}\left[\mathbf{U}_{\mathbf{x}^{\mathbf{s}}\mathbf{x}^{\mathbf{s}}}\right](\mathbf{A}_{\mathbf{x}^{\mathbf{s}}})^{\mathrm{T}}\,\mathbf{A}_{\mathbf{x}\gamma}\ . \tag{62}$$

Equations (61) and (62) were programmed and tested for the level ellipsoid (with $n_{max} = 10$); the agreement with the results from closed formulas on the basis of ellipsoidal harmonics (Heiskanen and Moritz 1967) was better than 10^{-5} m^2 s^{-2} for the potential U and 10^{-11} m s^{-2} in γ (everywhere in space; the results are based on 8-byte variables and the remaining differences are mainly due to rounding errors, etc.). Regarding the level ellipsoid, further testing is possible, as the components of the matrix (62) must fulfil the following conditions (Tscherning 1976a):

$$\left.\begin{aligned} U_{x^{\gamma}y^{\gamma}} &= U_{y^{\gamma}z^{\gamma}} = 0 \\ U_{x^{\gamma}x^{\gamma}} + U_{y^{\gamma}y^{\gamma}} + U_{z^{\gamma}z^{\gamma}} - 2\omega_N^2 &= 0 \end{aligned}\right\} \text{ everywhere in space,}$$

$$\left.\begin{aligned} U_{x^{\gamma}x^{\gamma}} &= -\frac{\gamma}{M}, \quad U_{y^{\gamma}y^{\gamma}} = -\frac{\gamma}{N} \end{aligned}\right\} \text{ at the ellipsoid surface.} \tag{63}$$

The first set of conditions results from the fact the plumb lines of the level ellipsoid are only curved in the meridian plane, the second condition is based on the generalized Laplace equation, and third, at the surface of the level ellipsoid, the second derivatives of U in the direction of x^y, y^y are associated with the principal radii of curvature of the ellipsoid (M: meridian; N: prime vertical).

Traditionally, near the Earth's surface, the normal gravity of the level ellipsoid is computed from a Taylor series expansion with respect to the ellipsoidal height:

$$\gamma = \gamma_0 + \left(\frac{\partial\gamma}{\partial h}\right)_0 h + \frac{1}{2}\left(\frac{\partial^2\gamma}{\partial h^2}\right)_0 h^2 + \frac{1}{6}\left(\frac{\partial^3\gamma}{\partial h^3}\right)_0 h^3 + \frac{1}{24}\left(\frac{\partial^4\gamma}{\partial h^4}\right)_0 h^4 + \ldots \quad . \tag{64}$$

The normal gravity at the level ellipsoid is given by the (rigorous) formula of Somigliana (e.g., Torge 2001):

$$\gamma_0 = \frac{a_N\,\gamma_a \cos^2\varphi + b_N\,\gamma_b \sin^2\varphi}{\sqrt{a_N^2\cos^2\varphi + b_N^2\sin^2\varphi}} = \gamma_a \frac{1 + k\sin^2\varphi}{\sqrt{1 - e_N^2\sin^2\varphi}} \quad \text{with} \quad k = \frac{b_N\,\gamma_b}{a_N\,\gamma_a} - 1\,, \tag{65}$$

where a_N, b_N are the semimajor and semiminor axes of the ellipsoid, e_N is the first eccentricity, and γ_a, γ_b are the normal gravity values at the equator and pole, respectively. The computation of the partial derivatives in (64) was investigated in detail by Wenzel (1989), suggesting that the first derivative be computed from the Bruns equation and the higher derivatives be taken from a spherical harmonic expansion of U based on J_2^N only. This procedure can be slightly improved by also considering J_4^N in the second derivative term, yielding

$$\begin{aligned}
\left(\frac{\partial\gamma}{\partial h}\right)_0 &= -\gamma_0\left(\frac{1}{M} + \frac{1}{N}\right) - 2\omega_N^2 \\
&= -\frac{\gamma_0}{a_N\,(1 - e_N^2)}(1 - e_N^2\sin^2\varphi)^{1/2}(2 - e_N^2(1 + \sin^2\varphi)) - 2\omega_N^2\,, \\
\left(\frac{\partial^2\gamma}{\partial h^2}\right)_0 &= \frac{GM_N}{r^4}\left(6 - 60\left(\frac{a_N}{r}\right)^2 J_2^N P_2(\cos\theta) - 210\left(\frac{a_N}{r}\right)^4 J_4^N P_4(\cos\theta)\right), \\
\left(\frac{\partial^3\gamma}{\partial h^3}\right)_0 &= \frac{GM_N}{r^5}\left(-24 + 360\left(\frac{a_N}{r}\right)^2 J_2^N P_2(\cos\theta)\right), \\
\left(\frac{\partial^4\gamma}{\partial h^4}\right)_0 &= 120\frac{GM_N}{r^6}\,.
\end{aligned} \tag{66}$$

Equations (64)–(66) were also programmed, and the results were compared with those from closed formulas based on ellipsoidal harmonics; the differences were always below 2×10^{-9} m s^{-2} (0.2 μGal) for stations up to h = 10 km, with the fourth order term being insignificant (max. 3×10^{-10} m s^{-2} = 0.03 μGal). Furthermore, if the derivative terms in (64) are computed by expansions with respect to the flattening

f_N (see Heiskanen and Moritz 1967), terms up to the second order of f_N, $o(f_N^2)$, are needed for the first vertical derivative of γ (or better apply the Bruns equation, which is rigorous), terms up to $o(f_N)$ should be used for the second derivative, while the third derivative can be based on a spherical approximation, yielding an accuracy of about 1×10^{-8} m s^{-2} = 1 μGal. On the other hand, formulas considering only terms up to $o(f_N)$ in the first vertical derivative of γ and a spherical approximation of the second derivative (as found frequently in textbooks, e.g., Heiskanen and Moritz 1967; Torge 2001) may result in errors with a magnitude of about 1×10^{-6} m s^{-2} = 100 μGal (again for heights up to 10 km), which is insufficient.

Finally, the Taylor series (64) opens a simple way to compute the mean normal gravity value

$$\bar{\gamma} = \frac{1}{h}\int_0^h \gamma\, dh = \gamma_0 + \left(\frac{\partial\gamma}{\partial h}\right)_0 \frac{h}{2} + \left(\frac{\partial^2\gamma}{\partial h^2}\right)_0 \frac{h^2}{6} + \left(\frac{\partial^3\gamma}{\partial h^3}\right)_0 \frac{h^3}{24} + \left(\frac{\partial^4\gamma}{\partial h^4}\right)_0 \frac{h^4}{120} + \ldots \quad , \qquad (67)$$

as needed in connection with normal heights.

2.6 Temporal Gravity Field Variations and the Atmosphere

The Earth's body and gravity field undergo changes at different temporal and spatial scales, which has been described in detail, e.g., by Torge (1989). The acquisition, analysis, description, and interpretation of such changes are treated in the field of geodynamics. The largest temporal variations are due to tidal effects (mainly moon and sun, but also planets), leading to (mostly) periodical deformations of the Earth's crust with maximum amplitudes of about 30 cm and corresponding gravity changes with amplitudes up to about 200 μGal (roughly 10^{-7} g); for details see Torge (1989, 2001) and Timmen (2010). Generally, gravimetric measurements are reduced for the effect of tides, atmospheric mass redistributions (mainly by simple admittance functions), and Earth rotation variations (Torge et al. 1987; Torge 1989; Timmen 2010). As a matter of principle, the Earth's gravity field varies with time due to mass redistributions in the geosphere, atmosphere, hydrosphere (including the cryosphere), and biosphere; selected examples related to hydrology (ground water) and postglacial rebound (Fennoscandia) are presented in Timmen (2010). According to Torge (2001), gravity changes due to mass redistributions do not exceed the order of 10^{-9} to 10^{-8} g.

Since 2002, the US–German GRACE satellite mission is providing the Earth's time-variable and static gravity field globally with unprecedented temporal and spatial resolution, which has greatly improved the understanding of mass redistributions in the atmosphere, oceans, water reservoirs, and cryosphere. An overview on the GRACE mission and early results are given in Tapley et al. (2004a, b), while reviews of recent GRACE results can be found in Wahr (2009) as well as Cazenave and Chen (2010). The GRACE results are mainly provided as monthly global spherical harmonic models, which can then be employed for studying peri-

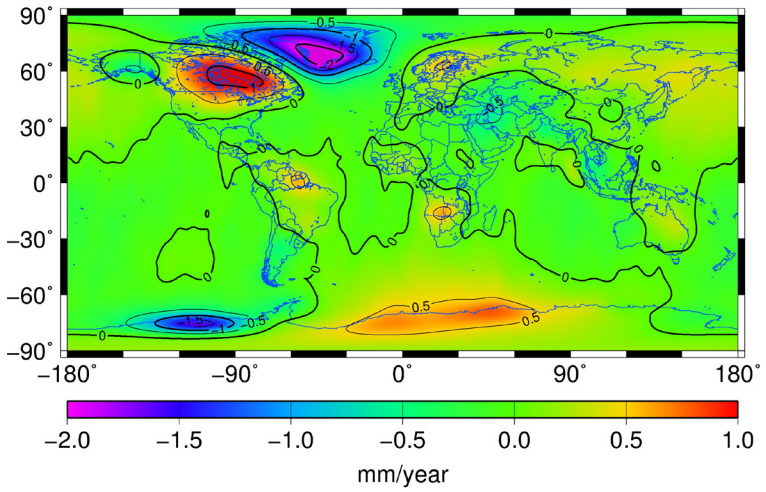

Fig. 4 Linear (secular) geoid trends derived from a sequence of 103 monthly GRACE solutions (Release 04) from GFZ, covering the time span August 2002 to September 2011, after Gaussian filtering with a radius of 400 km

odic and secular variations of the Earth's gravity field; for this purpose, the GRACE models are usually restricted to a ground resolution of about 300–400 km, because the GRACE errors become larger with increasing resolution (e.g., Tapley et al. 2004a; Wahr 2009). The largest-amplitude signals are related to water storage variability on land (Wahr 2009); they have mainly annual periods with amplitudes up to about 10 mm and 10 μGal in terms of geoid and gravity, respectively. Figure 4 shows the linear (secular) trend of the geoid as derived from a sequence of 103 monthly GRACE solutions (Release 04) from GFZ (Helmholtz-Centre Potsdam – German Research Centre for Geosciences, GFZ); the GRACE data, covering the time span August 2002 to September 2011, were smoothed by applying a Gaussian filter with a radius of 400 km. The largest geoid trends are related to the ice losses in Greenland (–2 mm/year), Alaska, and Antarctica, as well as water storage changes in the Amazon region, but also the post glacial rebound signals over North America (about +1 mm/year) and Fennoscandia (about 0.5 mm/year) are clearly visible.

In the following it is assumed that temporal variations of the Earth's body and gravity field have been taken into account by appropriate reductions or have been averaged out over sufficiently long time periods (this includes the station coordinates as realized, e.g., by the ITRF solutions). In this context, the largest variations are due to tidal effects, which can be reduced relatively easily with sufficient accuracy (e.g., Timmen 2010). On the other hand, effects like ground water changes or postglacial rebound are more difficult to handle (e.g., Timmen 2010). In general, the reduction of all relevant data sets to a certain epoch is an appropriate solution

to reach a (quasi) static state; considering the postglacial rebound signal in Fennoscandia as an example, this can be done by means of models (e.g., the existing uplift model of Ågren and Svensson 2007) or observation time series (e.g., from GRACE).

The tidal attraction acts in a direct and indirect way. The direct (or gravitational) attraction deforms the elastic Earth, which causes an (additional) indirect change of the gravitational potential (deformation potential). While the direct effects can be computed easily by astronomical tidal theory, the calculation of the indirect effects requires knowledge about the Earth's elastic parameters (primarily Love and Shida numbers). Regarding the tidal reductions of geodetic parameters (e.g., potential, gravity, station coordinates, physical heights), both the direct and indirect effects contain time-dependent (periodic) parts as well as time-independent (permanent, zero frequency) parts; the computation of the latter portion of the indirect (deformation) effects requires the fluid (secular) Love numbers, which differ substantially from the standard (second degree) elastic values and are unobservable (cannot be determined experimentally). In this context, a long-lasting and still ongoing discussion relates to the handling of the notable permanent parts of the tidal potential (see below), e.g., documented by the publication of Ekman (1996) with the title "the permanent problem of the permanent tide." A comprehensive treatise of the permanent tide subject is given in Ekman (1989a, b), and further reviews can be found, e.g., in Rapp et al. (1991), Ekman (1996), Poutanen et al. (1996), Heck (2004), or Mäkinen and Ihde (2009). As a consequence, based on the report from Rapp (1983b), the International Association of Geodesy (IAG) adopted at the IAG/IUGG General Assembly in Hamburg, 1983, the resolution no. 16, stating that "for the uniform treatment of tidal corrections to various geodetic quantities such as gravity and station positions, the indirect effect due to the permanent yielding of the Earth be not removed" (IAG 1984).

Altogether, the following cases are to be distinguished:

- The "zero tide system" is the one recommended by IAG. In this system, the direct effects are removed completely, but the indirect deformation effects associated with the permanent tidal deformation are retained. This implies that the masses of the moon, sun, and planets are shifted to infinity, while the permanent deformation effects are left untouched, avoiding the problem with the fluid Love numbers. Moreover, the zero tide system is also suitable for solving boundary value problems (BVPs) in physical geodesy, requiring that no masses exist external to the boundary surface (harmonicity condition; see Sect. 3).
- In the "mean tide system," only the periodic tidal effects are removed, but the permanent parts (both direct and indirect) are retained. Thus, the mean values reflect the mean situation (shape) in the presence of the moon, sun, and planets, which is the natural system in connection with oceanography and satellite altimetry observations as well as station positions, noting that the mean and zero crust (station positions) are identical (both include the permanent deformation effects). On the other hand, the mean tide system has the disadvantage that it is

not free of external masses (i.e., unsuitable for solving BVPs in physical geodesy); to overcome this problem, Zeman (1987) suggested modifying the normal gravity potential.

- The "tide-free system" (or non-tidal system) is aiming at the removal of all tidal effects (periodic and permanent direct and indirect effects). In this case, the required (unobservable) fluid Love numbers have to be replaced by conventional values; therefore, this system is also denoted sometimes as "conventionally tide-free."

Further discussions on advantages and disadvantages of each of the three concepts can be found in the references mentioned above. IAG has recommended the zero tide system, oceanographic applications may require the mean tide system, while the positioning domain (including the ITRF solutions; see IERS 2010) mainly uses the non-tidal system, thus not following the IAG recommendations.

Therefore, since different applications are usually associated with particular tidal systems, transformation formulas are needed for the conversion from one system to another. Considering only the dominating degree two terms of the tidal potential, each of the three tidal systems is directly associated with a corresponding $\overline{C}_{20}$ potential coefficient. Following IERS (2010), a quantity

$$\Delta\overline{C}_{20}^{perm} = A_0\, H_0\, k_{20} = -1.39141\times10^{-8}\, k_{20} \tag{68}$$

is introduced; then with the potential Love number k_{20}, the following relations hold:

$$\overline{C}_{20}^{nt} = \overline{C}_{20}^{zt} - \Delta\overline{C}_{20}^{perm}\,, \tag{69}$$

$$\overline{C}_{20}^{mt} = \overline{C}_{20}^{zt} + \Delta\overline{C}_{20}^{perm} \Big/ k_{20}\,, \tag{70}$$

where the superscripts *nt*, *zt*, and *mt* stand for non-tidal (tide-free), zero tide, and mean tide system, respectively. Starting with the zero tide coefficient $\overline{C}_{20}^{zt} = -484.16948\times10^{-6}$ (epoch J2000.0) and $k_{20} = 0.29525$ from IERS (2010), the above equations give the non-tidal and mean tide coefficients $\overline{C}_{20}^{nt} = -484.16537\times10^{-6}$ and $\overline{C}_{20}^{mt} = -484.18339\times10^{-6}$, respectively. Corresponding transformation formulas for geoid undulations can be obtained on the basis of the above coefficients and the spherical harmonic expansion (26) with $r = a$, $\varphi \approx 90° - \theta$, and a mean (normal) gravity value:

$$N_{[m]}^{nt} = N_{[m]}^{zt} + 0.0879_{[m]} \sin^2\varphi - 0.0293_{[m]}\,, \tag{71}$$

$$N_{[m]}^{mt} = N_{[m]}^{zt} - 0.2977_{[m]} \sin^2\varphi + 0.0992_{[m]}\,. \tag{72}$$

Further transformation formulas for other quantities such as gravity and heights can be found, e.g., in Ekman (1989a), or Mäkinen and Ihde (2009); the derivation of refined transformation formulas is described in Ihde et al. (2008).

So far, the atmospheric masses have been neglected, causing a small but not insignificant gravitational effect. As in conjunction with harmonic functions it is generally presupposed that there are no masses exterior to the Earth's surface, the effect of the atmosphere must be removed computationally. Because of the low density of the atmosphere ($\rho_A \approx 1$ kg/m^3), varying primarily with elevation, a simple normal atmosphere model can be used to calculate the effect.

To a first approximation, the atmospheric effect can be computed by using spherical approximations and a radially layered spherical density model, ignoring the topography. Then for a point P with radius r above the reference sphere (with radius R) the gravitational attraction can be split into an exterior and interior part, associated with the masses below and above the point P, respectively. Now it is well known from potential theory that the potential inside a spherical shell is constant, and thus the attraction is zero. Since the exterior gravitational field of concentric homogeneous mass shells is equal to the effect of the entire mass being concentrated at the center of mass of the object, the effect of the atmosphere on gravity is given by

$$g^A = \frac{G\,m(r)}{r^2} \quad , \tag{73}$$

where $m(r)$ is the mass of all atmospheric layers below P. Introducing the total mass of the atmosphere, M_A, and $m(r) = M_A - M(r)$, yields

$$g^A = \frac{G\,M_A}{r^2} - \frac{G\,M(r)}{r^2} = \frac{G\,M_A}{r^2} - \delta g^A \quad , \tag{74}$$

where $M(r)$ is the atmospheric mass above P. Accordingly, the gravitational potential of the atmosphere is given by

$$V^A = \frac{G\,M_A}{r} + G\int_r^\infty \frac{G\,M(r)}{r^2}dr = \frac{G\,M_A}{r} - \delta V^A \quad , \tag{75}$$

$$M(r) = 4\pi\int_r^\infty \rho_A(r)\,r^2 dr \quad . \tag{76}$$

The respective first terms on the right side of (74) and (75) represent the effect of a point mass (M_A); they are included in the normal potential (GM_N includes the mass of the solid Earth and atmosphere). On the other hand, the second terms on the right side represent the non-harmonic contributions; they are denoted as the atmospheric gravity and potential corrections δg^A and δV^A, respectively. The sign convention is here in accordance with IAG (1970), and Moritz (2000); the sign is defined such that the corrections have to be added to the observed quantities (i.e., the

non-harmonic atmospheric contribution is reduced); then after gravity field modeling, the correction terms may be subtracted again from the final results to be consistent with what is being observed within the atmosphere. The correction terms can be tabulated easily based on an atmospheric model; examples are the values recommended by IAG (1970), which are based on ellipsoidal density models suggested by Ecker and Mittermayer (1969), or those computed by Wenzel (1985), using spherical approximations. The potential effect, δV^A, has a maximum value of only about 0.06 m^2/s^2 (at the reference sphere with radius R), and is commonly neglected. The atmospheric gravity corrections, δg^A, can be approximated by the following formula derived by Wenzel (1985):

$$\delta g^A{}_{[\mathrm{mGal}]} = 0.874 - 9.9\times10^{-5} h_{[\mathrm{m}]} + 3.5625\times10^{-9} h^2_{[\mathrm{m}]} \ . \tag{77}$$

The above formula is based on spherical theory and applicable for heights up to about 8 km; the results differ by not more than 0.005 mGal from the values recommended by IAG (1970), considering ellipsoidal density models. Both quantities, the atmospheric gravity and potential corrections δg^A and δV^A, depend on the masses above a given station P, and hence go to zero for large radii (elevations); therefore, they need not be considered at satellite altitude. Further details on atmospheric effects can be found in Ecker and Mittermayer (1969), Rummel and Rapp (1976), Christodoulidis (1979), Moritz (1980), as well as Andersen et al. (1975), Andersen (1976), and Sjöberg and Nahavandchi (2000), also considering topographic information. The accuracy of the atmospheric potential based on the simple spherical model without topography may be estimated as about 0.1 m^2/s^2 (Christodoulidis 1979; Denker 1988). In the future, improvements of the atmospheric correction scheme may be necessary (see also Forsberg 2010), as implemented already in connection with the GRACE gravity field mission (Flechtner et al. 2010) or absolute gravimetry (Gitlein and Timmen 2006).

3 Gravity Field Modeling

3.1 Geodetic Boundary Value Problems

In mathematics, within the field of differential equations, a boundary value problem (BVP) is a differential equation together with a set of additional constraints, called the boundary conditions, which the solution to the BVP must satisfy. BVPs arise in several branches of physics, engineering, etc., in connection with any differential equation (e.g., Morse and Feshbach 1953). To be useful in applications, a BVP should be well-posed, i.e., a unique solution should exist with respect to the given input. Much theoretical work in the field of partial differential equations is devoted to proving that boundary value problems arising from scientific and engineering applications are in fact well-posed.

Potential theory may be defined as the study of potential functions related to conservative vector fields (or potential fields). With regard to gravitation, solutions of the Laplace and Poisson differential equations are sought (divergence-free and divergence-involving problems). Sometimes, potential theory is also defined exclusively as the study of harmonic functions, i.e., the solution of Laplace's equation. In this context, a BVP consists of finding a harmonic function V in the space outside of the closed (star-shaped) boundary surface, which fulfils the boundary conditions and is regular at infinity. Commonly, three types of BVPs are distinguished (Sigl 1985; Jekeli 2009):

- BVP of the first kind, also known as the Dirichlet problem. Solve for the potential function V in the exterior space, given its values on the boundary surface.
- BVP of the second kind, also known as the Neumann problem. Solve for V in the exterior space, given its normal derivatives on the boundary surface (derivatives in the direction of the surface normal).
- BVP of the third kind, also known as the mixed BVP or Robin problem. Solve for V in the exterior space, given a linear combination of V and its normal derivative on the boundary surface.

In addition, the category of oblique derivative problems can be introduced, related to the cases where the derivatives of the potential function are not given in the direction of the boundary surface normal. Furthermore, interior and exterior problems can be distinguished, related to the space interior and exterior to the boundary. However, in geodesy, the exterior BVPs are of prime importance.

Geodetic boundary value problems (GBVPs) may be considered as the combined determination of the Earth's figure and gravity field from geodetic observations (at the Earth's surface or its exterior). Besides the traditional terrestrial geodetic observations, such as potential (differences), gravity, and astronomical latitudes and longitudes, new types of boundary data become available from satellite techniques, etc., involving new types of GBVPs (e.g., mixed and overdetermined GBVPs). A comprehensive overview on GBVPs is given in Sansò (1995) as well as Heck (1997), where the latter publication specifically highlights that the primary unknown, to be solved in the framework of the GBVPs, is the exterior gravity potential W outside the boundary surface. In this connection, W can only be computed indirectly from the boundary data by solving a GBVP, while a direct computation is not possible, mainly due to insufficient knowledge about the Earth's density structures. However, once the potential function W is known, all relevant quantities can be derived from it (see Sect. 2.3). The basic assumptions in the following are that the Earth behaves like a rigid and non-deformable body, uniformly rotating about a body-fixed axis (Moritz 1980; Heck 1997); i.e., all time-variable effects have to be taken into account by appropriate reductions in order to reach a quasi-static state (e.g., by referring all quantities to a given epoch; see Sect. 2.6).

Depending on the type of boundary data as well as the type and number of unknown functions to be solved from geodetic observational data, several GBVP

formulations can be distinguished (Heck 1997). At first, a subdivision into fixed and free GBVPs is appropriate, involving the assumption of a known or unknown boundary surface, respectively. Hence, fixed GBVPs are always associated with a completely known boundary surface (e.g., fixed by coordinate vectors **X** derived from GNSS techniques), and therefore the only remaining unknown is the potential function W; this leads to the fixed gravimetric GBVP when employing gravity observations (provide the magnitude of the gravity vector) as the most important boundary data. On the other hand, regarding the free GBVPs, the information on the geometry of the boundary is either incomplete or missing entirely. When employing again gravity observations as boundary data, this results in Molodensky's boundary value problem (Molodenskii et al. 1962), i.e., the classical free gravimetric GBVP, which can be further subdivided into the vectorial free GBVP (astronomical variant of Molodensky's problem), where the position of the boundary is completely unknown (in total four unknowns; i.e., three coordinates in **X** and the potential W), and the scalar free GBVP (geodetic variant of Molodensky's problem), where the horizontal positions are known (e.g., gravity points with given ellipsoidal latitudes and longitudes), resulting in only two unknowns, one for the vertical coordinate (e.g., the ellipsoidal height) and a second one for the potential W (Heck 1997). The latter case can be considered as quite close to the hitherto applied geodetic practice, where, e.g., the horizontal coordinates of gravity stations were traditionally based on geodetic networks, mostly allowing a transformation to the Earth-fixed system with sufficient accuracy.

3.2 Linearization of the Boundary Conditions

The most important boundary data are gravity observations, carried out at (or near) the Earth's surface. Two essential cases can be distinguished with respect to the available station coordinates. The first case is related to the scalar-free GBVP and corresponds to the more traditional geodetic practice, where the vertical coordinates (physical heights) are mainly derived from geometric leveling, while the horizontal station coordinates (ellipsoidal latitudes and longitudes) are usually based on corresponding national horizontal control networks. In this context, it is assumed that the ellipsoidal coordinates are finally referred to the Earth-fixed system, either by adequate transformations from the national networks or directly by GNSS observations. Hence, in the scalar free GBVP, the horizontal coordinates are known, but the vertical spatial positions (ellipsoidal heights) of the observation sites (boundary) are unknown. The second case is related to the (scalar) fixed GBVP, where the geometry of the boundary is assumed to be completely known. This corresponds to the modern geodetic practice, where in many cases GNSS techniques are employed, giving directly the entire position vector **X** of all observation sites (boundary) with respect to the Earth-fixed system (either coordinates X, Y, Z or φ, λ, h). However, also with GNSS techniques, the vertical accuracy is

never as good as the horizontal accuracy, and, in addition, some effort is required to get an accurate connection to the ITRF.

The boundary conditions for various geodetic boundary value problem (GBVP) formulations are in general nonlinear. This means that the relevant observations (boundary data) depend in a nonlinear way on the unknown gravity potential function W; they can be considered as nonlinear functionals of W, see (44). As no mathematical tools exist for solving nonlinear GBVPs (Heck 1997), the boundary conditions (observation equations) must be linearized. For this purpose, a known reference potential must be introduced, and, in addition, a known reference surface has to be adopted in the case of the free GBVPs. Regarding the reference potential, traditionally the level ellipsoid is used, but today one of the highly accurate satellite models from the recent satellite missions GRACE and GOCE can also be employed. The question of the reference surface is related to the definition of telluroid; for details on different telluroid mappings (Molodensky, Hirvonen, isozenithal, Marussi, and gravimetric telluroid) see Heck (1986). With respect to both the reference potential and the reference surface, it is important that the approximate values are sufficiently close to the real situation, such that a one-step solution is sufficient, or a convergent iteration process can be constructed (e.g., Rummel 1988; Heck 1997).

In the first instance, the normal gravity field of the level ellipsoid is employed for approximating the gravity potential. Moreover, it is supposed that at least the horizontal positions (ellipsoidal latitudes and longitudes) and in the case of fixed GBVPs also the ellipsoidal heights, referring to the Earth-fixed system, are known for the observation sites; this is considered as realistic with respect to today's geodetic practice. In addition, without going into detail about different telluroid mappings (Grafarend 1978a; Heck 1986), the reference surface or telluroid is defined according to Molodensky (Heck 1986, 1997):

$$\varphi_Q = \varphi_P \,, \qquad \lambda_Q = \lambda_P \,, \qquad U_Q = U_0 - C = U_0 - (W_0 - W_P) \,. \tag{78}$$

The above equations associate each point P at the Earth's surface with a corresponding telluroid point Q, serving then as a known linearization point. The first two conditions fix the horizontal position of the telluroid point Q, requiring that the surface point P and the telluroid point Q are located on the same ellipsoidal normal, while the third condition defines the vertical position of Q based on the (observable) geopotential number C and the reference potential U_0, which is usually identified with the constant potential of the surface of the level ellipsoid; in principle, a known value of W_0 could also be employed, but this option is not pursued any further here. Regarding most of the existing geopotential numbers, these were historically referred to a fundamental datum point P_0^i with a corresponding local reference surface W_0^i (with the exact numerical value being typically unknown); in the following, no distinction is made between a local vertical datum (W_0^i) and the global case (with W_0 related to the geoid; for further details see Sect. 2.4). Fur-

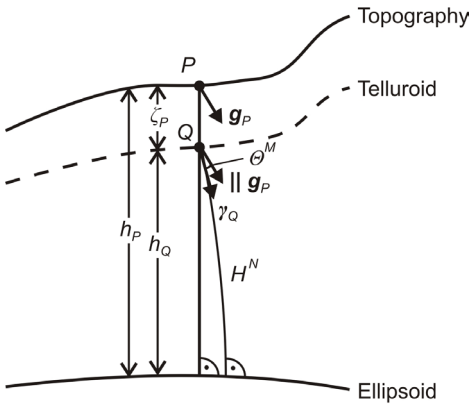

Fig. 5 Earth's surface, telluroid, ellipsoid, actual and normal gravity, deflection of the vertical according to Molodensky

thermore, the reference potentials (W_0 and W_0^i) may be considered as additional unknowns in the solution of the GBVPs, which must be counterbalanced by additional observations (GNSS and leveling); for details see Rummel and Teunissen (1988) or Heck and Rummel (1990). Finally it is also worth mentioning that the above telluroid definition according to Molodensky and the definition from Hirvonen, where the point Q is put on the same normal plumb line as P, are practically equivalent (Heck 1986); especially for the vertical component, the difference between both telluroid definitions is completely negligible due to the very small curvature of the normal plumb lines.

If the normal potential U is associated with the level ellipsoid, then the ellipsoidal height of the telluroid point Q, defined according to (78), is virtually identical with the normal height H^N (see Fig. 5); this results from (53) with $C = U_0 – U_Q$ and the fact that the ellipsoidal height (h) and the normal height (H^N) of Q differ by less than 10^{-7} m for heights up to 10 km (see Sect. 2.4). In addition, the position anomaly vector, defined as the difference of the position vectors of P and Q, respectively, has zero horizontal components with respect to the local ellipsoidal system in Q, while the vertical component is the height anomaly ζ_P (see Fig. 5).

The disturbing (or anomalous) potential is defined for an arbitrary point P in space by

$$T_P = W_P - U_P \,. \tag{79}$$

Assuming that the centrifugal parts in W and U are identical, the disturbing potential T may also be expressed as, see (35) and (57),

$$T_P = V_P - V_P^N \,, \tag{80}$$

and hence T is harmonic outside the Earth's surface and regular at infinity, see (19) and (21):

$$\Delta T = 0, \qquad \lim_{l\to\infty} T = 0 \ . \tag{81}$$

With regard to the solution of the free GBVPs, the domain of harmonicity of T has to be extended down to the surface of the (known) telluroid, which causes a small problem from the theoretical side (Heck 1997).

Corresponding to the disturbing potential T, the gravity disturbance vector is defined as

$$\boldsymbol{\delta g}_P = \mathbf{g}_P - \boldsymbol{\gamma}_P = \operatorname{grad} W_P - \operatorname{grad} U_P = \operatorname{grad} T_P \ , \tag{82}$$

while the scalar gravity disturbance is given by

$$\delta g_P = g_P - \gamma_P \ , \tag{83}$$

noting that the term disturbance is always used for one-point functions related to the same point in space (Grafarend 1978a; Heck 1997). Besides the observations in $\mathbf{g}_P$ (Φ, Λ, g), the computation of the gravity disturbance vector $\boldsymbol{\delta g}_P$ requires the spatial coordinates of P with respect to the Earth-fixed system (e.g., from GNSS) in order to be able to compute $\boldsymbol{\gamma}_P$.

Corresponding to (79) and (82) or (83), the potential anomaly

$$\Delta W_P = W_P - U_Q = T_P + (U_P - U_Q) \, , \tag{84}$$

and the gravity anomaly vector

$$\boldsymbol{\Delta g}_P = \mathbf{g}_P - \boldsymbol{\gamma}_Q = \boldsymbol{\delta g}_P + (\boldsymbol{\gamma}_P - \boldsymbol{\gamma}_Q) = \operatorname{grad} T_P + (\operatorname{grad} U_P - \operatorname{grad} U_Q) \, , \tag{85}$$

are introduced. Thus the "anomalies" are two-point functions related to the surface point P and the telluroid point Q (Grafarend 1978a; Heck 1997). The computation of the normal gravity vector $\boldsymbol{\gamma}_Q$ requires the spatial position vector of Q, e.g., its ellipsoidal latitude, longitude, and height, the latter being virtually identical with the normal height H^N (see above and Sect. 2.4), derived from geometric leveling through the geopotential number C.

Moreover, the gravity anomaly vector, $\boldsymbol{\Delta g}_P$, according to (85), can be expressed by the scalar equations (Heck 1997)

$$\begin{aligned} \Delta\varphi_P^{\gamma} &= \Phi_P - \varphi_Q^{\gamma} = \xi_P^M \ , \\ \Delta\lambda_P^{\gamma} &= \Lambda_P - \lambda_Q^{\gamma} = \eta_P^M \ / \cos\varphi_Q^{\gamma} \ , \\ \Delta g_P &= g_P - \gamma_Q \ , \end{aligned} \tag{86}$$

where ξ_P^M, η_P^M are the deflections of the vertical in north–south and east–west direction according to the definition of Molodensky (angles between the gravity vector at P and the normal gravity vector at Q), and Δg_P is the scalar gravity anomaly, also denoted as the surface free-air gravity anomaly.

In this context, the height anomaly is also a two-point function, given by

$$\zeta_P = h_P - h_Q \,. \tag{87}$$

Considering now the Molodensky telluroid, the combination of (78) and (84) yields $\Delta W_P = W_0 - U_0$, while a Taylor development of the normal potential U around the telluroid point Q gives

$$U_P = U_Q + \left(\frac{\partial U}{\partial h}\right)_Q \zeta_P + \ldots = U_Q - \gamma_Q \zeta_P + \ldots \quad . \tag{88}$$

Finally, by inserting both expressions into (84), Bruns's formula is obtained as

$$\zeta_P = \frac{T_P}{\gamma_Q} - \frac{W_0 - U_0}{\gamma_Q} \,. \tag{89}$$

In the above formula, the second term is neglected in many cases, thus assuming that the condition $W_0 = U_0$ holds. Furthermore, (89) is based only on the first term of the series expansion (88), i.e., a linear approximation, neglecting the nonlinear terms. In addition, it is noted that within the framework of linear approximations, e.g., the quantities T, ζ, δg, Δg, etc., are considered as small of first order, while products of such terms are small, of second order, and thus negligible, leading to $T_Q \approx T_P$, $\mathrm{grad}T_Q \approx \mathrm{grad}T_P$, etc. (Moritz 1980). Consequently, if the point P is unknown, which applies to the free GBVPs, T_P cannot be evaluated and has to be replaced by T_Q in (89). However, if the position of the point P in space is known, e.g., associated with the fixed GBVPs, a virtually rigorous version of formula (89), neglecting only the slightly different directions of the ellipsoidal normal and the normal plumb line, can be derived by expressing $U_P - U_Q = -\overline{\gamma}_{QP}\zeta_P$, corresponding to (53), where $\overline{\gamma}_{QP}$ is the mean normal gravity value along the line from Q to P (e.g., Wenzel 1985), giving

$$\zeta_P = \frac{T_P}{\overline{\gamma}_{QP}} - \frac{W_0 - U_0}{\overline{\gamma}_{QP}} \quad \text{with} \quad \overline{\gamma}_{QP} = \frac{1}{h_P - h_Q}\int_{h_Q}^{h_P} \gamma \, dh \,. \tag{90}$$

Given the point P in space, the use of (89) instead of (90) leads to maximum errors in the height anomalies of about a few millimeters (see also Wenzel 1985), and hence, as the mean normal gravity value $\overline{\gamma}_{QP}$ is easy to compute, in the simplest case as $\frac{1}{2}(\gamma_Q + \gamma_P)$, (90) should be preferred (noting that it is not consistent with the concept of linear approximations explained above).

The linearization of the nonlinear boundary conditions (observation equations) related to the scalar fixed (δg_P), the vectorial free ($\mathbf{\Delta g}_P$), and the scalar free GBVP (Δg_P) is treated in detail in Heck (1997) and Seitz (1997), also investigating the nonlinear terms and the resulting linearization errors (the nonlinearities arise from the free boundary as well as the use of the norm operator to compute the vector lengths, e.g., (83) and (86)). A rigorous linearization of the boundary conditions is

not intended here. Therefore, considering only linear approximations (see above) of (89), (83), and (86), results in

$$\zeta_P = \frac{T}{\gamma} - \frac{W_0 - U_0}{\gamma} \quad , \tag{91}$$

$$\delta g_P = -\frac{\partial T}{\partial z^e} = -\frac{\partial T}{\partial h} \quad , \tag{92}$$

$$\xi_P^M = -\frac{1}{\gamma}\frac{\partial T}{\partial x^e} = -\frac{1}{\gamma (M+h)}\frac{\partial T}{\partial \varphi} \quad , \tag{93}$$

$$\eta_P^M = -\frac{1}{\gamma}\frac{\partial T}{\partial y^e} = -\frac{1}{\gamma (N+h)\cos\varphi}\frac{\partial T}{\partial \lambda} \quad , \tag{94}$$

$$\Delta g_P = -\frac{\partial T}{\partial h} + \frac{1}{\gamma}\frac{\partial \gamma}{\partial h} T - \frac{1}{\gamma}\frac{\partial \gamma}{\partial h}(W_0 - U_0) \quad , \tag{95}$$

where the right sides of the above formulas have to be evaluated at the boundary surface, i.e., the telluroid in the case of the free GBVPs. The negative sign in the vertical deflection components follows from the sign conventions for the height anomalies and the vertical deflections (Torge 2001). For the derivation of (95), a Taylor series expansion of γ_P–γ_Q, analogous to (88), is used; the equation is also denoted as the fundamental equation of physical geodesy. Furthermore, the introduction of spherical approximations in the above formula system, i.e., the omission of terms of the order $o(f)$ with $f \approx 1/300$ (often called ellipsoidal effects), not affecting (91), gives

$$\delta g_P = -\frac{\partial T}{\partial r} \quad , \tag{96}$$

$$\xi_P^M = -\frac{1}{\gamma r}\frac{\partial T}{\partial \varphi} \quad , \tag{97}$$

$$\eta_P^M = -\frac{1}{\gamma r \cos\varphi}\frac{\partial T}{\partial \lambda} \quad , \tag{98}$$

$$\Delta g_P = -\frac{\partial T}{\partial r} - \frac{2}{r} T + \frac{2}{r}(W_0 - U_0) \quad , \tag{99}$$

where $\partial\gamma/\partial h = \partial\gamma/\partial r = -2\gamma/r$ (spherical approximation) is utilized. Moreover, the subscripts P and Q are dropped on the right sides of (91) to (99), noting again that the linearized boundary conditions hold on the (known) boundary surface, which is the Earth's surface for the fixed GBVPs and the telluroid for the free GBVPs, respectively; hence, the linearization process is associated with a transformation of

the free GBVPs into fixed ones, with the telluroid then serving as the (known) boundary. In this context, it has to be stressed that the boundary conditions in spherical approximation also still relate to the Earth's surface (fixed GBVPs) or the telluroid (free GBVPs); in other words, spherical approximations include only the omission of ellipsoidal terms, but do not imply that the boundary is replaced by a sphere (see also Moritz 1980 and Heck 1997). In addition, planar approximations, also neglecting terms of the order $o(h/R)$ associated with a mean Earth radius R, may be used for very local applications (e.g., Moritz 1980), but are not discussed here. Considering the linearized boundary conditions (91)–(99), it is clear that the derivatives of T are in general not normal to the (known) boundary surface (Earth's surface or telluroid, respectively), leading to the so-called oblique derivative BVPs (Heck 1997; Sideris 2011a). Furthermore, in the boundary condition for the gravity disturbance the radial derivative of T appears, while in the corresponding equation for the gravity anomaly a linear combination of the radial derivative of T and T itself occurs, similar to the second (Neumann) and third (Robin) BVP of potential theory, involving normal derivatives.

So far it has been assumed that the level ellipsoid is used for the linearization of the observation equations, implying that the height anomalies, i.e., the separation between the Earth's surface and the telluroid, following closely the Earth's surface, reach maximum values of about 100 m with an RMS (root-mean-square) value of roughly 30 m. Thus the use of spherical approximations, i.e., the omission of terms of the order $o(f)$ with $f \approx 1/300$, may in certain cases lead to significant errors at the milligal and decimeter level in the derived gravity and height anomalies, respectively (Heck 1997; Hipkin 2004). Obviously, the non-spherical and nonlinear terms cannot be neglected in precise gravity field modeling, and thus have to be considered by appropriate reductions (see, e.g., Heck 1991), especially in view of the present accuracy requirements for regional and global computations (e.g., the GRACE and GOCE satellite missions), aiming at accuracies at the millimeter to centimeter level for height anomalies.

On the other hand, the effect of the linearization and spherical approximation errors can be substantially reduced by introducing a higher degree reference field, e.g., a complete spherical harmonic model derived from the satellite missions GRACE (e.g., Mayer-Gürr et al. 2010; Kurtenbach et al. 2009) and GOCE (e.g., Pail et al. 2011) or the combined model EGM2008 (Pavlis et al. 2008), extended by a centrifugal component. In this context, it is important to stress that the satellite-only models are inherently unaffected by any spherical approximations, etc., while EGM2008 is derived on the basis of ellipsoidal harmonics and thus also hardly affected by such effects. In addition, it is essential that the gravity field parameters derived from the high-degree models are computed rigorously without any (spherical, etc.) approximations, as outlined in Sect. 2.3, such that the residuals with respect to the global model are virtually exact. Now, if the normal gravity field of the level ellipsoid is replaced by a global geopotential model complete to degree and order 100, 200, and 360, the residual height anomalies reduce to about 1.0, 0.4, and 0.2 m RMS, with corresponding maximum values of about 18, 11, and

4 m, respectively. Hence, a high-degree reference field leads to a much better approximation of the real situation, with the separation between the Earth's surface and the corresponding telluroid reducing by about one to two orders of magnitude, as compared to the linearization with respect to the level ellipsoid. Accordingly, the effect of linear and spherical approximations decreases in the modeling of the (rigorously derived) residual gravity field parameters, such that height anomalies may be deduced with accuracies at the centimeter to a few millimeters level; this is also supported by the numerical investigations in Heck (1997) and Seitz (1997). Further insight into this problem can be gained as well through closed-loop simulations with synthetic data (see, e.g., Wolf 2008).

The rigorous implementation of a high-degree geopotential model as a reference field in the linearization process must strictly follow the procedure described above for the level ellipsoid; the geopotential model is associated with a gravity potential

$$W^M = V^M + Z^M \,, \tag{100}$$

based on a spherical harmonic expansion of the gravitational part V^M as well as a centrifugal component Z^M. Correspondingly, the gravity vector is defined as

$$\mathbf{g}^M = \operatorname{grad} W^M = \operatorname{grad} V^M + \operatorname{grad} Z^M \,. \tag{101}$$

The notation is chosen here in line with the real gravity potential of the Earth and its functionals, because the currently available high-degree geopotential models allow a quite good approximation of the real gravity field. Now, within the linearization process, W^M and $\mathbf{g}^M$ have to take the place of U and $\boldsymbol{\gamma}$, respectively. Hence, the disturbance quantities related to a single point P in space with given coordinates can be computed directly, while the anomaly quantities require the definition of a telluroid associated with the geopotential model. In accordance with (78) it follows that

$$\varphi_{Q^*} = \varphi_P \,, \quad \lambda_{Q^*} = \lambda_P \,, \quad W^M_{Q^*} = U_Q = U_0 - C = U_0 - (W_0 - W_P) \,, \tag{102}$$

where Q^* is the telluroid point in conjunction with the geopotential model. The advantage of employing a high-degree reference field instead of the level ellipsoid is that the point Q^* is much closer to P than Q (see above as well as Fig. 6). Again it is assumed that the ellipsoidal latitude and longitude of P and thus Q^* are given, while the ellipsoidal height of P is unknown and that of Q^* can in principle be computed iteratively, starting with $h_{Q^*(0)} = h_Q = H^N$ and $W^M_{Q^*(0)}(\varphi_{Q^*}, \lambda_{Q^*}, h_{Q^*(0)})$, while then the equation

$$h_{Q^*(i)} = h_{Q^*(i-1)} + \frac{1}{g^M_{Q^*(i-1)}} \left(W^M_{Q^*(i-1)}(\varphi_{Q^*}, \lambda_{Q^*}, h_{Q^*(i-1)}) - W^M_{Q^*} \right), \qquad i = 1, \ldots, \infty \,, \tag{103}$$

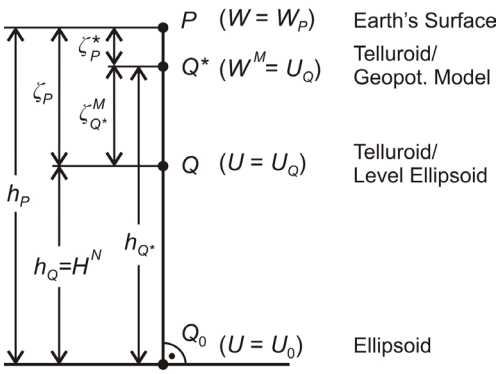

Fig. 6 Telluroid associated with level ellipsoid and high-degree reference geopotential model

has to be iterated until convergence, with the nominal potential value being $W_{Q^*}^M = U_Q = U_0 - C$, which is deduced from leveling and a conventional U_0 value. The time-consuming part in this iteration process is the calculation of the potential values W^M, requiring the evaluation of the spherical harmonic expansion; however, the convergence of (103) is very good, e.g., regarding a geopotential model complete to degree and order 360, the maximum error of h_{Q^*} was found to be less than 1×10^{-5} m after only two iterations ($i = 2$). Furthermore, it is noted that the geopotential model gravity value $g_{Q^*\,(i-1)}^M$ in (103) can be replaced by practically any constant (normal) gravity value γ, as the term in parentheses on the right side of (103) goes to zero within the iteration process.

After all, it is convenient to express also W^M as the sum of the potential of the level ellipsoid U and a corresponding disturbing potential T^M. Considering (79), this leads directly to the disturbing potential, associated with the high-degree geopotential model

$$T_P^* = W_P - W_P^M = (U_P + T_P) - (U_P + T_P^M) = T_P - T_P^M \,, \tag{104}$$

and the corresponding height anomaly (of P with respect to Q^*; see Fig. 6)

$$\zeta_P^* = h_P - h_{Q^*} = (h_P - h_Q) - (h_{Q^*} - h_Q) = \zeta_P - \zeta_{Q^*}^M \,, \tag{105}$$

which, following the line of thought used to derive (89), can be expressed in linear approximation as

$$\zeta_P^* = \frac{T_P^*}{g_{Q^*}^M} - \frac{W_0 - U_0}{g_{Q^*}^M} \,, \tag{106}$$

and accordingly $\zeta_{Q^*}^M$ is given by

$$\zeta_{Q^*}^M = \frac{T_{Q^*}^M}{\gamma_Q} \ , \tag{107}$$

noting that more rigorous versions of the above two equations can be obtained analogous to (90) by introducing corresponding mean gravity values $\overline{g}_{Q^*P}^M$ and $\overline{\gamma}_{QQ^*}$, respectively.

In the same way, the gravity disturbance and anomaly vectors with respect to the geopotential model are given by

$$\boldsymbol{\delta}\mathbf{g}_P^* = \mathbf{g}_P - \mathbf{g}_P^M = (\boldsymbol{\gamma}_P + \boldsymbol{\delta}\mathbf{g}_P) - (\boldsymbol{\gamma}_P + \boldsymbol{\delta}\mathbf{g}_P^M) = \boldsymbol{\delta}\mathbf{g}_P - \boldsymbol{\delta}\mathbf{g}_P^M \ , \tag{108}$$

$$\boldsymbol{\Delta}\mathbf{g}_P^* = \mathbf{g}_P - \mathbf{g}_{Q^*}^M = (\boldsymbol{\gamma}_Q + \boldsymbol{\Delta}\mathbf{g}_P) - (\boldsymbol{\gamma}_Q + \boldsymbol{\Delta}\mathbf{g}_{Q^*}^M) = \boldsymbol{\Delta}\mathbf{g}_P - \boldsymbol{\Delta}\mathbf{g}_{Q^*}^M \ . \tag{109}$$

Consequently, the rigorous linearization with respect to a high-degree geopotential model leads to residual quantities, which closely correspond to those used in the well-known remove–compute–restore technique, in which topographic (or mass) information is additionally taken into account (see Sect. 3.9). In this context, it is pointed out again that the parameters from the geopotential model should be derived without (spherical, etc.) approximations at the appropriate positions in space, and it is also noted that the concepts introduced in Sect. 2.3, computing first the potential derivatives with respect to a local spherical system, followed by a transformation to the desired target system, can be applied as well for the anomalous gravity field quantities. Now for the case that only normal heights exist, the telluroid point Q^* can be computed with sufficient accuracy (see above) after only two iterations of (103); in practice this means that the geopotential model has to be evaluated only at the two heights $h_{Q^*(0)} = h_Q = H^N$ and $h_{Q^*(1)} = H^N + \zeta_{Q^*(0)}$, yielding T_Q and $T_{Q^*} \approx T_{Q^*(1)}$ in Q and Q^*, respectively. With regard to a geopotential model complete to degree and order 360, the maximum differences between T_Q and T_{Q^*} reach about 0.25 $\mathrm{m^2\,s^{-2}}$, while $T_{Q^*(1)}$ is accurate to better than 1×10^{-4} $\mathrm{m^2\,s^{-2}}$, corresponding to about 0.025 m and 1×10^{-5} m in terms of height anomalies. The maximum differences between T_Q and T_{Q^*} are considered as significant, and hence the geopotential model should be evaluated at the appropriate positions in space. This was also pointed out by Tscherning (2004), mentioning that in this way "it is possible to come close to making no approximation at all."

3.3 The Constant Radius Approximation

The geodetic boundary value problems (GBVPs) aim at the determination of the exterior gravity potential W from boundary data, as a direct computation is impossible due to insufficient knowledge of the Earth's density structure. Within the linearization process, described in the previous section, the task of computing W is reduced to the determination of the disturbing potential T, which is a harmonic function outside the masses and regular at infinity, see (81).

Now harmonic solutions for T are sought, which satisfy the boundary conditions (observations), e.g., (91)–(99). In this context, it is pointed out again that the linearized boundary conditions refer to the known boundary surface (i.e., the Earth's surface for the fixed GBVPs, and the telluroid for the free GBVPs), and the derivatives of T, appearing in the boundary conditions, are generally not normal to the boundary surface (oblique derivative GBVPs).

However, even the linearized GBVPs based on spherical approximations, e.g., (96)–(99), do not permit rigorous analytical solutions in closed form as long as the boundary is not spherically shaped (Heck 1997). Therefore, Rummel (1988) and Heck (1997) discuss iterative solutions, where terms due to the Earth's flattening and topography of order $o(f)$ and $o(h/a)$ are involved, respectively. The omission of all non-spherical terms (i.e., assuming a spherical boundary) leads to the so-called constant radius approximations, which also contribute the dominating terms in iterative GBVP solution schemes.

In the following, several well-known formulas are derived on the basis of the constant radius approximation. In the first instance, as the disturbing potential T is a harmonic function, it may be expanded in spherical harmonics based on (80), (26), and (59), resulting in

$$T(\theta,\lambda,r)=\sum_{n=0}^{\infty}\left(\frac{a}{r}\right)^{n+1}\sum_{m=-n}^{n}\overline{T}_{nm}\overline{Y}_{nm}(\theta,\lambda)=\sum_{n=0}^{\infty}\left(\frac{a}{r}\right)^{n+1}T_n(\theta,\lambda,a)\ , \qquad (110)$$

with

$$\overline{T}_{nm}=\frac{GM}{a}\left(\begin{Bmatrix}\overline{C}_{nm}\\ \overline{S}_{nm}\end{Bmatrix}-\frac{GM_N}{GM}\left(\frac{a_N}{a}\right)^n\begin{Bmatrix}\overline{C}^N_{nm}\\ \overline{S}^N_{nm}\end{Bmatrix}\right)\quad\text{for}\quad\begin{Bmatrix}m\ge 0\\ m<0\end{Bmatrix}\ , \qquad (111)$$

where the different GM and a values in V and V^N lead to a rescaling of the coefficients of the normal potential, noting that (110) and (111) may also be expressed with respect to a_N and GM_N, whatever is more convenient. The summation in the above equation starts at degree $n = 0$ to account for possible differences in the GM and GM_N quantities related to V and V^N, respectively. Another option would be to compute T directly as the difference of V and V^N, requiring no rescaling of any coefficients. Furthermore, $T_n(\theta, \lambda, a)$ are the Laplace surface harmonics of degree n, referring to the radius $r = a$.

Assuming now that T is given on a sphere with radius $r = a$, (110) can be inverted easily by applying the orthogonality relations (28), yielding

$$\overline{T}_{nm}=\frac{1}{4\pi}\iint_{\sigma}T(\theta',\lambda',a)\overline{Y}_{nm}(\theta',\lambda')\,d\sigma\ . \qquad (112)$$

Utilizing this result as well as the decomposition formula for the Legendre polynomials gives directly

$$T_n(\theta,\lambda,a)=\frac{2n+1}{4\pi}\iint_{\sigma}T(\theta',\lambda',a)P_n(\cos\psi)\,d\sigma\,, \tag{113}$$

where ψ is the spherical distance between the two points $P\,(\theta,\lambda,a)$ and $P'\,(\theta',\lambda',a)$ with

$$\cos\psi=\cos\theta\cos\theta'+\sin\theta\sin\theta'\cos(\lambda-\lambda')\,. \tag{114}$$

Correspondingly, the gravity disturbance may be expressed in spherical approximation according to (96) as

$$\delta g(\theta,\lambda,r)=-\frac{\partial T}{\partial r}=\sum_{n=0}^{\infty}\left(\frac{a}{r}\right)^{n+2}\frac{n+1}{a}T_n(\theta,\lambda,a)=\sum_{n=0}^{\infty}\left(\frac{a}{r}\right)^{n+2}\delta g_n(\theta,\lambda,a)\,. \tag{115}$$

The above approach can be applied to other gravity field parameters as well and leads to the so-called Meissl scheme, which in its extended form, based on tensor spherical harmonics, is also applicable to the first and second horizontal derivatives of T (Rummel and van Gelderen 1995; Rummel 1997). Thus in spherical approximation, the following simple spectral relations (eigenvalue expressions) hold:

$$\delta g_n(\theta,\lambda,a)=\frac{n+1}{a}T_n(\theta,\lambda,a)\;, \tag{116}$$

$$\Delta g_n(\theta,\lambda,a)=\begin{cases}-\dfrac{1}{a}T_0(\theta,\lambda,a)+\dfrac{2}{a}(W_0-U_0) & \text{for } n=0\\[2ex] \dfrac{n-1}{a}T_n(\theta,\lambda,a) & \text{for } n>0\end{cases}\,, \tag{117}$$

$$T_n(\theta,\lambda,r)=\left(\frac{a}{r}\right)^{n+1}T_n(\theta,\lambda,a)\;, \tag{118}$$

$$\delta g_n(\theta,\lambda,r)=\left(\frac{a}{r}\right)^{n+2}\delta g_n(\theta,\lambda,a)\;, \tag{119}$$

$$\Delta g_n(\theta,\lambda,r)=\left(\frac{a}{r}\right)^{n+2}\Delta g_n(\theta,\lambda,a)\;. \tag{120}$$

Basically, the spherical harmonic expansion (110) together with (112) represents a solution to the Dirichlet BVP for a spherical boundary. Now, the spherical harmonic series has its advantages mainly in global analyses and the spectral interpretation, while integral formulas (Green's function representations) are better suited for local applications; this is easily recognized by the fact that a change in one boundary value leads to changes in all spherical harmonic coefficients, while a change in a remote boundary value affects the local field computed by integral

formulas only marginally, as the integration kernels essentially depend on the inverse distance or higher powers thereof (Jekeli 2009).

Combining (110) and (113) and assuming that the disturbing potential T is given on a sphere with radius $r = R$ (instead of $r = a$ used above) leads to the well-known Poisson integral (Heiskanen and Moritz 1967; Jekeli 2009)

$$T(\theta,\lambda,r) = \frac{1}{4\pi}\iint_{\sigma} T(\theta',\lambda',R)\,U(\psi,r)\,d\sigma \tag{121}$$

with the Poisson kernel

$$\begin{aligned} U(\psi,r) &= \sum_{n=0}^{\infty}\left(\frac{R}{r}\right)^{n+1}(2n+1)\,P_n(\cos\psi) \\ &= \frac{R(r^2-R^2)}{l^3} \end{aligned} \tag{122}$$

and the spatial distance

$$l = \sqrt{r^2 + R^2 - 2rR\cos\psi}\ . \tag{123}$$

The above equations allow the upward continuation of any harmonic function from a sphere with radius R to another sphere with radius $r > R$, e.g., they can be directly applied to the (spatial) function $r\,\Delta g$, which is harmonic, while Δg itself is not a harmonic function (for details see Heiskanen and Moritz 1967).

Furthermore, utilizing (113) correspondingly for the derivation of the gravity disturbance surface harmonics and inserting this result into (116) and (110) yields the Hotine integral (Hotine 1969; Heck 1997)

$$T(\theta,\lambda,r) = \frac{R}{4\pi}\iint_{\sigma} \delta g\,(\theta',\lambda',R)\,H(\psi,r)\,d\sigma \tag{124}$$

with the Hotine kernel

$$\begin{aligned} H(\psi,r) &= \sum_{n=0}^{\infty}\left(\frac{R}{r}\right)^{n+1}\frac{2n+1}{n+1}P_n(\cos\psi) \\ &= \frac{2R}{l} - \ln\frac{l+R-r\cos\psi}{r\,(1-\cos\psi)}\,. \end{aligned} \tag{125}$$

It should be noted that the summation in (122) and (125) starts at degree $n = 0$, and thus the complete spectrum including the degrees zero and one can be determined from the boundary data. However, with regard to gravity anomalies, the situation is different, as (117) has to be employed accordingly, where the factor $(n–1)$ appears; i.e., the gravity anomalies have no first degree harmonics and hence the corresponding disturbing potential harmonics cannot be determined from gravi-

ty anomalies. This leads to a non-unique solution of the BVP, and therefore additional constraints are necessary to achieve a unique solution for T. The first-degree harmonic coefficients are proportional to the center-of-mass coordinates and can be enforced to zero with an appropriate definition of the coordinate system (for further details see Rummel 1995 and Heck 1997). Corresponding to (124) and (125), the complete solution for the disturbing potential based on gravity anomalies is given by

$$T(\theta,\lambda,r) = \sum_{n=0}^{1}\left(\frac{R}{r}\right)^{n+1} T_n(\theta,\lambda,R) + \frac{R}{4\pi}\iint_{\sigma} \Delta g\,(\theta',\lambda',R)\,S(\psi,r)\,d\sigma\,, \qquad (126)$$

with the (extended) Stokes kernel

$$\begin{aligned} S(\psi,r) &= \sum_{n=2}^{\infty}\left(\frac{R}{r}\right)^{n+1}\frac{2n+1}{n-1}P_n(\cos\psi) \\ &= \frac{2R}{l} + \frac{R}{r} - 3\frac{Rl}{r^2} - \frac{R^2}{r^2}\cos\psi\left(5 + 3\ln\frac{l + r - R\cos\psi}{2r}\right). \end{aligned} \qquad (127)$$

In the above equations, the zero-degree and first-degree terms of T are handled separately, because the Stokes integral, the right term in (126), conventionally excludes these components (e.g., Heiskanen and Moritz 1967; Jekeli 2009); this is also evident from the Stokes kernel (127), where the summation only starts at degree $n = 2$. Furthermore, according to (110) and (111), the zero-degree term of T in (126) can be expressed as

$$T_0(\theta,\lambda,R) = \frac{GM - GM_N}{R}\,, \qquad (128)$$

and the corresponding zero-degree term of ζ follows from Bruns's formula as

$$\zeta_0(\theta,\lambda,R) = \frac{1}{\gamma_0}T_0(\theta,\lambda,R) - \frac{1}{\gamma_0}(W_0 - U_0)\,. \qquad (129)$$

In addition, it is noted that (124) and (125) solve the Neumann BVP, while (126)–(128) solve the Robin BVP, provided the boundary is a sphere. Furthermore, all integral kernels (Green's functions) introduced above, have singularities at $\psi = 0$, when the computation point is on the sphere with radius R. Therefore, the inner zone contributions have to be evaluated separately by expanding the boundary data in a Taylor series and performing the integration term by term (Heiskanen and Moritz 1967; Bian 1997, Torge 2001).

For the Stokes integral (with $r = R$), the inner zone contribution can be computed by approximating $S(\psi) = S(\psi, R) = 2/\psi = 2\,R/s$, with s being the planar distance (the first term in (127) dominates for $\psi \to 0$); then integration over a spherical cap with radius s_0 gives the inner zone contribution

$$T_i = \Delta g_P \, s_0 + \ldots \quad , \tag{130}$$

while an integration over a rectangular area (see also Haagmans et al. 1993) results in

$$\begin{aligned} T_i &= \Delta g_P \, \frac{1}{2\pi} \int_{-\Delta x/2}^{+\Delta x/2} \int_{-\Delta y/2}^{+\Delta y/2} \frac{1}{\sqrt{x^2 + y^2}} \, dx \, dy + \ldots \\ &= \Delta g_P \, \frac{1}{2\pi} \left(\Delta x \ln \frac{d + \Delta y}{d - \Delta y} + \Delta y \ln \frac{d + \Delta x}{d - \Delta x} \right) \quad \text{with} \quad d = \sqrt{\Delta x^2 + \Delta y^2} , \end{aligned} \tag{131}$$

where Δx, Δy are the side lengths (in meters) of the rectangle in x (north–south) and y (east–west) direction, respectively. If the area sizes of the spherical cap and the rectangle are chosen to be identical ($\pi \, s_0^2 = \Delta x \, \Delta y$), (131) always gives slightly larger inner zone contributions than (130); the differences are at the few percent level, depending on the ratio of $\Delta x \, / \, \Delta y$ (for further details see Haagmans et al. 1993).

Finally, based on the spherical and constant radius approximations, virtually any gravity field quantity can be obtained in space from any other quantity on a spherical boundary (Jekeli 2009). Further examples are the Vening-Meinesz integral formulas, which allow the computation of deflections of the vertical from gravity anomalies by applying (97) and (98) to the Stokes integral, as well as the inverse Stokes, Hotine, and Vening-Meinesz integral formulas, which are all presented, e.g., in Jekeli (2009).

3.4 Solutions to Molodensky's Boundary Value Problem

In the previous section, different GBVP solutions are derived based on the spherical and constant radius approximation, assuming that the boundary is a sphere. Now, more complicated boundaries require additional corrections or iterative solution schemes. The scalar free GBVP, formulated first by Molodensky (e.g., Molodenskii et al. 1962), is based on gravity observations at the Earth's surface. Within the linearization process, the scalar free GBVP is transformed into a fixed one by approximating the Earth's surface by means of the telluroid, serving then as the (known) boundary surface, to which the boundary conditions as well as the boundary data (i.e., the gravity anomalies) refer (see Sect. 3.2). Furthermore, the scalar free GBVP in linear and spherical approximation is often called the simple Molodensky problem (Moritz 1980; Heck 1997).

Molodensky's problem can be solved in various ways; detailed derivations can be found in Moritz (1980). An efficient solution, avoiding integral equations, is provided by the method of analytical continuation (Moritz 1980;, Sideris 1987, 2011a). In this method, the gravity anomalies Δg (at any point on the telluroid) are

reduced to the normal level surface passing through the given computation point P (point level); the resulting anomalies are denoted as $\Delta g'$ and can be obtained by

$$\Delta g' = \sum_{n=0}^{\infty} g_n\,,\;\; g_n = -\sum_{j=1}^{n} (H^N - H_P^N)^j L_j(g_{n-j})\,,\;\; \text{starting with}\;\; g_0 = \Delta g\,. \qquad (132)$$

Thus the g_n terms are evaluated recursively based on the vertical derivative operator L_j with

$$L_j = \frac{1}{j!}\frac{\partial^j}{\partial h^j} = \frac{1}{j}\frac{1}{(j-1)!}\frac{\partial^{j-1}}{\partial h^{j-1}}\frac{\partial}{\partial h} = \frac{1}{j}L_{j-1}L_1 = \frac{1}{j!}L^j = \frac{1}{j!}LLL\ldots L \;\; (j \text{ times}). \qquad (133)$$

In the above equation, the abbreviation $L = L_1$ is introduced, and in planar approximation ($R \to \infty$) L becomes the surface operator

$$L(f) = L_1(f) = \frac{R^2}{2\pi}\iint_{\sigma} \frac{f - f_P}{l_0^3}\, d\sigma\,, \qquad l_0 = 2R\sin\frac{\psi}{2}\,. \qquad (134)$$

Now, the analytically continued gravity anomalies $\Delta g'$ refer to the normal level surface passing through the computation point P, and hence the disturbing potential T at P can be obtained by applying Stokes's integral operator $\mathbf{S}$ (right term of (126)) to $\Delta g'$, yielding

$$T = \mathbf{S}(\Delta g') = \mathbf{S}(\Delta g) + \sum_{n=1}^{\infty} \mathbf{S}(g_n) = \sum_{n=0}^{\infty} T_n\,. \qquad (135)$$

Thus, the main contribution to the Molodensky solution is provided by the Stokes term, while the further so-called Molodensky terms consider that the data are not given on a level surface. Moreover, the zero-degree and first-degree terms of T are omitted in the above equation, but the notes given for the Stokes integral apply to the Molodensky solution as well (see previous section). Finally, it should be noted that the Molodensky terms T_n and the Laplace surface harmonics of T have nothing in common.

Regarding the above computation procedure, it is important to realize that the g_n terms depend on the computation point P, which is rather impractical, as a new set of g_n values has to be computed for every new computation point. This difficulty can be overcome, e.g., by performing the analytical continuation in two steps, where the surface gravity anomalies are first analytically continued to zero level (giving $\Delta g^{0\prime}$), then the Stokes operator is applied to compute the harmonically continued disturbing potential $T^{0\prime}$, and finally $T^{0\prime}$ is analytically continued back to the telluroid (Sideris 1987; Forsberg and Tscherning 1997), yielding

$$T = T^{0\prime} + \sum_{n=1}^{\infty} (H^N)^n L_n(T^{0\prime})\,. \qquad (136)$$

The two-step formulas are much better suited for numerical computations and allow the application of Fast Fourier Transform (FFT) techniques (Sideris 1987).

Furthermore, the first order solution of (135) is known as the gradient solution (Moritz 1980), which can be expressed as

$$T \approx \mathbf{S}\left(\Delta g + g_1\right) = \mathbf{S}\left(\Delta g - \frac{\partial \Delta g}{\partial h}(H^N - H_P^N)\right). \tag{137}$$

Regarding the gradient solution, it is also worth mentioning that

$$\mathbf{S}\left(g_1\right) \approx \mathbf{S}\left(c\right) \tag{138}$$

holds in linear approximation for gravity anomalies Δg linearly dependent on the elevations, where c is the classical terrain correction (Moritz 1980). Besides this, the gravity anomalies $\Delta g_{\text{Faye}} = \Delta g + c$ are denoted as Faye anomalies, giving

$$T \approx \mathbf{S}\left(\Delta g + c\right) = \mathbf{S}\left(\Delta g_{\text{Faye}}\right). \tag{139}$$

For the two-step procedure based on (135) and (136), the gradient solution leads to

$$T \approx \mathbf{S}\left(\Delta g - \frac{\partial \Delta g}{\partial h} H^N\right) + \frac{\partial T^{0\prime}}{\partial h} H^N \,. \tag{140}$$

Considering the relations (92), (91), and (95), yielding

$$\frac{\partial T}{\partial h} = -\delta g \,, \qquad \frac{\partial \zeta}{\partial h} = -\frac{1}{\gamma}\Delta g \,, \tag{141}$$

the gradient solution results in a very simple scheme for the computation of the height anomalies (Forsberg and Tscherning 1997):

1. Predict vertical gradient $\partial \Delta g/\partial h \approx -T_{zz}$ from Δg.
2. Continue Δg downward, giving $\Delta g^{0\prime} \approx \Delta g - (\partial \Delta g/\partial h)\, H^N$.
3. Apply Stokes operator, yielding $\zeta^{0\prime} = \mathbf{S}(\Delta g^{0\prime})$.
4. Continue the height anomalies upward to obtain $\zeta = \zeta^{0\prime} - (\Delta g^{0\prime}/\gamma)\, H^N$.

The above procedure is preferable over (139), as it contains fewer approximations, avoiding the assumption that the gravity anomalies are linearly dependent on the elevations.

Finally, it is noted that $\zeta^{0\prime}$, ζ, and the geoid undulation N (as well as the corresponding disturbing potentials $T^{0\prime}$, T, and T^0) are fundamentally different quantities. Initially, $T^{0\prime}$ is a disturbing potential obtained by harmonic continuation (to zero level), which is identical to T outside the Earth's surface; e.g., this is also the quantity obtained from a global geopotential model or least-squares collocation applied spatially. On the other hand, T^0 relates to the geoid (see next section),

which is in general located inside the topography on the continents and hence not an equipotential surface of a harmonic function (because T^0 is not harmonic inside the topography). The differences between ζ and $\zeta^{0\prime}$ depend on the free-air gravity anomaly, see (141), while the differences between ζ and N depend on the Bouguer gravity anomaly, see (56). In typical mountainous areas with, e.g., 1 km changes in elevation, the differences between $\zeta^{0\prime}$, ζ, and N are at the level of 10 cm (Forsberg and Tscherning 1997).

3.5 Solutions to Stokes's Boundary Value Problem

Stokes's classical geodetic boundary value problem (GBVP) aims at the determination of the geoid from gravimetric data. The calculation of the geoid within the GBVP framework has two important consequences: first, the gravity values must refer to the geoid, which initially serves as the boundary surface, and second, there must be no masses outside the geoid. The latter requirement results from the boundary value problem approach of potential theory, which always involves harmonic functions satisfying the Laplace equation. Consequently, since no masses are allowed outside the geoid, the topography of the Earth must be eliminated mathematically by appropriate reductions.

Stokes's as well as Molodensky's GBVP may both be considered as scalar free problems (see above), the main difference being that Molodensky's problem is based on gravity data at the Earth's surface, while Stokes's problem involves gravity data at the geoid. Accordingly, Stokes problem is in principle easier to solve than Molodensky's problem, because the initial boundary surface, i.e., the geoid, is a level surface with the gravity vectors perpendicular to it; this corresponds to a BVP of the third kind (Robin problem) of potential theory, see boundary condition (95) or (99). However, the main drawback of Stokes's problem is that complicated topographic reductions are necessary.

For the solution of Stokes's GBVP, the geoid is approximated by an ellipsoid, and then after spherical and constant radius approximation the general solution is given by (126) with $r = R$, the right term being the Stokes integral (for further details see above). Now, in order to get the boundary values (gravity anomalies) at the geoid, the external masses outside the geoid must be either removed completely or moved inside the geoid. This so-called regularization obviously also changes the shape of the level surfaces and hence the geoid, leading to the cogeoid. In this context, it is advantageous to preserve the total mass of the Earth. Therefore, usually Helmert's second condensation reduction is applied, where the masses above the geoid are condensed onto a layer on the geoid (e.g., Sideris 1994, 2011a).

Accordingly, the entire procedure for the computation of the geoid may be described as follows (Heiskanen and Moritz 1967; Sideris 2011a):

1. The masses above the geoid are removed computationally, i.e., the attraction effect (A_P) is subtracted from the gravity value at the surface point P.

2. The gravity station is lowered from P to P_0 on the geoid using the free-air reduction (F) or harmonic downward continuation.
3. The topographic masses are condensed on the geoid, and the attraction effect at P_0 is restored ($A^c_{P_0}$).
4. The indirect effect (for details see Wichiencharoen 1982) on the potential (δT_{ind}) due to the shifting of the topographic masses is computed at P_0.
5. The indirect effect on gravity (δg_{ind}), which reduces gravity from the geoid to the cogeoid, is taken into account, finally yielding the gravity anomalies on the cogeoid as $\Delta g^c = g_P - A_P + F + A^c_{P_0} + \delta g_{ind} - \gamma_0$.
6. The disturbing potential for the cogeoid (T^{0c}) is computed by applying Stokes's operator to Δg^c .
7. The disturbing potential for the geoid (T^0) is computed by adding the indirect effect to the Stokes contribution, yielding

$$T^0 = \mathbf{S}(\Delta g^c) + \delta T_{ind} \ . \tag{142}$$

8. Finally, the geoid undulation (omitting the zero-degree term) is obtained from Bruns's formula as

$$N = \frac{T^0}{\gamma_0} = \frac{1}{\gamma_0}\mathbf{S}(\Delta g^c) + \frac{1}{\gamma_0}\delta T_{ind} \ . \tag{143}$$

In addition, with the quantity $\delta A = A^c_{P_0} - A_P \approx c$ and $\delta g_{ind} \approx 0$, the gravity anomaly at the cogeoid becomes $\Delta g^c \approx g_P + F - \gamma_0 + c \approx \Delta g_P + c = \Delta g_{\text{Faye}}$ (Forsberg and Tscherning 1997). Thus, the Faye anomalies play a role in the first order solutions of Stokes's as well as Molodensky's problem, see (139); further relationships and discussions on this matter can be found in Sideris (1994) and Forsberg and Tscherning (1997). Practical examples of large-scale geoid computations are the models derived for the United States (e.g., Smith and Roman 2001; Wang et al. 2011) and Canada (Véronneau and Huang 2007).

In conclusion, the computation of the geoid is in the details quite complicated and requires several approximations as well as assumptions about the density of the topographic masses above the geoid, which is the classical dilemma in determining the geoid as well as the orthometric heights. Furthermore, it is not an easy task to ensure that the orthometric heights and the corresponding geoid undulations are consistent, such that the equation $h = H + N$ is satisfied. This is also pointed out clearly by Forsberg and Tscherning (1997), mentioning that "if refined expansions are used for the downward continuation, consistency is lost with the conventional Helmert orthometric heights;" therefore, they suggest one works with height anomalies (or the disturbing potential) related to the Earth's surface as far as possible, and only at the end of the computation chain to shift back to the geoid if neces-

sary, e.g., by using (56). In addition, this proposal is in accordance with the strategy applied for the modeling of the quasigeoid and geoid in Europe, performed at the Institut für Erdmessung (IfE), Leibniz Universität Hannover (e.g., Denker and Torge 1998; Denker et al. 2009).

3.6 The Spectral Combination Technique

The spectral combination technique encompasses all procedures to combine heterogeneous data by spectral weights (depending on spherical harmonic degree n); it was initially developed to combine terrestrial gravity data and a global geopotential model in an optimal way for the purpose of calculating the geoid or quasigeoid. The spectral combination approach is based on the Laplace surface harmonics derived from different data sets, which are then combined by employing spectral weights. The method was promoted mainly by Sjöberg (1980, 1981, 2003) and Wenzel (1981, 1982), with the basic idea of the procedure already being outlined in Moritz (1976).

The development of the basic formulas is based on the spherical harmonic expansion of the disturbing potential (110) as well as the spectral relations given in (116)–(120). The following derivations are consistently based on the spherical and constant radius approximation (see also previous sections), assuming that the observations are given on a sphere with radius $r = R$. The first data set to be considered is the global geopotential model, giving the disturbing potential Laplace surface harmonics referring to $r = R$ in the form

$$T_n^M(\theta,\lambda,R) = \left(\frac{a}{R}\right)^{n+1} T_n^M(\theta,\lambda,a) = \left(\frac{a}{R}\right)^{n+1} \sum_{m=-n}^{+n} \overline{T}_{nm}^M \, \overline{Y}_{nm}(\theta,\lambda)\,, \qquad (144)$$

which can be evaluated by means of the given coefficients $\overline{T}_{nm}^M$.

On the other hand, corresponding surface harmonics can also be deduced from gravity anomalies in the form

$$T_n^G(\theta,\lambda,R) = \frac{R}{n-1}\Delta g_n^G(\theta,\lambda,R) = \frac{R}{4\pi}\frac{2n+1}{n-1}\iint_\sigma \Delta g(\theta',\lambda',R)\,P_n(\cos\psi)\,d\sigma\,, \qquad (145)$$

where $\Delta g_n^G(\theta,\lambda,R)$ is derived analogous to (113).

The combined disturbing potential surface harmonic can now be computed as the weighted mean in the form

$$\hat{T}_n(\theta,\lambda,R) = w_n^M T_n^M(\theta,\lambda,R) + w_n^G T_n^G(\theta,\lambda,R)\,, \qquad (146)$$

where $w_n{}^M$ and $w_n{}^G$ are the spectral weights related to the geopotential model and the terrestrial gravity data, respectively. The spectral weights can either be determined empirically, e.g., as filter coefficients (Haagmans et al. 2003), or within the

framework of a least-squares adjustment or a least-squares collocation solution (see also Kern 2004). The least-squares methods allow the taking into account of the error estimates of the spectral components $T_n{}^M$ and $T_n{}^G$, which are represented by the corresponding error degree variances (referring to the radius $r = R$)

$$\sigma_n^2(\varepsilon_{T^M}, R) = M\{\varepsilon_{T^M}^2(\theta, \lambda, R)\} = \left(\frac{a}{R}\right)^{2(n+1)} \sum_{m=-n}^{+n} \sigma_{\overline{T}_{nm}^M}^2 \tag{147}$$

for the global geopotential model, and

$$\begin{aligned} \sigma_n^2(\varepsilon_{T^G}, R) &= \left(\frac{R}{n-1}\right)^2 \sigma_n^2(\varepsilon_{\Delta g^G}, R) \\ &= \left(\frac{R}{n-1}\right)^2 \frac{2n+1}{2} \int_0^\pi Cov(\varepsilon_{\Delta g^G}, \varepsilon'_{\Delta g^G}, \psi, R)\, P_n(\cos\psi) \sin\psi \, d\psi \end{aligned} \tag{148}$$

for the terrestrial gravity data; $M\{\cdot\}$ is a homogeneous and isotropic averaging (mean value) operator for the sphere (for details see Moritz 1980), and $\sigma_n^2(\varepsilon_{\Delta g^G}, R)$ are the gravity anomaly error degree variances. For the evaluation of the above two equations, the standard deviations $\sigma_{\overline{T}_{nm}^M}$ of the corresponding coefficients $\overline{T}_{nm}^M$, see (144), and an (isotropic) error covariance function of the terrestrial gravity data are required. In this context, the degree variance approach neglects possibly existing error correlations between individual geopotential model coefficients, and, in addition, error correlations between different data sets (here geopotential model and terrestrial gravity observations) are usually disregarded due to lacking information.

In principle, the above scheme can also be extended to employ further data sets (e.g., satellite altimetry; Wenzel 1982) for the derivation of corresponding disturbing potential surface harmonics and error degree variances. The general least-squares adjustment and collocation solutions with N components can be found, e.g., in Wenzel (1982) and Denker (1988), respectively. Furthermore, the truncation error due to a limited integration cap size may be considered (e.g., Sjöberg 2003), but is omitted here, as it can be made negligibly small (see Sect. 4.4). Returning to the case of only two different data sources, the least-squares adjustment solution gives the following spectral weights for the gravity components:

$$w_n^G = \frac{\sigma_n^2(\varepsilon_{T^M}, R)}{\sigma_n^2(\varepsilon_{T^M}, R) + \sigma_n^2(\varepsilon_{T^G}, R)}. \tag{149}$$

Correspondingly, the weights $w_n{}^M$ can be derived, and the sum of both weights may be expressed as

$$s_n = w_n^M + w_n^G, \tag{150}$$

yielding $s_n = 1.0$ for the least squares adjustment solution (as well as the case of empirically determined weights; e.g., Haagmans et al. 2003), and $s_n \leq 1.0$ for the collocation solution due to the smoothing property inherent in this method.

Combining (146) and (150) in the form $w_n^M = s_n - w_n^G$ gives the following result for the combined disturbing potential surface harmonics:

$$\begin{aligned} \hat{T}_n(\theta,\lambda,R) &= s_n T_n^M(\theta,\lambda,R) + w_n^G \left(T_n^G(\theta,\lambda,R) - T_n^M(\theta,\lambda,R) \right) \\ &= \hat{T}_n^M(\theta,\lambda,R) + \hat{T}_n^G(\theta,\lambda,R) . \end{aligned} \tag{151}$$

The major advantage of rewriting the surface harmonics terms in the above equation is, that this basically results in a remove–compute–restore procedure, i.e., the first part of (151) is the usual geopotential model component (for s_n = 1.0), and the second part is related to the difference between the terrestrial gravity anomalies and the corresponding global model values. This yields significant advantages in the numerical evaluation, because the difference quantities are small and average out at larger distances (see also below). Now, summing up all combined surface harmonics $\hat{T}_n(\theta,\lambda,R)$ from degrees 2 to ∞, and considering (144) and (145), yields the final computation formulas for the disturbing potential:

$$\hat{T}(\theta,\lambda,r) = \hat{T}^M(\theta,\lambda,r) + \hat{T}^G(\theta,\lambda,r) , \tag{152}$$

with the contribution from the global geopotential model

$$\hat{T}^M(\theta,\lambda,r) = \sum_{n=2}^{\infty} s_n \left(\frac{a}{r} \right)^{n+1} \sum_{m=-n}^{+n} \overline{T}_{nm}^M \overline{Y}_{nm}(\theta,\lambda) , \tag{153}$$

and the terrestrial gravity data

$$\hat{T}^G(\theta,\lambda,r) = \frac{R}{4\pi} \iint_{\sigma} \left(\Delta g(\theta',\lambda',R) - \Delta g^M(\theta',\lambda',R) \right) W(\psi,r)\, d\sigma , \tag{154}$$

associated with the (modified Stokes) kernel

$$W(\psi,r) = \sum_{n=2}^{\infty} \left(\frac{R}{r} \right)^{n+1} w_n^G \frac{2n+1}{n-1} P_n(\cos\psi) . \tag{155}$$

In (154), Δg^M are the gravity anomalies related to the global geopotential model. The global model is used in a remove–compute–restore fashion, i.e., the residual anomalies are used to compute the residual disturbing potential, and finally the disturbing potential contribution from the global model is added. However, this procedure can be applied to Stokes's formula as well. Hence, the only difference between the spectral combination approach and Stokes's formula relates to the spectral weights $w_n{}^G$ in (155); thus Stokes's formula results as a special case of the above formulas by setting all weights $w_n{}^G = 1.0$ for degrees n equal 2 to ∞. There-

fore, while the Stokes formula always extracts all degrees from 2 to ∞ from the terrestrial gravity data, the spectral weights allow control of which degrees are taken from the terrestrial gravity data; e.g., only the short wavelengths should be computed from the gravity data, while the long wavelength structures should be defined mainly by a global geopotential model (e.g., from GRACE, GOCE, etc.). Another important feature of the (modified Stokes) kernel in (155) is that the kernel function remains finite if the weights go to zero for very high degrees or the summation is limited to some maximum degree (e.g., because mean gravity anomalies are utilized); hence, in principle, no special consideration of the inner zone contribution is required, but due to the rapid change of the integration kernel near $\psi = 0°$ it is recommended to integrate numerically the kernel function within the innermost zone (see also Sect. 4.4). Lastly, the zero-degree and first-degree terms of T are omitted again in the above equations (see notes related to the Stokes integral in Sect. 3.3).

In addition, the spectral combination technique also permits the derivation of error estimates for the results based on the degree variance approach. Based on (151) and (152), the error estimates for the combined disturbing potential $\hat{T}$ can be derived by straightforward error propagation. The error covariance function (related to points P and P') is given by

$$Cov(\varepsilon_{\hat{T}}, \varepsilon'_{\hat{T}}, \psi, r, r') = \sum_{n=2}^{\infty} \left(\frac{R^2}{rr'} \right)^{n+1} \sigma_n^2(\varepsilon_{\hat{T}}, R)\, P_n(\cos\psi)\,, \tag{156}$$

with the error degree variances of the combined disturbing potential

$$\sigma_n^2(\varepsilon_{\hat{T}}, R) = \begin{cases} (s_n - w_n^G)^2 \sigma_n^2(\varepsilon_{TM}, R) + (w_n^G)^2 \sigma_n^2(\varepsilon_{TG}, R) & \text{for } n \le n_{max} \\ \sigma_n^2(\varepsilon_{TG}) & \text{for } n > n_{max} \end{cases}, \tag{157}$$

where n_{max} is the maximum degree of the global geopotential model employed.

The spectral combination approach results in integral formulas, which initially have to be evaluated over the entire unit sphere σ. However, as residual anomalies $\Delta g – \Delta g^M$ are employed in (154), a limited integration to some maximum distance ψ_{max} (spherical cap σ_0) should lead to only a small truncation error. This truncation error (also denoted as omission error) may be estimated based on Molodensky's truncation coefficients (e.g., Sjöberg 2003) or by means of the frequency transfer function (Wenzel 1982). The latter approach is outlined in the following. Assuming that a limited integration of (154) over a spherical cap σ_0 results in $\tilde{T}^G$ (instead of $\hat{T}^G$), which may be expressed by corresponding Laplace surface harmonics $\tilde{T}_n^G$ (related to $r = R$), the truncation error can be expressed as

$$\begin{aligned}\varepsilon_n^{tr} &= \hat{T}_n^G - \tilde{T}_n^G = w_n^G (T_n^G - T_n^M) - \tilde{T}_n^G = (T_n^G - T_n^M)\left(w_n^G - \frac{\tilde{T}_n^G}{T_n^G - T_n^M} \right) \\ &= (T_n^G - T_n^M)(w_n^G - FTF_n)\,,\end{aligned} \tag{158}$$

where the relation (151) is considered with the independent variables being dropped for the sake of simplicity. After some mathematical manipulations, the frequency transfer function, known from signal processing, follows as

$$FTF_n = \frac{n-1}{2} \int_{\psi=0}^{\psi_{\max}} W(\psi, R)\, P_n(\cos\psi) \sin\psi \, d\psi \,, \tag{159}$$

and, corresponding to (156), the covariance function of the truncation error is given by

$$Cov(\varepsilon^{tr}, \varepsilon^{tr'}, \psi, r, r') = \sum_{n=2}^{\infty} \left(\frac{R^2}{rr'} \right)^{n+1} \sigma_n^2 (T^G - T^M, R)(w_n^G - FTF_n)^2 P_n(\cos\psi)\,, \tag{160}$$

with

$$\sigma_n^2 (T^G - T^M, R) = \begin{cases} \sigma_n^2 (\varepsilon_{T^M}, R) + \sigma_n^2 (\varepsilon_{T^G}, R) & \text{for } n \le n_{\max} \\ \sigma_n^2 (T, R) + \sigma_n^2 (\varepsilon_{T^G}) & \text{for } n > n_{\max} \end{cases}, \tag{161}$$

where $\sigma_n^2(T, R)$ are the disturbing potential (signal) degree variances, which have to be derived from a given model, e.g., the degree variance model of Tscherning and Rapp (1974). Finally, the spectral combination approach can be extended to other input and output gravity field parameters; examples can be found in Wenzel (1982), Denker (2003), and Wolf (2007). Moreover, an extension of the spectral combination technique by a heterogeneous error model, with several accuracy classes for the gravity data, was investigated by Behrend (1999), while the use of a full error covariance matrix for the geopotential model has not yet been attempted. In addition, numerical results are provided in Sect. 4.

3.7 Least-Squares Collocation

Within the framework of physical geodesy, least-squares collocation (LSC) is a method for determining the anomalous gravity field by a combination of geodetic observations of different kinds (Moritz 1980). LSC allows the calculation of unknown deterministic parameters (e.g., station coordinates), and besides being able to propagate the input data noise into the results, it can utilize as input as well as predict (output) heterogeneous signals related to the anomalous gravity field; hence, LSC can be considered as a method, combining least-squares adjustment, filtering, and prediction (Moritz 1980). The mathematical foundation of LSC is

related to the fields of statistics and functional analysis, in particular the theory of reproducing kernel Hilbert spaces. The method was introduced in geodesy by Moritz (1962), while Krarup (1969) succeeded in unifying the functional analytic and statistical viewpoints. Further information on the mathematical foundation of LSC can be found, e.g., in the articles from Tscherning (1985, 1986, 1994), Sansò (1986), and the textbooks from Meschkowski (1962) and Moritz (1980).

The simultaneous determination of station coordinates and gravity field quantities is denoted as "integrated" or "operational geodesy" (e.g., Eeg and Krarup 1973; Grafarend 1978b; Hein 1986); however, this approach has not gained much acceptance in practice because it is extremely computation-intensive. Therefore, only the parameter-less case of LSC (least-squares prediction) is discussed briefly in the following. The basic formula for the prediction of signals in unsurveyed points is

$$\hat{\mathbf{s}} = \mathbf{C}_{\mathbf{st}}(\mathbf{C}_{\mathbf{tt}} + \mathbf{C}_{\mathbf{nn}})^{-1}\mathbf{l} = \mathbf{C}_{\mathbf{st}}\,\bar{\mathbf{C}}^{-1}\mathbf{l}, \qquad \bar{\mathbf{C}} = \mathbf{C}_{\mathbf{tt}} + \mathbf{C}_{\mathbf{nn}}, \tag{162}$$

where $\mathbf{C}_{\mathbf{tt}}$ and $\mathbf{C}_{\mathbf{st}}$ are the auto and cross covariance matrices related to the signals $\mathbf{t}$ at the observation sites and $\mathbf{s}$ at the unsurveyed stations, $\mathbf{l}$ is the observation vector, consisting of a signal and noise component (i.e., $\mathbf{l} = \mathbf{s} + \mathbf{n}$), and $\mathbf{C}_{\mathbf{nn}}$ is the noise covariance matrix. The LSC solution is based on a least-squares hybrid minimum condition on the weighted quadratic sum of the signal and noise parts, or equivalently, the prediction results satisfy the least error variance condition (Moritz 1980). The input and output signals may be heterogeneous (e.g., T, Δg, ξ, η, etc.), but as all these quantities depend on the (harmonic) disturbing potential T, corresponding relations must also be considered for the calculation of the signal covariances in the matrices $\mathbf{C}_{\mathbf{tt}}$ and $\mathbf{C}_{\mathbf{st}}$. In this context, the covariance function of the disturbing potential, $K(P,P')$, is typically chosen as the basic covariance function, from which all other required covariances are derived by covariance propagation, considering the harmonicity of T and the analytical relations between T and its functionals. Moreover, it is assumed that the signal and noise quantities have an expected (or mean) value equal to zero; regarding the disturbing potential T, this condition is fulfilled at the global scale if T does not contain a zero-degree harmonic.

The (spatial) homogeneous and isotropic covariance function of the disturbing potential is given by

$$\begin{aligned} K(P,P') &= Cov(T,T',\psi,r,r') = M\left\{T(\theta,\lambda,r)\cdot T(\theta',\lambda',r')\right\} \\ &= \sum_{n=2}^{\infty}\left(\frac{R^2}{rr'}\right)^{n+1}\sigma_n^2(T,R)\,P_n(\cos\psi)\,, \end{aligned} \tag{163}$$

with the disturbing potential degree variances

$$\sigma_n^2(T,R) = M\left\{T_n^2(\theta,\lambda,R)\right\}, \tag{164}$$

where $M\{\cdot\}$ is the homogeneous and isotropic averaging (mean value) operator. In principle, the covariance function cannot be exactly determined empirically, as this would require a complete knowledge of the disturbing potential function. Therefore, an empirical covariance function has to be used, which is typically obtained by fitting an analytical expression to the given data within the area of interest (local covariance function; for details see Goad et al. 1984). In this context, the degree variance model of Tscherning and Rapp (1974), resulting in closed formulas for all covariance expressions, is widely used, and a corresponding planar model was derived by Forsberg (1987). Furthermore, for the residual disturbing potential with respect to a global geopotential model, the degree variances in (163) have to be replaced by corresponding error degree variances of the global model up to the maximum degree n_{max} of the global model. Finally, it is noted that the LSC estimates have the minimum variance property if the kernel function is identified with the empirical covariance function, while this property is lost if arbitrary kernel functions are employed according to the analytical aspect of collocation (Moritz 1980).

LSC also allows the computation of error estimates, e.g., the error covariance matrix for the signals estimated by (162) is given by

$$\mathbf{E}_{ss} = \mathbf{C}_{ss} - \mathbf{C}_{st}(\mathbf{C}_{tt} + \mathbf{C}_{nn})^{-1}\mathbf{C}_{ts} \,. \tag{165}$$

The main advantage of LSC is its flexibility, being able to handle all quantities related to the disturbing potential as input and output data, including the associated error estimates. The data may be located at arbitrary (discrete) points in space, and hence no additional gridding is necessary. Furthermore, the varying heights of the observation and prediction sites are taken into account if LSC is applied spatially; the method inherently includes the harmonic continuation, and therefore the non-level surface corrections (Molodensky terms) are irrelevant in this case (Forsberg and Tscherning 1997). Usually, the spatial covariance functions, e.g., (163), are based on spherical approximations, but this is not considered as a serious problem when residuals with respect to a global geopotential model are processed (for further discussions see Tscherning 2004).

The main drawback of LSC is, however, that a system of equations as large as the number of observations has to be solved, see (162). In addition, numerical problems may arise from identical points or points at a short distance, when, depending on the input data noise, the matrix $\bar{\mathbf{C}}$ may become nearly singular; therefore, such duplicate points should be excluded from the input data. Today, with modern computers, several thousands of observations can be handled without problems. Moreover, the computational effort can be significantly reduced for the simple case of interpolating a single gravity field quantity (typically gravity anomalies), as then the input data can be restricted to several points near the prediction site. Furthermore, the fast collocation method can be applied, requiring gridded data sets (Sansò and Tscherning 2003).

Finally, the LSC method may be considered as data-driven, starting from discrete data and information about their noise and signal covariances, while the GBVP solutions by integral formulas may be characterized as model-driven (Sideris 2011a). For the limiting case of homogeneous and continuous data, least-squares collocation transforms into integral formulas such as Stokes's integral, etc. (Moritz 1976).

3.8 Astronomical Leveling

More recently, the method of astronomical leveling has again attracted some interest within the framework of special projects, including the high-precision geoid and quasigeoid determination along selected lines as well as the independent validation of corresponding regional gravimetric models and global geopotential models (e.g., Hirt and Flury 2008; Hirt et al. 2008; Ihde et al. 2010). The efficiency of astronomical latitude and longitude observations could be substantially improved by using transportable zenith cameras together with CCD technology, precise electronic tilt meters, and GNSS for timing and positioning, associated with automated processing of the digital images. At present, two such systems exist, one at the Institut für Erdmessung (IfE), Leibniz Universität Hannover, and the other at the ETH (Eidgenössische Technische Hochschule), Zurich, Switzerland (Bürki et al. 2004; Hirt 2004). Besides the enhanced observation efficiency, allowing the occupation of 10–20 stations per night, the accuracy could also be substantially improved; while the new digital zenith camera systems reach an observation accuracy of 0.05″ (1 h observation time) to 0.08″ (20 min observation time; see Hirt and Seeber 2008), the standard classical analog zenith camera, astrolabe, and theodolite systems attained an accuracy of at most 0.5″ (e.g., Wildermann 1988), often accompanied by systematic errors, in particular in the longitudes (Bäumker 1984).

The astronomical latitude and longitude provide the direction of the gravity vector and hence the inclination of the corresponding level surface. The deflection of the vertical describes the angle between the actual plumb line and a reference direction; the deflection of the vertical is a vectorial quantity and usually expressed by its components in north–south and east–west direction. Besides the deflection of the vertical according to Molodensky (see Sect. 3.2), the deflection of the vertical at the Earth's surface with respect to the ellipsoidal normal at P (Helmert's definition) and the corresponding quantity at the geoid (Pizzetti's definition) are to be distinguished (e.g., Torge 2001). Thus the components of the deflection of the vertical according to Helmert are given by

$$\xi_P^H = \Phi_P - \varphi_P \,, \qquad \eta_P^H = (\Lambda_P - \lambda_P)\cos\varphi_P \,. \tag{166}$$

Integrating the deflections of the vertical along a path on the geoid or the Earth's surface yields the geoid undulation difference

$$\Delta N_{12} = N_2 - N_1 = -\int_1^2 \varepsilon^0 \, ds = -\int_1^2 \varepsilon^H \, ds - \int_1^2 \delta\varepsilon \, ds = -\int_1^2 \varepsilon^H \, ds - E_{12} \,, \qquad (167)$$

where ε^0 and ε^H are the azimuthal deflection components (in the azimuth α) according to Pizetti and Helmert at the geoid and Earth's surface, respectively, e.g.,

$$\varepsilon^H = \xi^H \cos\alpha + \eta^H \sin\alpha \,, \qquad (168)$$

$\delta\varepsilon$ is the correction for the curvature of the plumb line, and E_{12} is the orthometric height reduction known from geometric leveling (for further details see Torge 2001).

Regarding the height anomalies, the relation

$$d\zeta = \frac{d\zeta}{ds} ds + \frac{d\zeta}{dh} dh \qquad (169)$$

has to be utilized (Molodenskii et al. 1962), which considers that the height anomalies are not related to a level surface, in contrast to the geoid undulations treated above (i.e., $dN = (dN/ds)\, ds = \varepsilon^0 \, ds$ can be considered as a special case of (169)). Considering that $d\zeta/ds$ is the azimuthal deflection component according to Molodensky, while taking $d\zeta/dh$ from (141), leads to

$$\Delta\zeta_{12} = \zeta_2 - \zeta_1 = -\int_1^2 \varepsilon^M \, ds - \int_1^2 \frac{\Delta g}{\gamma} dh \,. \qquad (170)$$

Alternatively, utilizing the deflections of the vertical according to Helmert, the above equation can be expressed as

$$\Delta\zeta_{12} = \zeta_2 - \zeta_1 = -\int_1^2 \varepsilon^H \, ds - E_{12}^N \,, \qquad (171)$$

where E_{12}^N is the normal height reduction; for a detailed derivation of the equations for the height anomalies see Campbell (1971) and Torge (2001). The negative sign of the ε components in (167), (170), and (171) follows from the sign conventions for the geoid/quasigeoid heights and the deflections of the vertical.

The accuracy of astronomical leveling mainly depends on the accuracy of the vertical deflections as well as the quality of the interpolation between the observation sites. The latter component, i.e., the interpolation error, arises from the approximation of the line integrals by discrete observations; it can be substantially reduced by considering topographic information. The purely random observation errors propagate with the square root of the number of individual set-ups. The standard deviation of ΔN_i or $\Delta\zeta_i$ from a single set-up is given by $\sigma_{\Delta N_i\,[\mathrm{mm}]} = 4.8\, \sigma_{\varepsilon['']}\, \Delta S_{[\mathrm{km}]}$, where $\sigma_{\varepsilon['']}$ is the vertical deflection standard deviation in arc seconds, and ΔS is the station distance in kilometers. Hence, for a line

of length S with n segments ($n = S/\Delta S$), the standard deviation is given by $\sigma_{\Delta N\,[\mathrm{mm}]} = 4.8\ \sigma_{\varepsilon[''\,]}\ \Delta S_{[\mathrm{km}]}\sqrt{n}$, assuming uncorrelated errors; on the other hand, errors with a correlation of $r = 1.0$ and systematic errors propagate linearly with n or the distance S, resulting in $\sigma_{\Delta N\,[\mathrm{mm}]} = 4.8\ \sigma_{\varepsilon[''\,]}\ S_{[\mathrm{km}]}$. Regarding the correlation due to anomalous refraction, Hirt and Seeber (2008) mention values of $r \approx 0.05$ between single observations.

Regarding the digital zenith camera results, an accuracy of about 0.1″ can be safely assumed for a standard observation period of 20 min (Hirt and Seeber 2008), which leads to a formal accuracy of the ΔN or $\Delta\zeta$ quantities at the few millimeters level for shorter lines up to about 100 km, depending on the station distance. Accordingly, for longer lines of 500–1,000 km, the random errors accumulate to a level of about 1–3 cm, and systematic errors become more critical, e.g., a systematic error of only 0.01″ transforms into a corresponding ΔN or $\Delta\zeta$ error of 2.4 cm (S = 500 km) and 4.8 cm (S = 1,000 km), respectively. Thus, on long traverses of several 100 km, the astrogeodetic results are getting into competition with the combined satellite (e.g., GOCE) and gravimetric solutions, as indicated by the practical results for two 500 km long traverses in Germany (e.g., Ihde et al. 2010). On the other hand, an independent verification of the astrogeodetic results at the millimeter level for spatial scales of a few 100 m to several 10 km is extremely difficult, as practically no other comparable data exists. While geometric leveling is accurate at the millimeter level, the GNSS techniques usually give worse results due to station dependent effects, etc.; however, based on 48-h GPS observations and sophisticated new approaches to reduce station dependent effects, Hirt et al. (2010) quote an RMS difference between GPS/leveling and astrogeodetic results of about 2–3 mm (max. 5 mm). In addition, considering the spectral relation between gravity anomalies and vertical deflection components with a conversion factor of 6.7 mGal/″ for higher degrees n, it should also be possible to verify at least the fine structures of the astrogeodetic calculations, provided that the local and regional gravity anomaly field is reasonably represented by observations, while the far-zone is modeled by a global geopotential model; in principle, an accuracy of 0.1″ for the astronomical observations corresponds to an accuracy of about 0.7 mGal in terms of gravity, which is easily achieved by regional gravimetric surveys, being in most instances more accurate by at least one order of magnitude. To the best knowledge of the author, such an experiment is still lacking, and therefore would be an interesting topic for the future.

The main advantage of the astrogeodetic method is its independence from any data outside the area of calculation, in contrast to the gravimetric method where basically global data coverage is needed. Therefore, the main applications for the astrogeodetic method are seen in local geoid and quasigeoid calculations (especially for the case that gravity field observations in the surrounding areas are lacking or inaccessible for political reasons) as well as the independent validation of corresponding gravimetric results and global geopotential models up to distances of a few 100 km. A regional gravity field survey, particularly for larger areas, can be

performed more effectively by land, sea, and airborne gravimetry than by astronomical observations, which require more time per station occupation and have to be done during the night outside normal working hours.

3.9 The Remove–Compute–Restore Technique and Topographic Effects

In practice, local and regional gravity field modeling is usually based on discrete data covering the area of interest and the immediate surroundings. This leads to two difficulties. First, the very short wavelength gravity field information is not properly represented by the discrete observations, leading to aliasing effects; this problem is counteracted by employing digital elevation models to obtain the high-frequency gravity field signals. Second, as the observation data cover only a certain region, the long wavelength gravity field information (i.e., longer than the extent of the region) must be computed in another way; this problem is remedied by using a state-of-the-art global geopotential model. Hence, the short and long wavelength gravity field structures are obtained from digital elevation models and a global geopotential model, respectively, while the medium wavelength field structures are derived from the regional discrete gravity field observations. This leads directly to the remove–compute–restore (RCR) technique, in which the short and long wavelength information is first removed from the observations, then the residual quantities are used for gravity field modeling (e.g., transformation from residual gravity to height anomalies), while finally the short and long wavelength contributions are restored again.

The general scheme of the RCR technique is based on a residual disturbing potential given by

$$T^{res} = T - T^{M} - T^{T} , \tag{172}$$

where T^M and T^T are the contributions from the global geopotential model and the topographic information (or more generally the anomalous masses; see below). Correspondingly, all observations, described as linear functionals L of T, are consistently reduced by

$$L_{obs}(T^{res}) = L_{obs}(T) - L_{obs}(T^{M}) - L_{obs}(T^{T}) , \tag{173}$$

where the global geopotential model should be utilized rigorously as a high-degree reference field (see Sect. 3.2). Then, after applying the gravity field modeling techniques, the effects of the global geopotential model and the topography are restored, leading to the final predictions

$$L_{pred}(\hat{T}) = L_{pred}(\hat{T}^{res}) + L_{pred}(T^{M}) + L_{pred}(T^{T}) . \tag{174}$$

The removal of the short and long wavelength gravity field information corresponds to a spectral (low-pass and high-pass) filtering; this leads to residual quantities which are typically much smaller and smoother (as well as statistically more homogeneous and isotropic) than the original ones, facilitating, e.g., the tasks of interpolation, gridding, as well as field transformations by integral formulas or LSC, with the additional side effect that the collection of observational data can be restricted to the region of interest plus a narrow edge zone around it. The RCR technique has become a standard procedure for local and regional gravity field modeling as documented in textbooks (e.g., Torge 2001) and numerous journal articles (e.g., Sideris 2011b; Forsberg 2010; Denker et al. 2009; Tscherning 2004; Smith and Roman 2001).

Until recently, high-degree geopotential models were mainly developed up to degree and order $n_{max} = 360$ from satellite and terrestrial data, corresponding to a resolution of 0.5° or about 55 km; examples are the EGM1996 (Lemoine et al. 1998) as well as the EIGEN (e.g., Förste et al. 2008a, b) and GGM (e.g., Tapley et al. 2007) models. However, the situation changed considerably with the advent of the EGM2008 model (Pavlis et al. 2008), which includes coefficients up to spherical harmonic degree $n_{max} = 2{,}190$, corresponding to a resolution of 5' or about 9 km. Hence, regarding areas with high-quality data included in EGM2008, it should only be necessary to add the very short wavelength gravity field structures (about 2–3 cm RMS for the geoid/quasigeoid) by means of local gravity and terrain data, but the situation may be quite different in areas where only poor data were available for EGM2008. At present, there is not very much practical experience on how to make optimal use of the ultra-high-degree EGM2008 model in regional gravity field modeling, and certainly more investigations on this topic are needed (e.g., according to Forsberg 2010). Further discussions in this direction, e.g., related to the impact on topographic reductions, follow below and in Sect. 4.4.

In mountainous regions, the gravity field is strongly correlated with the local topography; the gravitational attraction of the topographic masses causes a strong signal, which dominates at shorter wavelengths. Therefore, topographic information can be used to smooth the gravity field prior to any modeling process in order to avoid aliasing effects. For example, gravity stations are by tendency located in valleys along roads, and thus the observations are related to a level which is systematically below the average topography. Such aliasing errors can be very big and devastating for gravity field modeling (Forsberg and Tscherning 1997). Besides the direct gravitational effect, the topography implies that the observations are related to a non-level surface, which can be considered by LSC, but requires additional corrections (Molodensky terms) for the integral formula approaches (see Sect. 3.4).

In addition to the topography, other information about local density anomalies, e.g., due to salt domes, etc., may also be taken into account (Denker 1988). This leads to a so-called mass model, which may be considered as “source information” (the masses are the sources of the gravitational field), in contrast to the “effect

information" from a global geopotential model (Sünkel 1983). The effect of the anomalous masses can be computed by Newton's law according to (19), giving

$$L_{obs}(T^T) = G\iiint_V \Delta\rho\, L_{obs}\left(\frac{1}{l}\right) dv\,, \tag{175}$$

where $\Delta\rho$ are (appropriately defined) density anomalies (see Forsberg 1984; Forsberg and Tscherning 1997). In this context, it is important to note that the topographic (or mass) potential T^T has to be a harmonic function, because otherwise the above RCR scheme is not valid (Forsberg and Tscherning 1997). This condition is fulfilled if either a fixed area is taken into account (e.g., specified by latitude and longitude limits), or if the reductions are – at least in principle – computed globally. The classical terrain reduction as well as reductions based on fixed spherical cap sizes do not fit into this scheme, as for every new station another area of the mass model is evaluated.

Different terrain reduction schemes and the associated advantages and disadvantages are discussed in detail in Forsberg and Tscherning (1981, 1997) as well as Forsberg (1984). The complete topographic (or Bouguer) reduction is not suited for gravity field modeling because it causes a very large change of the potential function due to the complete removal of all topographic masses (ideally shifted to infinity). The topographic-isostatic reduction is useful for gravity field modeling as it provides a smooth residual field; however, it has the disadvantage of generating long wavelength signals, and thus also the potential coefficients of a global model need to be reduced accordingly, which is a costly and time-consuming procedure. Furthermore, as a global high-degree spherical harmonic reference expansion is used within the RCR procedure, which obviously also includes the effect of the global topography, preferably only short wavelength topographic effects should be considered, leading to the so-called residual terrain model (RTM) reduction, introduced by Forsberg and Tscherning (1981).

The RTM procedure is based on a smooth reference topography surface, usually obtained by applying a moving average or other filter (e.g., a Gaussian filter; see Forsberg 2010) to the existing high-resolution digital elevation model (DEM), and then only the differences between the actual topography and the reference topography are taken into account within the reduction process; this leads to balanced positive and negative density anomalies, representing areas where the topography is either above or below the reference topography, and hence the RTM effects will cancel out for zones at larger distances (Forsberg and Tscherning 1997). Thus, the remote contributions become negligibly small, and the RTM reduction computations can be limited to a distance of about two to three times the resolution of the reference topography (Forsberg and Tscherning 1997). In summary, the RTM reduction has the advantage that only short wavelength gravity field structures are considered (without changing the long wavelengths), and in addition the reductions can be limited to some distance ψ_{max}, while still satisfying the harmonicity condition for the topography potential function T^T. Furthermore, the RTM reduced grav-

ity anomalies based on a mean elevation surface of about 100 km resolution will typically be quite similar in magnitude to the isostatic anomalies (Forsberg and Tscherning 1997).

The mass displacements associated with the RTM technique (also denoted as regularization) lead to the situation that stations above the mean elevation surface are left in the mass-free domain, whereas the gravity field quantities at stations in valleys with $h_P < h_{ref}$ are transformed into corresponding quantities inside the masses, where the associated potential function is not harmonic. The latter problem is usually remedied by a simple "harmonic correction", which is based on downward continuation through a Bouguer plate, being valid only if the reference topography is sufficiently long-wavelength (Forsberg and Tscherning 1997; Forsberg 2010). The non-harmonicity of the reduced potential below the reference height surface is considered today as a major theoretical problem with the RTM method (Forsberg and Tscherning 1997), and some attention was given to it recently by Elhabiby et al. (2009), Omang et al. (2011), and Forsberg (2010). In principle, the quantities related to a harmonically continued topography potential function T^T are needed, which may be obtained by first removing the effect of the entire topography, followed by a harmonic continuation of the observations to the reference elevation surface, plus finally the restoration of the effect of the reference topography. Another option would be to condense the masses of the reference topography at a lower level. For further details on this topic, requiring additional investigations, see the references mentioned above.

The RTM concept is widely applied in practice, employing a mean elevation surface (reference topography) with a resolution ranging typically from 100 km to 50 km, but also smaller values have been applied (e.g., Forsberg and Tscherning 1997; Denker 1988; Forsberg 2010). In this context, Forsberg (2010) describes quasigeoid computations based on local gravity and terrain data in connection with the full EGM2008 model (n_{max} = 2,190) and RTM reductions associated with a 5' and 30' reference topography, as well as a computation based on EGM2008 with n_{max} = 360 and RTM 30' reductions. In comparison to GPS/leveling data, the two solutions based on the RTM 30' reductions and EGM2008 to n_{max} = 360 and 2,190 showed the best performance (with a slight advantage for the results using EGM2008 to n_{max} = 2,190), while the solution with the RTM 5' reductions and EGM2008 (n_{max} = 2,190) fitted less well, which was attributed to the approximation errors in the harmonic correction (as discussed above). Interestingly enough, the solution based on EGM2008 to n_{max} = 2,190 and the RTM 30' reductions showed the best performance, and Forsberg (2010) mentions that this is "indicating that the 'double accounting' of the topography does not matter in practice (which it should not, since the remove–restore principle will account for this)."

The practical computation of terrain effects requires high-resolution DEMs and is mostly based on prism integration in the space domain, augmented by the much faster (but sometimes more approximate) FFT methods (e.g., Forsberg 1984; Schwarz et al. 1990; Forsberg and Tscherning 1997; Sideris 2011b). Regarding a rectangular prism of constant density $\Delta\rho$, closed formulas exist for the gravitational

potential and its derivatives (MacMillan 1958; Forsberg 1984; Denker 1988), e.g., the potential at a point P, located at the origin of a local Cartesian coordinate system (x, y, z), is given by

$$T^{prism} = G\Delta\rho \left| \left| \left| xy \ln(z+d) + xz \ln(y+d) + yz \ln(x+d) \right.\right.\right. - \frac{x^2}{2} \arctan \frac{yz}{xd} - \frac{y^2}{2} \arctan \frac{xz}{yd} - \frac{z^2}{2} \arctan \frac{xy}{zd} \Big|_{x1}^{x2} \Big|_{y1}^{y2} \Big|_{z1}^{z2} , \quad (176)$$

$$\text{with} \qquad d = \sqrt{x^2 + y^2 + z^2} .$$

The computation of terrain effects related to other gravity field parameters is described in detail in Forsberg (1984), including a computer program (TC) for the efficient evaluation of large terrain grids with sophisticated features such as an inner zone densification, the consideration of the given station elevations, a simple Earth curvature correction, as well as the use of a detailed and coarse grid for the inner and outer zones, respectively, associated with an automatic switching between different computation formulas in order to save computing time and to obtain stable results. The use of the rectangular prisms is considered as sufficiently accurate in connection with the RTM method, as the differences between rectangular and spherical bodies will also cancel out to some extent within the RCR procedure. However, further studies on this topic are necessary, such as that presented by Heck and Seitz (2007), using the so-called tesseroids based on spherical coordinates.

Finally, it should be noted that the RCR technique can be applied in combination with all gravity field modeling procedures described in the previous sections, ranging from the computation of spherical harmonic models, over the integral formula approaches, least-squares collocation, astronomical leveling, to the application of Molodensky's theory. The whole Molodensky theory may in principle be applied to the original surface free-air data as well as to terrain-reduced data, yielding much smaller correction terms g_n associated with a more stable solution scheme (e.g., Forsberg and Tscherning 1997; Denker and Tziavos 1999).

4 Practical Results

4.1 Data Requirements

Today's demands for accuracy within the scope of regional gravity field modeling are at the level of about 0.01–0.001 m for the geoid/quasigeoid, 1 mGal for gravity anomalies, and 1″ for vertical deflection components, e.g., regarding applications such as height determination by GNSS or dynamic ocean topography (DOT) modeling, interpolation of gravity data (for leveling stations, etc.), and local geodetic networks. In this context, terrestrial surface free-air gravity anomalies form one of

the most important input data sets because they exist in many regions of the world with good quality and coverage. Regarding the input data requirements with respect to accuracy and resolution, theoretical as well as numerical investigations, including spectral analysis can be utilized. An easy way to gain an idea about the necessary data quality is provided by the degree variance approach, based on the spectral decomposition of the anomalous gravity field. The root mean square (RMS) omission error, describing the gravity field signals above a certain harmonic degree n_{max} (i.e., the terms neglected in a spherical harmonic expansion complete up to degree and order n_{max}), can be computed simply as the square root of the sum of the corresponding degree variances for degrees $n_{max} + 1$ to infinity. The degree variance model of Tscherning and Rapp (1974) with $n_{max} = 10{,}000$ (corresponding to a spatial resolution of 2 km) yields an omission error of about 0.001 m for geoid/quasigeoid heights, 1.4 mGal for gravity anomalies, and 0.2″ for vertical deflection components, while the corresponding values for $n_{max} = 5{,}000$ (corresponding to a spatial resolution of 4 km) are about 0.005 m, 4.8 mGal, and 0.7″, respectively. Regarding high-degree geopotential models, the omission errors for $n_{max} = 360$ (standard over the past decades) and $n_{max} = 2{,}190$ (related to EGM2008; Pavlis et al. 2008) are of interest; for the latter case, the omission error is 0.023 m for geoid/quasigeoid heights, 11.1 mGal for gravity anomalies, and 1.7″ for vertical deflection components, while the corresponding values for $n_{max} = 360$ are 0.227 m, 25.2 mGal and 3.8″, respectively. The latter figures also document that the combination of a global geopotential model with local terrestrial data is important for modeling the complete gravity field spectrum; otherwise, for example, geoid/quasigeoid signals with a magnitude of about 2–4 cm for $n_{max} = 2{,}190$ (see also Jekeli et al. 2009) or a few decimeters for $n_{max} = 360$ are lacking.

The omission error for different gravity field parameters is depicted in Fig. 7, which also gives some insight into the spectral sensitivity of the quantities, the geoid/quasigeoid (or disturbing potential T) signal being concentrated mainly at the longer wavelengths, while for the first and second derivatives of T (Δg, ξ, η, and T_{zz}, respectively; 1 Eötvös (E) = 10^{-9} s^{-2} = 0.1 mGal/km) the signals are progressively focused at the shorter wavelengths. Another useful formula for estimating the omission error for geoid/quasigeoid heights can be deduced from Kaula's rule of thumb (a simple degree variance model, based on the assumption that the standard deviation of a single fully normalized coefficient of the gravitational potential is $\sigma\{\bar{C}_{nm}, \bar{S}_{nm}\} \approx 10^{-5} / n^2$; Kaula 1966), resulting in (see also Forsberg 1993)

$$\sigma_{\text{omission}}^{n\max}(\zeta) = \sqrt{\sum_{n=n_{max}+1}^{\infty} \sigma_n^2(\zeta)} \approx \frac{64_{[\text{m}]}}{n_{max}}. \tag{177}$$

The above formula gives an omission error of 0.006 m for n_{max} = 10,000, 0.013 m for $n_{max} = 5{,}000$, 0.029 m for $n_{max} = 2{,}190$, and 0.18 m for $n_{max} = 360$, which is in reasonable agreement with the results based on the Tscherning and Rapp (1974) model. Aiming at the computation of the geoid or quasigeoid with an accuracy of 0.01 m or better, the preceding simple and straightforward considerations

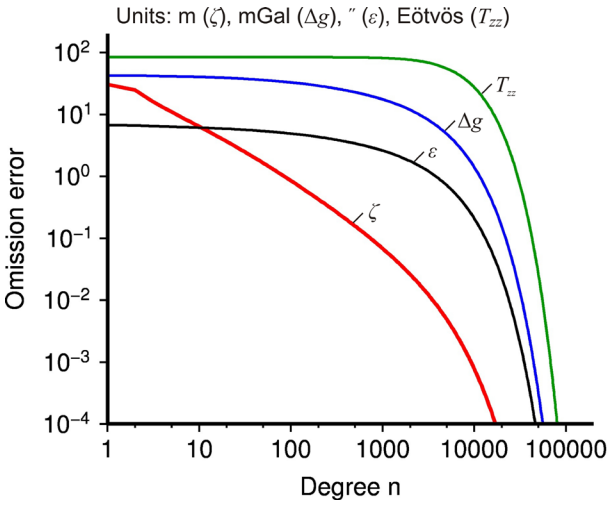

Fig. 7 Omission error for geoid/quasigeoid heights (N, ζ), gravity anomalies (Δg), single vertical deflection components (ε), and vertical gravity gradients (T_{zz})

suggest that corresponding harmonics up to degree and order 5,000–10,000 have to be modeled, requiring input data with a spatial resolution of roughly 2–4 km, while, e.g., the accuracy demands for gravity data are only at the level of about 1 mGal and hence not very severe. However, it has to be noted that these simple thoughts consider only random errors, and, furthermore, the omission and observation errors superimpose each other in the calculations.

On the other hand, small systematic gravity errors, affecting large regions, may also integrate up to significant geoid or quasigeoid errors. A rough estimation of such effects is possible on the basis of the formula for the inner zone geoid/quasigeoid contribution (130). For example, considering a systematic gravity error of 0.1 mGal over a circular cap with radius 100 km or 0.02 mGal over a 500 km cap, respectively, leads in each case to a systematic geoid/quasigeoid error of 0.01 m. With regard to the combination of terrestrial data with GOCE and GRACE geopotential models, the chosen radii approximately correspond to the resolutions where terrestrial data come into play. Therefore, it is desirable to connect at least the gravity base network to modern absolute gravity stations (with an accuracy of 0.01–0.02 mGal or better), while the requirements for regional detail surveys can be relaxed (with acceptable random errors up to about 1 mGal).

Another view on the data requirements is possible by looking at the gravitational effects of typical disturbing density anomalies. For example, in the north German lowlands, many saltdomes exist, which cause quite local gravity field structures. Figure 8 depicts the gravitational effect of a typical salt dome with an extension of $4 \times 4 \times 4$ km^3 and a density contrast of $\Delta\rho = 300$ kg/m^3, with the density of salt usually being lower than that of the surrounding rocks. Therefore, salt domes are frequently connected with (negative) gravity anomalies of about 20–30 mGal, associated with geoid/quasigeoid and vertical deflection effects of 5–6 cm and 2″, respectively. Hence, in order to capture such significant local gravity field varia-

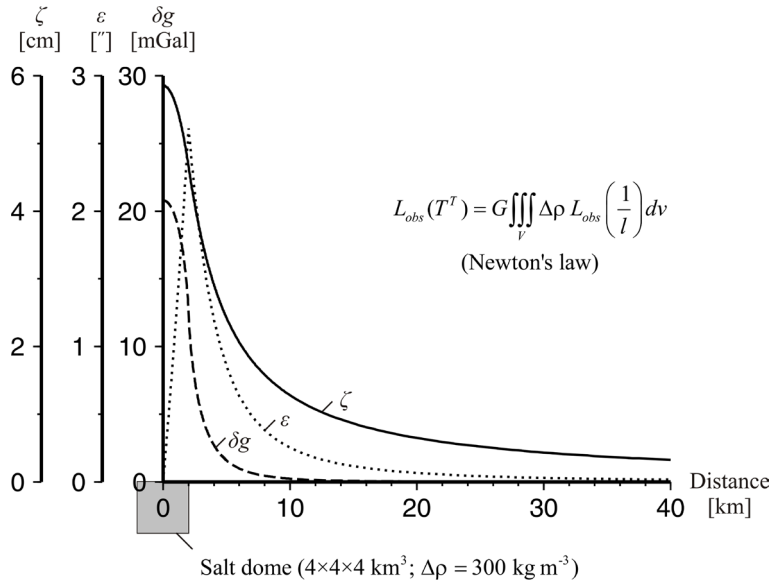

Fig. 8 Gravitational effect of a typical salt dome on height anomalies (ζ,), gravity disturbances (δg) and vertical deflections (ε)

tions, corresponding observations with a sufficient spatial resolution are needed, again leading to data spacings at the few kilometer level.

Besides the gravity observations themselves, the horizontal and vertical coordinates (either gravity field related heights from leveling or ellipsoidal heights from GNSS techniques) of the gravity sites must be known with sufficient accuracy. The station positions are required for the calculation of the normal gravity field parameters and the corresponding anomalous gravity field quantities (regarding the level ellipsoid, only the latitudes and heights are needed), as well as for the determination of the global geopotential model and terrain contributions within the framework of the remove–compute–restore (RCR) procedure. The horizontal and vertical position requirements should roughly conform with the gravity accuracy; considering, e.g., gravity observations with an accuracy of 0.01, 0.1, and 1.0 mGal, an actual gravity gradient of about 0.3 mGal/m for the vertical and 10 mGal/km (maximum) for the horizontal direction, respectively, results in position requirements of about 0.03, 0.3, and 3.0 m (vertically), and 1 m, 10 m, and 100 m (horizontally).

In addition, within the framework of the RCR technique, the digital elevation models (DEMs) must also have a sufficient spatial resolution and accuracy. In this context, comprehensive numerical investigations are presented, e.g., in Li et al. (1995) and Grote (1996); in summary, regarding the targeted modeling accuracies (see above), the DEMs should have a spatial resolution of about 100–1,000 m for alpine to flat areas, while an accuracy of approximately 10 m is sufficient, provid-

ed that, especially for the gravity sites, the available station heights are employed in the computation of the terrain effects, as suggested by Forsberg (1984).

Furthermore, a comprehensive study on the effect of systematic gravity anomaly errors due to gravity, horizontal, and vertical datum inconsistencies is given in Heck (1990), with a similar investigation (for Europe) being presented by Denker (2001). The effect of such small but systematic gravity anomaly errors on the geoid/quasigeoid is predominantly of long wavelength nature, and hence it can be kept small (below the level of 0.01 m) by using a global high-degree satellite geopotential model (from the GRACE or GOCE mission) as a reference (e.g., in connection with the spectral combination approach), while the pure terrestrial solutions based on Stokes's integral may lead to errors at the decimeter level (for further details see Heck 1990 and Denker 2001).

In summary, gravity surveys should preferably be connected to a high-precision gravity base network (relying on absolute gravity observations) in order to avoid large-scale systematic errors; the corresponding accuracies should be about 0.01 mGal for gravity, 0.03 m for the heights, and 1.0 m for the horizontal coordinates, or better, respectively. On the other hand, the accuracy requirements for detail surveys may be relaxed to the level of about 1 mGal and accordingly for the vertical and horizontal positions (see above), provided that the errors are purely random. These figures are also supported by simulation studies based on least-squares collocation, etc. (examples can be found, e.g., in Denker 1988 and Forsberg 1993).

4.2 The European Gravity and Geoid Project

The historical development of geoid and quasigeoid modeling in Europe has been described, e.g., in Torge and Denker (1998). Since the beginning of the 1980s, the Institut für Erdmessung (IfE), Leibniz Universität Hannover (LUH), has been involved in such computations. The first important result was the "European Gravimetric Geoid Number One" (EGG1; Torge et al. 1982); it was based on mean gravity anomalies and had an accuracy at the level of several decimeters. Then, with the advent of the Global Positioning System (GPS), the accuracy demands for the geoid/quasigeoid increased to the centimeter level, which can be achieved only by combining high-resolution point gravity field data with corresponding topographic information and a global geopotential model. In this context, several investigations were carried out initially for very local areas, and regarding a small test network near Hannover, Germany, it was proven for the first time that an agreement between gravimetric and GPS/leveling results at the centimeter level is in fact possible (Denker and Wenzel 1987). These computations were subsequently extended to larger regions and lead to a new quasigeoid model for the whole of Germany (Denker 1989). Based on these experiences, IfE proposed to perform corresponding computations for the whole of Europe; finally, this task was supported by the International Association of Geodesy (IAG), Geoid Sub-Commission for Europe,

and IfE served as the computing center in the period 1990–2003. A major result of this IAG enterprise was the high-resolution European geoid and quasigeoid model EGG1997 (Denker and Torge 1998), based on the global geopotential model EGM1996 (Lemoine et al. 1998) and high-resolution gravity and terrain data available at that time. The evaluation of EGG1997 by GPS and leveling data revealed the existence of long wavelength errors at the level of 0.1–1 ppm, while the agreement over shorter distances up to about 100 km was at the level of 0.01–0.02 m in many areas with good quality and coverage of the input data (Denker and Torge 1998; Denker 1998).

However, after a while, several advancements appeared to be possible, including strongly improved global satellite gravity fields (from the CHAMP, GRACE, GOCE missions), new or updated high-resolution data sets (gravity, terrain, satellite altimetry, GPS/leveling), as well as refined modeling techniques. Thus, a complete re-computation of the European geoid and quasigeoid was considered appropriate and promised significant accuracy improvements, especially at the longer wavelengths. As a result, after the IUGG General Assembly in Sapporo, 2003, when the new structure of the IAG was implemented, it was decided to support the development of an improved European geoid/quasigeoid model in the form of an IAG Commission 2 Project, named "CP2.1 – European Gravity and Geoid Project (EGGP)," and since 2011 this task has continued as IAG Sub-Commission 2.4a "Gravity and Geoid in Europe." The European geoid and gravity project has strong connections to the IAG International Gravity Field Service (IGFS) and its centers, as well as to several other IAG bodies, e.g., EUREF (IAG Reference Frame Sub-Commission for Europe). The project is chaired by H. Denker, IfE, and has about 50 national delegates (project members) from most of the countries in Europe. Due to the confidentiality of many data sets, only one data and computation center exists at IfE, Hannover. Further details on the project can be found, e.g., in Denker et al. (2009). Interim results and status reports of the project were presented roughly on an annual basis.

While the initial test computations within the framework of the EGGP were limited to central Europe, the first complete re-computation was finished in 2007 and is denoted as EGG2007 (European Gravimetric (Quasi)Geoid 2007). After that, the new global geopotential model EGM2008 (Pavlis et al. 2008) became available. As the comparisons of EGM2008 with the European gravity data sets revealed some systematic differences for a few gravity sources, these problem areas were corrected, and, besides a few other improvements, lead to a new computation, which was finished at the end of 2008 and is denoted as EGG2008. At present, investigations about the inclusion of a GOCE geopotential model and some further refinements are still going on. More details about the EGGP data and results are provided in the following sections.

4.3 The European Gravity and Terrain Data

Since the start of the European geoid project, significant improvements of the land gravity data base were made, including new or revised data sets for nearly all European countries. New gravity data sets became available for Austria, Belgium, Bulgaria, Croatia, Cyprus, Denmark, Estonia, Finland, France, Germany, Greece, Italy, Latvia, Luxemburg, the Netherlands, Norway, Portugal, Serbia, Slovenia, Spain, Sweden, Switzerland, and Turkey.

Significant progress was also made in the collection and reprocessing of marine gravity data. All marine gravity data collected until 2003 were edited and crossover adjusted (see Denker and Roland 2005), which led to significant data improvements. The comparisons with independent altimetric gravity anomalies from, e.g., the KMS2002 model (Andersen et al. 2005), showed an RMS difference of 18.0 mGal for the original data set, 10.2 mGal for the edited data set, and 7.8 mGal for the edited and crossover adjusted data set, respectively, which proves the effectiveness of the entire processing scheme (see Denker and Roland 2005).

In addition, after 2003, significant new marine gravity data sets became available, originating mainly from the authorities of the Scandinavian countries (coverage: Baltic Sea, North Sea, North Atlantic), France (coverage: western parts of the Mediterranean Sea, Atlantic), as well as the National Geospatial-Intelligence Agency (NGA), U.S.A. (coverage: central and eastern parts of the Mediterranean Sea). Moreover, some airborne data sets were also provided by the Scandinavian authorities, covering the Baltic Sea as well as parts of the North Atlantic and Greenland coastal waters. The aforementioned new gravity data sets were thus far not crossover adjusted together with the other marine gravity data sources, mainly because all of them are of high quality without the need for a crossover adjustment and also due to a lack of time.

In addition to this, the public domain data from the Arctic Gravity Project ArcGP (Forsberg and Kenyon 2004) were integrated in the project data base. Finally, data from the EGG1997 data base were utilized for some areas (e.g., Eastern Europe and Africa). Furthermore, in order to fill the remaining data voids in the marine gravity data, altimetric gravity anomalies were employed. Until 2007 (regarding the EGG2007 computation), the altimetric data set KMS2002 (Andersen et al. 2005) was used.

After that, when the global geopotential model EGM2008 (Pavlis et al. 2008) became available, some problem areas with systematic differences between the European gravity data sets and EGM2008 showed up. This led to the following updates of the gravity sources being carried out until September 2008 (related to the EGG2008 computation):

- The Greek and Turkish gravity values were corrected in absolute level (the errors were caused by imperfect gravity reference system information).
- A few minor new sources (nine) were added.

- The KMS2002 altimetric anomalies were replaced by a merger of the 1' × 1' DNSC2008GRA (Andersen et al. 2010) and V18.1 (Sandwell and Smith 2009) data sets; the merging procedure was done in accordance with the EGM2008 approach (Pavlis et al. 2008), where the DNSC2008GRA data were used near the coast (out to 200 km distance) and the Sandwell and Smith data were employed over the open ocean; in addition, the altimetric data were completely edited out within a distance of 10 km from the shore line, as comparisons with some high-quality ship data within a 10 km wide coastal zone showed an RMS difference twice as high as on the open ocean (approximately 8 mGal vs 4 mGal).
- The ship gravity data editing was improved and some sources with very poor quality were completely excluded (mainly older sources with RMS differences to the altimetric data exceeding about 10 mGal).
- Fill-in gravity anomalies were derived from the EGM2008 geopotential model for some 5' × 5' cells in Africa, the Caucasus region, and parts of Asia, where no gravity observations were available within a distance of 15 km; this approach was selected to stay close to EGM2008, even in regions with large gravity data voids outside the main area of interest, being Europe and the surrounding waters.

The updates described above were taken into account for the EGG2008 computation, but not for EGG2007. Further information on the different data sets is included in Table 1. The final EGG2007 gravity data set consisted of 5,354,653 observations from 709 sources, plus 195,840 gravity values from the ArcGP project and 951,251 altimetric anomalies from the KMS2002 data set. On the other hand, the corresponding EGG2008 data set consists of 5,355,206 gravity observations from 718 sources, plus 195,840 ArcGP, 13,222,260 (1' × 1') altimetric, as well as 120,747 EGM2008 fill-in values; thus, in comparison to the previous EGG1997 computation, the land and marine data from the project data base approximately doubled, while the total amount of data increased about sixfold.

The progress in the collection of gravity data is also documented for selected examples in Fig. 9. The left part of the figure shows the old status in 1997 (EGG1997; Denker and Torge 1998) and the right part shows the new status as of September 2008 (EGG2008) for the whole of Europe (top), Scandinavia (middle), and the Mediterranean Sea (bottom; ship data from Morelli et al. 1975 excluded). In this context, it should be noted that within the EGGP, the Morelli ship gravity data for the Mediterranean Sea were completely excluded, as comparisons with newer data sources revealed significant systematic discrepancies in several areas.

Finally, it is important to mention that all EGGP gravity sources were carefully checked regarding the underlying horizontal and vertical position as well as the gravity reference systems, and, if necessary, transformations were done to the target systems, being ETRS1989 (European Terrestrial Reference System 1989, coinciding with ITRS at epoch 1989.0, and co-moving with the stable part of the Eura-

Table 1 Main characteristics of EGG1997/2007/2008

EGG1997	EGG2007	EGG2008
Gravity data		
Project data base		
2,684,133 (744 sources)	5,354,653 (709 sources)	5,355,206 (718 sources)
Other data sources		
–	195,840 (ArcGP)	195,840 (ArcGP)
335,124 (KMS1996)	951,251 (KMS2002)	13,222,260 (1' × 1' altimetry)
–	–	120,747 (EGM2008 fill-ins)
3,019,257 (Total)	6,501,744 (Total)	18,894,053 (Total)
Terrain data		
7.5" … 5' grids	1" … 30" grids	1" … 30" grids
700 million elevations	8.3 billion elevations	8.3 billion elevations
15' × 20' RTM	30' × 45' RTM	15' × 20' RTM
Global geopotential model		
EGM1996 (n_{max} = 360)	EIGEN-GL04C (n_{max} = 360)	EGM2008 (n_{max} = 360/2190)
Computation procedure		
Remove-restore technique, spectral combination (1D FFT)		
GRS80 normal potential, zero-tide system		
Computation grid		
25° – 77°N, 35°W – 67.4°E	25° – 85°N, 50°W – 70°E	25° – 85°N, 50°W – 70°E
1.0' × 1.5'	1.0' × 1.0'	1.0' × 1.0'
3,120 × 4,096 points	3,600 × 7,200 points	3,600 × 7,200 points

sian tectonic plate; for further details see http://www.euref.eu/), EVRS (European Vertical Reference System, based on the zero tide system; see Ihde et al. 2008), and a gravity datum based on absolute gravity observations. In the merging process of the various data sources, emphasis was placed on a thorough check with respect to systematic and gross errors, which was one of the most time-consuming steps.

Apart from the improved gravity data, comparable progress was also made in the collection of high-resolution digital elevation models (DEMs). For the EGG1997 computation, digital elevation models (DEMs) with a resolution of about 200 m were only available for Central and Western Europe, while coarser grids with a resolution of 0.5–10 km had to be used for the remaining parts of Europe. As of 1997, only Germany had released a very high-resolution DEM with a grid size of 1" × 1" (approx. 30 m), but meanwhile Switzerland and Austria also provided 1" × 1" DEMs for the EGGP. At present, high-resolution national DEMs do not exist or are confidential for large parts of Eastern Europe. Hence, in all areas not covered by high-resolution national DEMs, fill-ins from public domain data sets had to be utilized. However, compared to EGG1997, significantly improved fill-ins are available now, e.g., from the Shuttle Radar Topography Mission (SRTM) with a resolution of 3" × 3" (SRTM3; JPL 2007) or the global public domain model GTOPO30 with a resolution of 30" × 30" (USGS 2007). As the

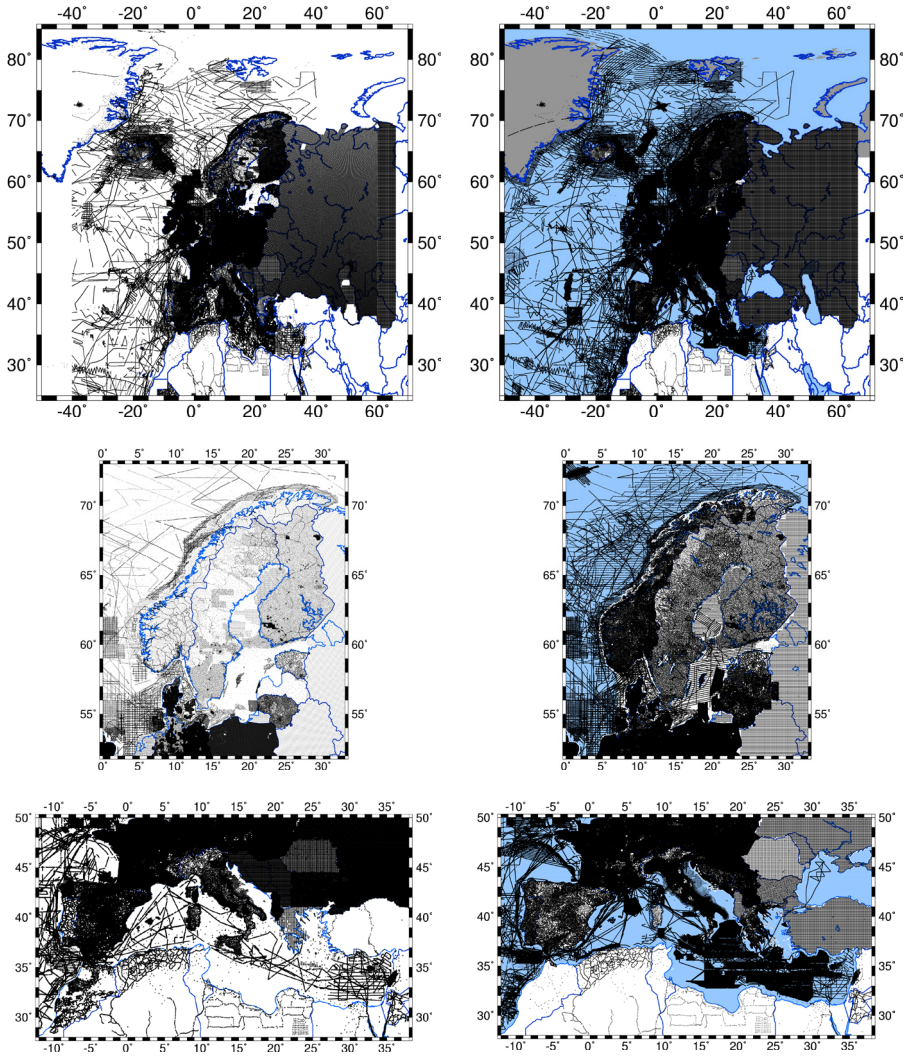

Fig. 9 Locations of terrestrial gravity data for entire Europe (*top*), Scandinavia (*middle*) and the Mediterranean Sea (*bottom*), excluding the Morelli data; the *left* part shows the status in 1997 (EGG1997) and the *right* part shows the status of September 2008 (EGG2008) with the ArcGP and altimetric data shown in *grey* and *blue*, respectively

SRTM3 model covers only the latitudes between 60°N and 54°S, the GTOPO30 model had to be used for the regions in the far North.

All available DEMs were merged into a new European DEM with a common grid size of 3" × 3", covering the area 25°N–85°N and 50°W–70°E. Furthermore, for the area of Germany, Austria, and Switzerland, a corresponding 1" × 1" DEM

was created. The 3" × 3" and 1" × 1" DEMs comprise about 6.6 and 1.7 billion elevations, respectively. In the merging process, the highest priority was given to the national DEMs, followed by the SRTM3 and GTOPO30 data. For testing purposes, a second 3" × 3" European DEM was created using only the public domain data sets SRTM3 and GTOPO30. Depth models were not considered so far, i.e., elevations for ocean cells were set equal to zero.

Within the merging process, the SRTM3 and GTOPO30 DEMs were also evaluated by comparisons with the high-resolution national DEMs. In Germany, the differences between the national and the SRTM3 DEMs showed a standard deviation of 7.9 m with maximum differences up to about 300 m. The largest differences were located in opencast mining areas and resulted from the different epochs of the data. Histograms of the differences showed a clear deviation from the normal distribution with a long tail towards too high SRTM3 elevations, which is expected due to the fact that SRTM is a "first return system," providing elevations of whatever the radar has bounced off from, and in many instances this is above the actual ground level (Denker 2005).

The evaluation of the GTOPO30 model by national and SRTM3 DEMs demonstrated that in large parts of Europe the longitudes of GTOPO30 should be increased by 30" (one block). In Central Europe, the longitude shift reduced the standard deviation of the differences to the national and SRTM3 models by roughly 75% to about 10 m. Altogether, the national DEMs augmented by the SRTM3 and GTOPO30 data provide a significantly improved European DEM, as compared to EGG1997. The DEMs were not updated between 2007 and 2008, and hence both the EGG2007 and EGG2008 computations rely on the same DEM for Europe, which is depicted in Fig. 10.

4.4 Development of the European Quasigeoid Model EGG2008

The general computation strategy is based on the spatial gravity field modeling approach, aiming at the determination of the disturbing potential at the Earth's surface and the associated height anomalies or quasigeoid undulations (e.g., Denker et al. 2005). This concept has the advantage that only gravity field observations at the Earth's surface and in its exterior enter into the calculations, avoiding assumptions about the Earth's interior gravity field (as needed in connection with the orthometric heights and the geoid). A conversion of the height anomalies to geoid undulations can then be performed afterwards by introducing a density hypothesis, which should be consistent with that used for deriving the corresponding orthometric heights (e.g., the so-called Helmert heights based on (52); for further discussions see Sects. 2.4 and 3.5).

The remove–compute–restore (RCR) technique is utilized for combining the high-resolution terrestrial gravity and terrain data with a state-of-the-art global geopotential model. Terrain reductions are performed according to the residual terrain model (RTM) technique to smooth the data and to avoid aliasing effects

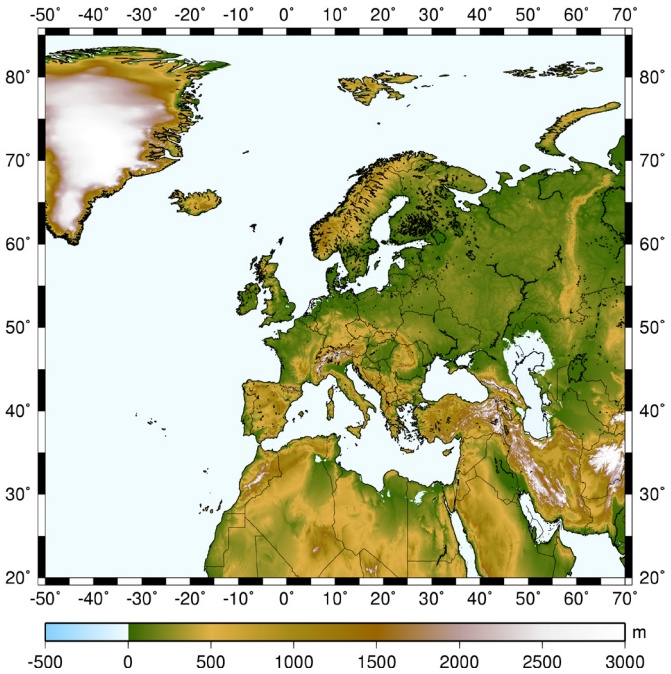

Fig. 10 Final digital elevation model (DEM) for Europe with a resolution of 3″ × 3″

(see Sect. 3.9). The transformation of the gravity anomalies into corresponding disturbing potential and height anomaly values is done by the spectral combination technique with integral formulas (see Sect. 3.6). In principle, the following steps are carried out:

1. Computation of surface free-air gravity anomalies based on (86), including the atmospheric correction (77), yielding

$$\Delta g_P = g_P + \delta g^A - \gamma_Q \quad . \tag{178}$$

2. Computation of residual gravity anomalies (remove step) for all stations according to equation (173), giving

$$\Delta g_P^{res} = \Delta g_P - \Delta g_{Q^*}^M - \Delta g_P^T \,, \tag{179}$$

   where $\Delta g_{Q^*}^M$ and Δg_P^T are the contributions from the global geopotential model and the topography, respectively (see Sects. 3.2 and 3.9).
3. Gridding of the irregularly distributed residual gravity anomalies, which are still referring to the actual observation positions, by least-squares collocation, taking into account the given standard deviations of the observations.

4. Transformation of the residual gravity anomaly grid into a corresponding disturbing potential grid (compute step) based on the spectral combination approach (154), resulting in

$$\hat{T}_P^{res}(\theta,\lambda,r) = \frac{R}{4\pi}\iint_{\sigma} \Delta g_{P'}^{res} W(\psi,r)\, d\sigma \quad . \tag{180}$$

5. Computation of the final disturbing potential by restoring the contributions from the geopotential model and the topography (restore step), yielding

$$\hat{T}_P = \hat{T}_P^{res} + T_P^M + T_P^T \quad . \tag{181}$$

6. Conversion of the disturbing potential to height anomalies by means of (90).
7. Derivation of geoid undulations by introducing a density hypothesis, e.g., based on (56) and (52).

Regarding the details of the practical implementation of the above steps, the following more general notes are given:

- It is assumed that all station coordinates are based on the ETRS1989 reference system, the physical heights are normal heights based on the EVRS (zero tide system), and the gravity values are referring to an absolute gravity datum; regarding the accuracy requirements for the station coordinates, gravity values, etc.; see Sect. 4.1.
- The geodetic reference system GRS80 (e.g., Moritz 2000) is used as the normal gravity field in all computations, being the latest system recommended by IUGG and IAG; in addition, the GRS80 ellipsoid is recommended by IERS (2010) for use with the ITRF solutions, and it is also mostly utilized for GNSS ellipsoidal coordinates.
- Atmospheric corrections for the observed gravity values are computed according to (77); the restore part δV^A (see (75), Sect. 2.6) is neglected due to its insignificant magnitude (of a few millimeters).
- The degree two zonal coefficient of the global geopotential model is always converted to the zero tide system, and hence the resulting height anomalies and geoid undulations also refer to the zero tide system.
- The different values of the constants GM (geocentric gravitational constant) and a (semimajor axis) in the global geopotential models and the GRS80 normal gravity field are handled rigorously throughout all computation steps; the resulting degree zero terms in the spherical harmonic expansions are taken into account in all calculations, see (110) and (111).
- The geopotential model parameters are so far not computed rigorously based on coordinate transformations of the relevant vectors and matrices (see Sects. 2.3 and 2.5), but instead ellipsoidal approximations based on Wenzel (1985) are employed, which also provide sufficiently accurate results. Furthermore, the

geopotential model values were until now only computed utilizing the normal heights H^N, and not $H^N + \zeta_{Q^*}$, as required within a rigorous linearization process with respect to a high-degree geopotential model (see Sect. 3.2). However, for future calculations the rigorous approach will be implemented, and it remains to be seen whether this also leads to improved results.

- Topographic reductions are computed based on the RTM technique (see Sect. 3.9), which results in a significant smoothing of the relevant gravity field quantities and reduces aliasing effects. The required reference topography was always computed by a moving average filter from the available DEMs; this ensures the consistency between the high-resolution DEMs and the reference topography, without creating undesirable long wavelength signals. The reference topography had a resolution (size of the moving average filter) of 30' × 45' for EGG2007, and 15' × 20' for EGG2008 (see also Table 1). The resolution of the reference topography was reduced for EGG2008, because even the RTM technique creates some small long wavelength signals, which lead to an inconsistency within the RCR procedure, as these signals are suppressed in the compute step (by the spectral combination approach), but are fully considered in the restore step on the other hand. All computations were done with the program TC based on prism integration; regarding the gravity stations, the DEM was forced to reproduce the given station elevations (see Sect. 3.9; Forsberg 1984). Figure 11 shows an example for the surface free-air gravity anomalies and the corresponding RTM reduced values; the figure clearly documents that the RTM reductions lead to a significant smoothing of the anomaly field, while preserving the long wavelength features.
- The spectral combination technique was employed so far for the compute step, because it allows an optimal combination of the terrestrial data with a global geopotential model based on the error characteristics of both data sets, and furthermore the resulting integral formulas can be evaluated rigorously and very effectively by 1D FFT techniques (Haagmans et al. 1993). In this context, the regional terrestrial data, with possibly existing (small) long wavelength systematic errors, and a global geopotential model, being highly accurate at the very long wavelengths, complement each other in an optimal way; hence, within the combination process, the very accurate long wavelength gravity field structures of the present global geopotential models (based on the GRACE and GOCE missions) should be retained, while the terrestrial data should mainly contribute the shorter wavelength components. In addition, previous investigations clearly showed that the application of the original Stokes formula, implying that the complete disturbing potential spectrum (from degree 2 to ∞) is computed from the terrestrial gravity data plus the geopotential model in the outer zone, leads to unreasonable long wavelength distortions of the results, and therefore it is not well suited in this context. Further specific details on the implementation of the spectral combination procedure are given below.

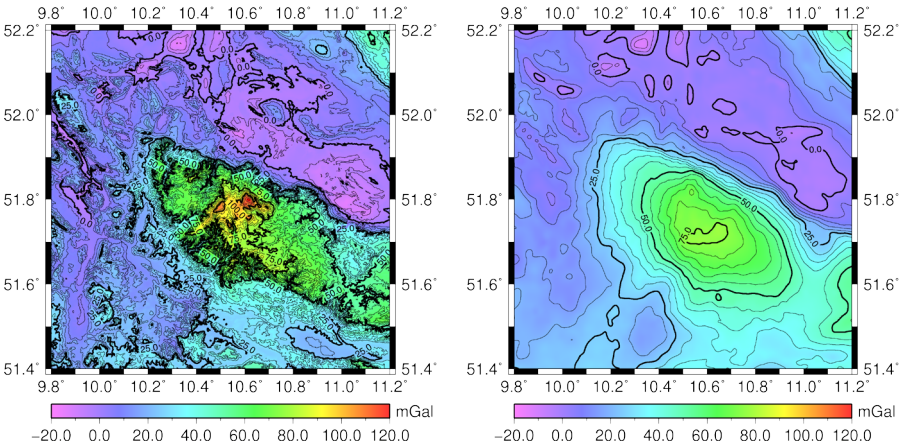

Fig. 11 Surface free-air gravity anomalies (*left*) and corresponding RTM 15' × 20' reduced values (*right*) for the area of the Harz mountains, Germany

- The computation area for the EGG2007 and EGG2008 models is 25°N–85°N and 50°W–70°E. The grid spacing is 1' × 1', yielding 3,600 × 7,200 = 25,920,000 grid points (see also Table 1).

The key ingredients within the spectral combination approach are the spectral weights according to (149), which depend on the error degree variances associated with the terrestrial gravity data and the geopotential model. Regarding the terrestrial gravity data, the starting point was the following error covariance function:

$$Cov(\varepsilon_{\Delta g^G}, \varepsilon'_{\Delta g^G}, \psi, R) = 1_{[\mathrm{mGal}^2]}\, e^{-4\psi[^\circ]} . \tag{182}$$

This covariance model considers correlated noise and was originally suggested and applied by Weber (1984). Then, based on (148), corresponding error degree variances can be computed, and, together with the error degree variances for the geopotential model according to (147), the spectral weights can be estimated from (149).

For the computation of EGG2007, the geopotential model EIGEN-GL04C (Förste et al. 2008a) was employed, because at that time it was the latest available high-degree model based on GRACE and terrestrial data. The spectral weights, computed as described above, are shown in Fig. 12 together with corresponding values related to a recent CHAMP model and the EGM1996 model (used for the EGG1997 computation). In addition, Fig. 12 also depicts the modified integral kernels associated with the corresponding spectral weights as well as the original Stokes kernel. With respect to EGG2007, it was decided to do the combination only up to degree 120, while between degrees 120 and 10,000 (corresponding to the used grid size) full weight ($w_n^G = 1.0$) was given to the terrestrial gravity data in

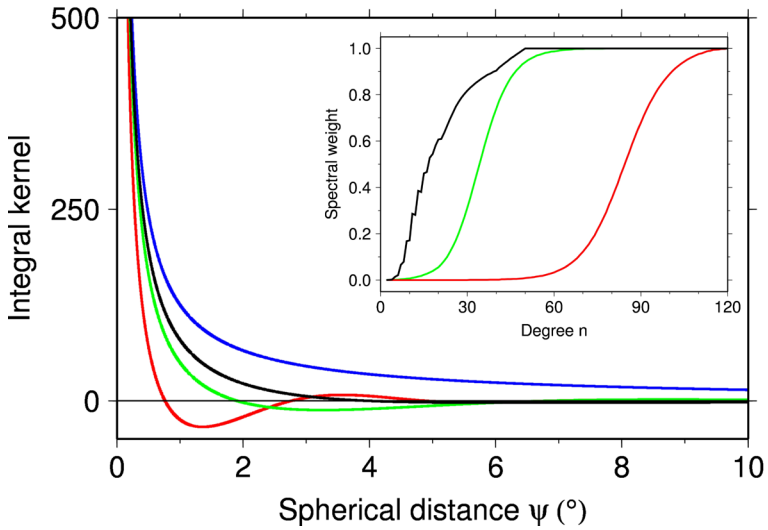

Fig. 12 Spectral weights and corresponding integral kernels related to a GRACE based geopotential model (*red*; used for EGG2007 and EGG2008), a recent CHAMP model (*green*), and EGM1996 (*black*; used for EGG1997), along with the classical Stokes kernel (*blue*)

order to exploit fully the collected European gravity sources. However, this does not imply that the global model is completely disregarded above degree and order 120, as, e.g., in areas with larger data gaps the high-degree gravity information of the model is considered in the gridding process and thus practically taken over in the final combined solution. In this context, it is also worth mentioning that previous studies revealed that it is advantageous to use a high-degree model up to degree $n_{max} = 360$, as this leads to smaller residual quantities accompanied with reduced effects of (e.g., linear) approximation errors in the mathematical modeling. In addition, a cosine tapering window was applied between degrees 10,000 and 30,000 in order to prevent oscillations of the integral kernel. As already mentioned in Sect. 3.6, the resulting modified integral kernels $W(\psi)$ remain finite if the weights go to zero for very high degrees or the summation is limited to some maximum degree; therefore, in principle, no special consideration of the inner zone contribution is required, but due to the rapid change of the integration kernel near $\psi = 0°$ (see Fig. 12) it is recommended to integrate numerically the kernel function within the innermost zone (see also Sect. 3.6). Consequently, a numerical kernel integration was implemented using 21 × 21 points for the innermost (central) grid cell and 11 × 11 points out to a distance of $\psi = 0.5°$; outside this distance, the kernel value is simply calculated based on the distance to the cell center. Moreover, to speed up the computations, internally a coarse grid is computed and employed for the remote zones, and in addition, kernel tabulation and interpolation are implemented.

In spring 2008, the new global geopotential model EGM2008 became available, given as spherical harmonic coefficients complete to degree and order 2,159, with additional coefficients going up to degree 2,190 and order 2,159 (Pavlis et al. 2008). The EGM2008 model is based on a corresponding GRACE-only model (ITG-GRACE03, $n_{max} = 180$, including GRACE data from September 2002 to April 2007, computation method described in Mayer-Gürr 2006), along with its complete covariance matrix, and a new and comprehensive worldwide 5' × 5' terrestrial gravity anomaly data set, combined by a least-squares adjustment, using internally ellipsoidal harmonic coefficients (Pavlis et al. 2008). At first the EGM2008 model was compared with corresponding GRACE static gravity field solutions. Figure 13 depicts the signal and error spectra related to EGM2008, along with the error spectra of the recent GRACE based models EIGEN-GL04C (Förste et al. 2008a; utilized for the EGG2007 calculation), EIGEN-5S (Förste et al. 2008b), and ITG-GRACE2010 (Mayer-Gürr et al. 2010; formal standard deviations scaled by factor 8), as well as the corresponding spectra of the differences to EGM2008, respectively. Now, regarding roughly the degree range 20–90, the EGM2008 error estimates are about five to six times higher than those from the more recent EIGEN-5S and ITG-GRACE2010 models, and about three times higher than those from the EIGEN-GL04C model. On the other hand, the depicted difference spectra are all very similar and show a reasonable agreement with the error spectra of the EIGEN-5S, ITG-GRACE2010 and EIGEN-GL04C models until about degrees 60–70, but the difference spectra significantly exceed the latter error curves in the degree range 60–100, while still being compatible with the EGM2008 error estimates; it is also worth mentioning that the same features show up with reference to the GGM03S/C models (Tapley et al. 2007), not shown in Fig. 13. Based on these findings, it appears that the EGM2008 error estimates are perhaps too pessimistic for the low degrees (degrees less than 60–70), while the bump in the difference signals (degrees 60–100) is probably related to the EGM2008 weighting procedure.

As a result, the spectral weights computed from (149) on the basis of the (perhaps too pessimistic) EGM2008 error estimates and the error covariance function for the terrestrial gravity data (1 mGal correlated noise; see (182)) turned out to be somewhat unrealistic, with too much weight given to the terrestrial data, dominating the combination solution (i.e., $w_n^G > 0.5$) already below degree 70. In principle, this could be counteracted by increasing the error estimates for the terrestrial data or decreasing the EGM2008 error estimates, as only the relative weighting matters. However, this was not attempted, but instead the spectral weights from the EGG2007 calculation were also adopted for EGG2008 in connection with the EGM2008 model, as these weights appear to be quite reasonable (with $w_n^G > 0.5$ at about degree 85; see Fig. 12); in addition, this weighting scheme is in very good agreement with the studies from Forsberg (2010), who found empirically from GPS/leveling comparisons that linearly increasing weights between degrees 80 ($w_n^G = 0.0$) and 90 ($w_n^G = 1.0$) are optimal. Furthermore, it is also noted that the combination solutions based on the original EGM2008 spectral weights, in contrast

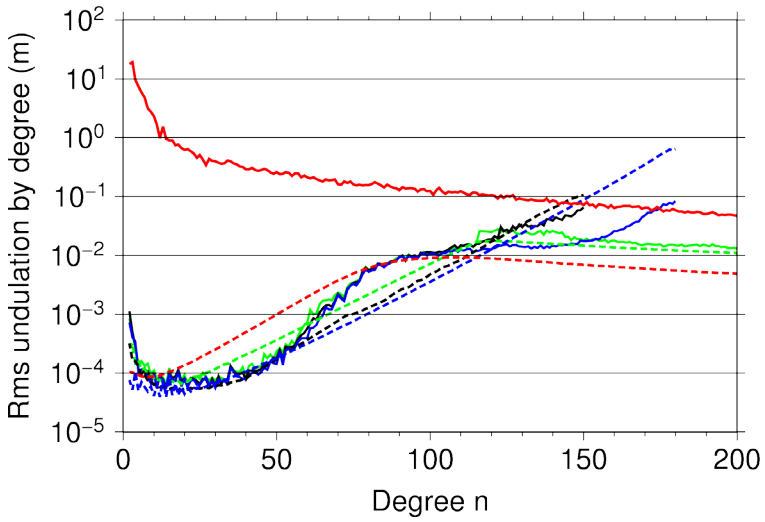

Fig. 13 Signal and error spectra for EGM2008 (*red thick* and *dashed lines*, respectively), along with the error spectra (*dashed lines*) for EIGEN-GL04C (*green*), EIGEN-5S (*black*), and ITG-GRACE2010 (*blue*; formal standard deviations scaled by factor 8), as well as the corresponding difference spectra with respect to EGM2008 (*thick lines*)

to those shown in Fig. 12, performed slightly worse in some of the GPS/leveling comparisons.

Another issue relates to the maximum degree of the employed geopotential model in conjunction with the reference topography used for the RTM reductions. This item, mainly concerning the ultra-high-degree model EGM2008, has been discussed already in Sect. 3.9 with reference to the studies in Forsberg (2010), showing "some inherent problems in implementing the RTM method for a highly varying reference topography" with "best results obtained for a relatively low-resolution (30') reference height, irrespective of whether EGM2008 is used at a corresponding resolution (n_{max} = 360) or to full resolution (n_{max} = 2,190)." With respect to the European calculations, RTM reductions based on a 30' × 45' (EGG2007) and 15' × 20' (EGG2008) reference topography were tested and used in combination with the full resolution EGM2008 model (n_{max} = 2,190); however, the GPS/leveling comparisons indicated a slight deterioration in a few but not all cases as compared to the solutions based on EGM2008 with n_{max} = 360, and further studies are needed to understand fully this matter. Possible reasons may be related to the "double consideration" of the short wavelength topographic signals in the RTM reductions and the EGM2008 model, the non-rigorous linearization with respect to the geopotential model (i.e., the use of heights H^N instead of $H^N + \zeta_{Q^*}$; see above and Sect. 3.2), as well as due to the RTM reductions themselves. Therefore, it was ultimately decided to employ the EGM2008 model only with n_{max} = 360 in the EGG2008 calculation, accompanied by some fill-ins over large data voids (see

above) to ensure that the full resolution EGM2008 model and the EGG2008 quasigeoid stay reasonably close together even there.

In principle, the Molodensky corrections terms, considering data on a non-level surface, also have to be taken into account in connection with the spectral combination approach (because the employed residual gravity anomalies are still referring to the actual observation positions). In this context, Molodensky's theory (see Sect. 3.4) and terrain reductions (see Sect. 3.9) are complementary, because the application of terrain reductions results in a significant smoothing of the gravity field observations, associated with a corresponding reduction of the Molodensky correction terms and a more stable computing scheme (Forsberg and Tscherning 1997). The magnitude of the Molodensky terms was studied in Denker and Tziavos (1999) in conjunction with different terrain reduction techniques, indicating that the maximum values associated with the RTM technique may reach about 5–10 cm in extremely rugged areas of the European Alps (≈ 1 cm RMS) and about 1 cm in low mountain ranges (≈ 1 mm RMS). However, utilizing the so-called gradient solution (see Sect. 3.4) for Switzerland and Austria did not lead to any improvements in the GPS/leveling comparisons, with similar findings reported by Forsberg (2010). Therefore, the Molodensky terms have been neglected so far in the EGG2007 and EGG2008 calculations.

One final item concerns the European Vertical Reference System (EVRS), where the vertical datum (zero level surface) is defined as the (zero tide) equipotential surface of the Earth's gravity field, which passes through the "Normaal Amsterdams Peil" (NAP; fundamental tide gauge in Amsterdam, the Netherlands) and which has the (constant) gravity potential W_0^{EVRS} (see Ihde et al. 2008). The latest EVRS realization is the EVRF2007 (European Vertical Reference Frame 2007), consisting of a set of points with precisely determined geopotential numbers and normal heights relative to the aforementioned zero level surface through the NAP at epoch 2000.0 (Ihde et al. 2008); EVRF2007 is the recommended reference frame for all pan-European applications. However, to remain general, the notation W_0^i is used for the potential of the zero level surface of a local vertical datum (i). Now W_0^i, being initially unknown, will in general differ from U_0, which has to be considered accordingly in (89) as well as (95) or (99) for the height and gravity anomalies, respectively. While the (small) constant term in the gravity anomaly equations has practically no effect on the computed disturbing potential T (because it is of long wavelength nature, and such signals are almost entirely defined by the global geopotential model; see above), and the zero-degree term of T (i.e., T_0 due to the different GM values; see (128)) is already taken into account within the calculation process (see above), Bruns's formula (89) together with (87) results in

$$\zeta_P^i = h_P - H^{N(i)} = \frac{T_P}{\gamma_Q} - \frac{W_0^i - U_0}{\gamma_Q} = \frac{T_P}{\gamma_Q} + \zeta_0^i \,, \tag{183}$$

Table 2 Statistics of 18,154,254 irregularly distributed gravity anomalies (without error flag) that were used as input for EGG2008; units are mGal

Parameter	Mean	Std. dev.	Minimum	Maximum
Δg	+6.59	34.11	–333.36	+498.88
Δg^M (EGM2008, $n_{max}=360$)	+7.49	31.27	–226.32	+236.25
Δg^T (RTM 15' × 20')	–0.34	4.98	–215.21	+182.72
$\Delta g - \Delta g^M$	–0.90	14.95	–268.74	+290.52
$\Delta g - \Delta g^M - \Delta g^T = \Delta g^{res}$	–0.57	13.90	–163.43	+263.23

Std. dev.: standard deviation

Table 3 Statistics of 3,600 × 7,200 = 25,920,000 quasigeoid heights of the EGG2008 grid; units are m

Parameter	Mean	Std. dev.	Minimum	Maximum
$\zeta^{res} = \mathbf{S}(\Delta g^{res})$	0.000	0.161	–1.657	+2.361
ζ^T (RTM 15' × 20')	0.000	0.036	–0.493	+0.934
ζ^M (EGM2008, $n_{max}=360$)	+26.498	24.257	–48.665	+67.551
$\zeta_0^{\text{EVRF2007}}$	+0.300	0.000	+0.300	+0.300
ζ (EGG2008)	+26.798	24.258	–48.858	+68.104

Std. dev.: standard deviation

where T_P is the disturbing potential (including the zero-degree term, as obtained directly from the above described computations) relative to the (GRS80) normal potential (U_P, U_0, respectively), $H^{N\,(i)}$ is the normal height based on the vertical datum (i), and ζ_0^i is a virtually constant term to account for the potential difference $W_0^i - U_0$. Regarding the EVRF2007, the latter constant was determined by comparisons with GPS and leveling data (i.e., $h_P - H^{N\,(\text{EVRF2007})}$) from the European EUVN_DA data set (Kenyeres et al. 2010; see Sect. 4.5) as +0.302 m. As a result, a slightly rounded value for ζ_0^i (based also on an earlier EUVN_DA release) was employed for the computation of the final EGG2008 height anomalies (quasigeoid heights), yielding

$$\zeta_P^{EGG2008} = \frac{T_P}{\gamma_Q} + \zeta_0^{\text{EVRF2007}}, \quad \text{with} \quad \zeta_0^{\text{EVRF2007}} = +0.300 \text{ m} . \tag{184}$$

The above correction ensures the compatibility between the European GPS (ETRS1989) and leveling data (EVRS, normal heights, zero tide system, etc.) on the one hand, and the EGG2008 height anomalies on the other hand.

Table 2 shows the statistics of the 18,154,254 irregularly distributed gravity anomalies without an error flag, which were used as input for the computation of the EGG2008 residual gravity anomaly grid; the number of points is smaller than that given in Table 1, because Table 2 excludes the stations which received an

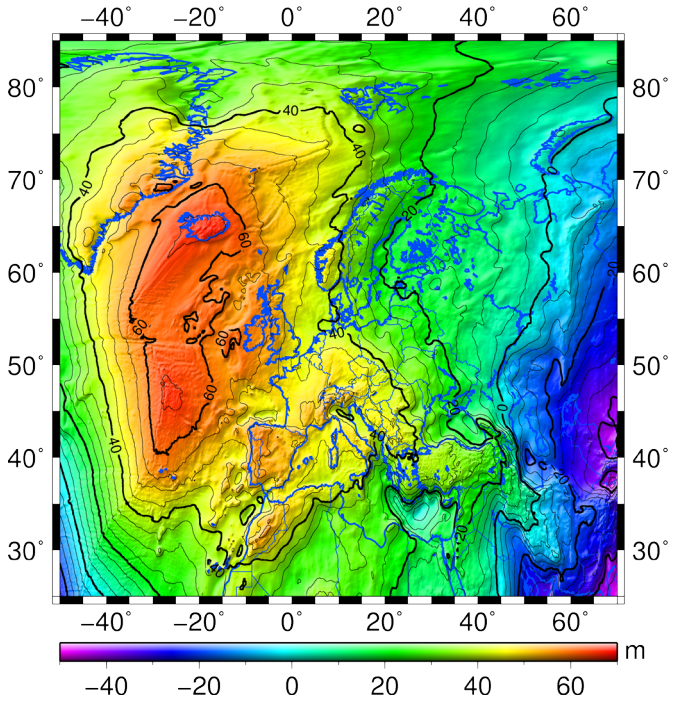

Fig. 14 Final EGG2008 quasigeoid referring to GRS80 (see text; units are m)

error flag (mainly edited altimetry data near the coast as well as some very bad and duplicate marine gravity sources; see Sect. 4.3). The standard deviation (std. dev.) of the original gravity anomalies is 34.11 mGal, which reduces to 14.95 mGal after subtracting EGM2008 ($n_{max} = 360$) and 13.90 mGal after also subtracting the RTM contributions. The minimum and maximum values also reduce accordingly, and the mean value of the final residual anomalies is –0.57 mGal and thus reasonably close to zero (as it should be).

The statistics of the corresponding quasigeoid height or height anomaly terms for EGG2008 are given in Table 3. The major contribution to the final quasigeoid comes from the global geopotential model EGM2008 ($n_{max} = 360$) with values ranging from –48.655 m to +67.551 m and a standard deviation of 24.257 m. The standard deviations of the contributions from the topography and the terrestrial gravity data are 0.036 m and 0.161 m, respectively. However, the maximum RTM effects are about 0.9 m, while the maximum effects of terrestrial gravity data are about 2.4 m (all large values are located in Asia or Africa). In addition, the final EGG2008 quasigeoid is depicted in Fig. 14.

Table 4 Standard deviations for quasigeoid heights based on 1 mGal correlated noise for the terrestrial gravity data and error degree variances from different geopotential models; units are m

Degree range	EGM2008	EIGEN-GL04S1/C	EIGEN-5S/5C
2 – 50	0.0028	0.0012	0.0007
51 – 100	0.0213	0.0114	0.0097
101 – 200	0.0184	0.0184	0.0184
201 – 360	0.0115	0.0115	0.0115
361 – 2,000	0.0071	0.0071	0.0071
2,001 – ∞	0.0006	0.0006	0.0006
2 – ∞	0.0314	0.0256	0.0248

The spectral combination technique also permits the derivation of error estimates for the computed quasigeoid heights on the basis of corresponding error degree variances. According to (156) and (157) the error degree variances related to the terrestrial gravity data and the global geopotential model are required. Table 4 shows the results based on 1 mGal correlated noise for the terrestrial gravity data, see (182), and the error degree variances from different geopotential models; as the EGM2008 error estimates may be a little too pessimistic (see the discussion above), corresponding estimates from the EIGEN-GL04S1/GL04C and EIGEN-5S/5C models were also taken into consideration. In this context, the results based on the error estimates of the "S" (satellite-only) and "C" (combined) models do not differ significantly, because due to the selected weighting scheme (see Fig. 12), the error degree variances of the global model come into play only up to degree $n_{max} = 120$, see (157), where the "S" and "C" values do not differ significantly. Table 4 gives a standard deviation for the quasigeoid heights of 3.1 cm related to the EGM2008 model and about 2.5 cm related to the EIGEN models, which can be viewed as the pessimistic and optimistic case, respectively. Table 4 also shows that the major error contributions are coming from the spectral band with n = 50–360, while today the very long wavelengths ($n < 50$) are accurately known from the GRACE mission and the short wavelengths ($n > 360$) can be obtained from high-quality terrestrial data. However, once GOCE can deliver the quasigeoid up to a resolution of 100 km ($n \approx 200$) with an accuracy of about 1 cm, the total error (complete spectrum) will reduce to 1.7 cm (for a corresponding study related to EGG1997, see Denker 1998). In addition to this, an error covariance function was derived for the quasigeoid heights based on (156), utilizing the more optimistic EIGEN-5S/5C error estimates; the result is depicted in Fig. 15, showing significant error correlations up to distances of about 300 km. Finally, it should be noted that the aforementioned error estimates apply only to those regions in Europe, where high-quality terrestrial gravity data exists, while in other areas (mainly Eastern Europe) less accurate results have to be expected. In the end, the future perspectives for calculating gravimetric geoid/quasigeoid models with an accuracy of 1 cm are quite good with respect to well-surveyed regions, where such

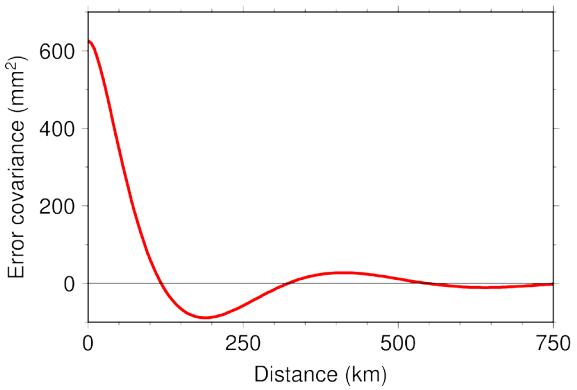

Fig. 15 Error covariance function for quasigeoid heights based on 1 mGal correlated noise for the terrestrial gravity data and error degree variances from the EIGEN-5S/5C models

models can then replace geometric leveling and serve as a vertical datum, e.g., as planned in Canada and the U.S.A. (see Sect. 2.4).

Besides the commission error, the truncation error, resulting from the truncation of the kernel function (or integration) at some distance ψ_{max}, is also of interest. The truncation error can be derived from (160) and (161) by means of the frequency transfer function FTF_n, see (159). For ψ_{max} = 10°, 7.5°, and 5.0°, the truncation error is estimated as 0.7 mm, 1.6 mm, and 3.5 mm, respectively. Moreover, the truncation error remains below 1 cm for ψ_{max} larger than about 3°, while truncation errors of about 18 mm and 25 mm are obtained for ψ_{max} = 2° and 1° (all figures given in terms of standard deviation). In addition, the frequency transfer function (FTF_n) and the spectral weights differ by no more than about 1.5% for ψ_{max} = 10°. Finally, it is noted that in the practical computations, kernel truncation is not used at all, i.e., for every computation point the complete input grid is employed; this was done because kernel truncation offers no computational advantages and previous studies showed that kernel truncation may lead to unfavorable results, as for every computation point another input data field is utilized (which does not conform with the harmonicity condition, see the corresponding discussion on the computation of terrain reductions in Sect. 3.9 as well as Wolf 2008).

4.5 Evaluation of the European Quasigeoid Model EGG2008

The EGG2008 quasigeoid model and all other interim solutions as well as the previous EGG1997 release were evaluated by independent national and European GPS and leveling data sets. The ellipsoidal GPS heights as well as the leveled heights (all given as normal heights) were converted to the zero tide system based on the transformation formulas published by Ihde et al. (2008). Regarding the GPS heights, it was generally assumed that they refer to the (conventional) tide-free system, as this is common practice and standard for the ITRF products (see Sect. 2.1); the transformation to the zero-tide system decreases the ellipsoidal

Table 5 Comparison of 907 GPS and leveling stations in Germany with quasigeoid models based on different terrestrial data sets and geopotential models; the GPS/leveling data were converted to the zero tide system; the differences are defined in the sense GPS/leveling minus gravimetric quasigeoid; the mean values refer to the raw differences without applying the constant $\zeta_0^{EVRF2007}$; the other statistical parameters are calculated after subtracting the mean value; units are m

Terrestrial data	Geopotential model	Mean	RMS	Minimum	Maximum
1997 (EGG1997)	EGM1996	+0.431	0.096	–0.188	+0.331
1997	EGM2008	+0.302	0.029	–0.095	+0.089
2007 (EGG2007)	EIGEN-GL04C	+0.298	0.036	–0.159	+0.075
2008	EGM1996	+0.416	0.074	–0.132	+0.300
2008	EIGEN-CHAMP03S	+0.288	0.050	–0.116	+0.262
2008	EIGEN-GRACE01S	+0.290	0.038	–0.111	+0.152
2008	EIGEN-GRACE02S	+0.295	0.037	–0.080	+0.123
2008	EIGEN-GL04S1	+0.299	0.029	–0.097	+0.086
2008	EIGEN-GL04C	+0.300	0.028	–0.093	+0.082
2008	EIGEN-5S	+0.300	0.027	–0.097	+0.073
2008	EIGEN-5C	+0.298	0.028	–0.098	+0.073
2008 (EGG2008)	EGM2008	+0.297	0.027	–0.091	+0.078
–	EGM2008 ($n_{max}=2190$)	+0.302	0.031	–0.110	+0.148

heights by approximately 4.5 cm on average over the European continent. The leveling heights were usually treated as mean tide quantities, as this is a reasonable approximation for the typical case of not applying any tidal reductions to the leveling; the conversion from the mean tide system to the zero tide system was carried out relative to the central latitude of the GPS/leveling data set, which does not change the average height level of all stations, but in principle the corrections should be calculated relative to the fundamental datum point.

Table 5 shows the statistics of the differences between a German GPS/leveling data set, consisting of 907 stations (data from Bundesamt für Kartographie und Geodäsie, BKG, Frankfurt; e.g., Liebsch et al. 2006), and various quasigeoid calculations based on different terrestrial data sets (1997, 2007, 2008) and geopotential models; the differences were always computed in the sense GPS/leveling minus gravimetric quasigeoid. All quasigeoid models were computed by the spectral combination technique based on 1 mGal correlated noise for the gravity data, see (182), and the error estimates for the geopotential model, where the spectral weights related to the EGM2008 geopotential model are a special case, as described in Sect. 4.4. As a result, the long wavelength components of the regional quasigeoid models and the underlying global geopotential model match to a great extent, and hence the comparisons of such regional quasigeoids with GPS/leveling data can also be considered as a validation tool for the respective global geopotential model. Table 5 provides the mean values of the raw differences without applying the constant ζ_0^i, while the other statistical parameters (RMS, Minimum, Maximum) are related to the centered differences (i.e., after subtracting the corresponding mean value). The results in Table 5 clearly demonstrate the

enormous progress resulting from improved gravity and terrain data on the one hand and the global geopotential models based on the satellite missions CHAMP and GRACE on the other, with the RMS differences reducing by about a factor of 3.5 from 9.6 cm for EGG1997 to 2.7 cm for EGG2008. In detail, the combination of the older EGM1996 model with the terrestrial data sets from 1997 and 2008 leads to RMS differences of 9.6 cm and 7.4 cm, respectively, corresponding to an improvement of about 23% (related to the updated terrestrial data), but, on the other hand, the combination of the 1997 terrestrial data with the EGM2008 model results in an RMS difference of only 2.9 cm (improvement 70%); thus, most of the total improvement is due to the better satellite data in this case. Furthermore, considering the different EIGEN models from GFZ, the RMS differences improve in the course of time, where the newer models, associated with longer observation series, yield the best results; for example, the combination of the 2008 terrestrial data with EGM1996 gives an RMS difference of 7.4 cm, which reduces to 5.0 cm related to the CHAMP model (EIGEN-CHAMP03S), about 3.8 cm for the early GRACE models (EIGEN-GRACE01S/02S), and finally 2.7 cm for the recent GRACE based models (EIGEN-5S/C, EGM2008). Consequently, the new satellite mission data (CHAMP, GRACE) have a significant impact on the accuracy of regional quasigeoid models, and further improvements down to the level of about 1 cm are anticipated from the GOCE mission. In addition, the mean values associated with the CHAMP and GRACE based geopotential models are remarkably stable, differing by no more than about 1 cm. Besides the results given in Table 5, the differences between the German GPS/leveling data and EGG1997 as well as EGG2008 are illustrated in Fig. 16, showing again the progress from the 1997 to the 2008 quasigeoid models, especially with regard to the long wavelengths.

The statistics from further comparisons of national GPS and leveling data sets as well as the European EUVN_DA enterprise (Kenyeres et al. 2010) with selected quasigeoid solutions are presented in Tables 6 and 7. The comparisons were carried out in conformity with the German GPS/leveling data set (i.e., zero tide system, normal heights, no ζ_0^i constant considered, etc.), with the normal heights referring to the respective national vertical datums. Again, several combinations of the terrestrial data and geopotential models were utilized to assess the progress associated with the improved input data sets; besides the quasigeoid model EGG1997 (1997 terrestrial data, geopotential model EGM1996, denoted as EGG1997/EGM1996), the solutions EGG1997/EGM2008 (1997 gravity and terrain data, EGM2008 geopotential model), EGG2008 (2008 terrestrial data, EGM2008 geopotential model, denoted as EGG2008/EGM2008), as well as the pure EGM2008 model with $n_{max} = 2{,}190$ are addressed in Tables 6 and 7. Besides a summary of the comparisons with the German GPS/leveling data, Table 6 includes corresponding results for the Netherlands, Belgium, a French traverse from Marseille to Dunkerque (1,100 km long) with new leveling data (NIREF; Duquenne et al. 2007), a French national data set (based on the older leveling network IGN69), Switzerland, Austria, and Russia (Demianov and Majorov 2004),

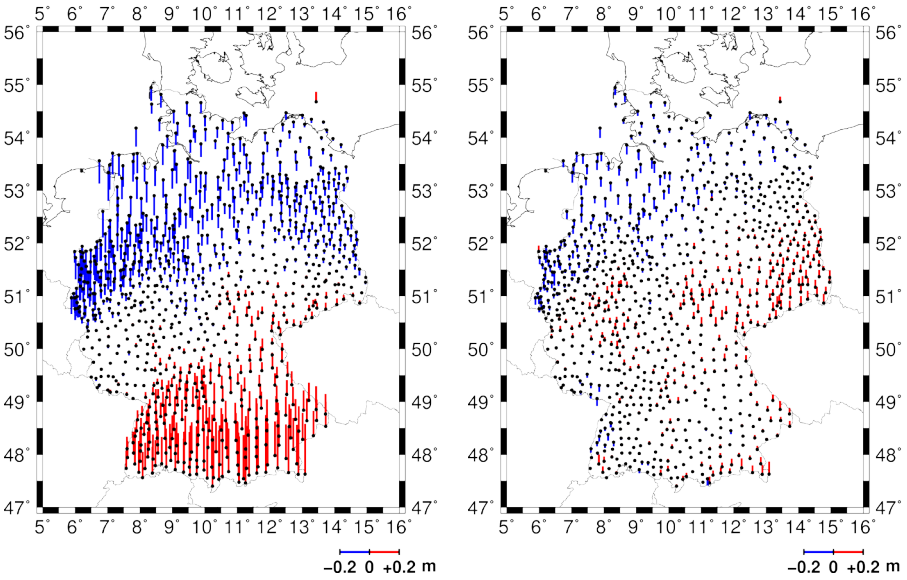

Fig. 16 Comparison of 907 GPS and leveling stations in Germany with the quasigeoid solutions EGG1997 (*left* part) and EGG2008 (*right* part); a constant bias is subtracted; stations (*dots*) and differences (positive: up in *red*; negative: down in *blue*) are depicted

while the results relating to the EUVN_DA project (Kenyeres et al. 2010) are listed in Table 7. The EUVN_DA project aimed at a densification of the previous EUVN campaign (Ihde et al. 2000) by collecting high-quality GPS and leveling data from participating European countries. At present, about 1,400 points are available with interstation distances ranging from about 50 to 100 km. The EUVN_DA data set is based on the reference systems ETRS1989 (GPS) and EVRS (leveling data, present realization EVRF2007; see Ihde et al. 2008), with the zero tide system implemented for both GPS and leveling data; the normal heights were derived in part directly from geopotential numbers as well as by simple transformations with up to three parameters (Kenyeres et al. 2010).

In addition to the numerical results given in Tables 6 and 7, the differences of the EUVN_DA as well as the Russian GPS/leveling campaign with respect to EGG1997 and EGG2008 are illustrated in Fig. 17. On the whole, the EGG2008 model performs significantly better than EGG1997. The improvements result from the updated gravity and terrain data as well as from the utilization of better geopotential models (based on the GRACE mission). Tables 6 and 7 show that solely through the introduction of the (GRACE based) EGM2008 geopotential model (i.e., EGG1997/EGM1996 vs EGG1997/EGM2008), the RMS differences reduce by between 28% (Switzerland) and 70% (Germany). However, the update and reprocessing of the gravity and terrain data also leads to substantial improvements in

Table 6 Comparison of different GPS and leveling campaigns with quasigeoid models based on different terrestrial data sets and geopotential models; the GPS/leveling data were converted to the zero tide system; the differences are defined in the sense GPS/leveling minus gravimetric quasigeoid; the mean values refer to the raw differences without applying the constant $\zeta_0^{EVRF2007}$; the other statistical parameters are calculated after subtracting the mean value; units are m

Quasigeoid (Δg / geopotential model)	#	Mean	RMS	Minimum	Maximum	Improvement vs EGG1997
Germany						
EGG1997/EGM1996	907	+0.431	0.096	–0.188	+0.331	–
EGG1997/EGM2008	907	+0.302	0.029	–0.095	+0.089	70%
EGG2008/EGM2008	907	+0.297	0.027	–0.091	+0.078	72%
EGM2008 (n_{max} = 2,190)	907	+0.302	0.031	–0.110	+0.148	–
The Netherlands						
EGG1997/EGM1996	84	+0.244	0.034	–0.061	+0.118	–
EGG1997/EGM2008	84	+0.234	0.021	–0.047	+0.050	38%
EGG2008/EGM2008	84	+0.255	0.010	–0.040	+0.027	71%
EGM2008 (n_{max} = 2,190)	84	+0.263	0.030	–0.135	+0.036	–
Belgium						
EGG1997/EGM1996	31	–2.005	0.061	–0.103	+0.102	–
EGG1997/EGM2008	31	–2.054	0.031	–0.055	+0.046	49%
EGG2008/EGM2008	31	–2.065	0.028	–0.053	+0.048	54%
EGM2008 (n_{max} = 2,190)	31	–2.060	0.019	–0.047	+0.037	–
France (North-South traverse with new leveling)						
EGG1997/EGM1996	16	–0.027	0.086	–0.188	+0.124	–
EGG1997/EGM2008	16	–0.088	0.032	–0.051	+0.068	63%
EGG2008/EGM2008	16	–0.097	0.026	–0.024	+0.059	70%
EGM2008 (n_{max} = 2,190)	16	–0.100	0.038	–0.066	+0.082	–
France (Nationwide campaign)						
EGG1997/EGM1996	965	–0.132	0.125	–0.295	+0.351	–
EGG1997/EGM2008	965	–0.180	0.080	–0.227	+0.258	36%
EGG2008/EGM2008	965	–0.188	0.076	–0.221	+0.191	39%
EGM2008 (n_{max} = 2,190)	965	–0.181	0.084	–0.271	+0.346	–
Switzerland						
EGG1997/EGM1996	188	+0.535	0.080	–0.129	+0.258	–
EGG1997/EGM2008	188	+0.117	0.058	–0.201	+0.282	28%
EGG2008/EGM2008	188	+0.174	0.052	–0.157	+0.230	35%
EGM2008 (n_{max} = 2,190)	188	+0.141	0.056	–0.170	+0.170	–
Austria						
EGG1997/EGM1996	170	+0.660	0.108	–0.202	+0.248	–
EGG1997/EGM2008	170	+0.356	0.064	–0.129	+0.197	41%
EGG2008/EGM2008	170	+0.361	0.037	–0.098	+0.100	66%
EGM2008 (n_{max} = 2,190)	170	+0.338	0.071	–0.212	+0.171	–
Russia						
EGG1997/EGM1996	48	+0.574	0.256	–0.776	+0.707	–
EGG1997/EGM2008	48	+0.560	0.124	–0.261	+0.300	52%
EGG2008/EGM2008	48	+0.555	0.076	–0.134	+0.163	70%
EGM2008 (n_{max} = 2,190)	48	+0.555	0.072	–0.120	+0.141	–

Table 7 Comparison of the EUVN_DA GPS and leveling data set with quasigeoid models based on different terrestrial data sets and geopotential models; the GPS/leveling data were converted to the zero tide system; the differences are defined in the sense GPS/leveling minus gravimetric quasigeoid; the mean values refer to the raw differences without applying the constant $\zeta_0^{EVRF2007}$; the other statistical parameters are calculated after subtracting the mean value; units are m

Quasigeoid (Δg / geopotential model)	#	Mean	RMS	Minimum	Maximum	Improvement vs EGG1997
EUVN_DA (all)						
EGG1997/EGM1996	1,395	+0.287	0.243	–0.899	+0.708	–
EGG1997/EGM2008	1,395	+0.253	0.188	–0.693	+0.527	23%
EGG2008/EGM2008	1,395	+0.250	0.173	–0.688	+0.443	29%
EGM2008 (n_{max} = 2,190)	1,395	+0.254	0.171	–0.643	+0.481	–
EUVN_DA (excuding Great Britain and Italy)						
EGG1997/EGM1996	1,139	+0.359	0.161	–0.599	+0.636	–
EGG1997/EGM2008	1,139	+0.300	0.108	–0.607	+0.428	33%
EGG2008/EGM2008	1,139	+0.302	0.076	–0.302	+0.391	53%
EGM2008 (n_{max} = 2,190)	1,139	+0.305	0.077	–0.250	+0.430	–

the GPS and leveling comparisons in all cases. The additional improvements from the upgraded terrestrial data (EGG1997/EGM2008 vs EGG2008/EGM2008) range from 2% (Germany), 18% (Russia; see Fig. 17, bottom), 20% (EUVN_DA, excluding Great Britain and Italy, see below), 25% (Austria), to about 33% (the Netherlands); the improvements are particularly high in those areas where the data basis was significantly extended, e.g., in the Netherlands, Austria, Russia, as well as other regions of Europe. The overall improvement of EGG2008 over EGG1997 ranges from about 35% to 72%, and also the long wavelength discrepancies are significantly reduced from 0.1–1.0 ppm for the EGG1997 model to typically below 0.1 ppm for all GRACE based solutions (see also Denker et al. 2009). Therefore, the consideration of additional tilt parameters in north–south and west–east directions between the respective quasigeoid heights from GPS/leveling and EGG2008 (see Sect. 2.1, formula (5)) leads to only marginal improvements of the RMS differences in most cases, the only two exceptions being the French nationwide data set of 965 stations (as well as the corresponding French data set within EUVN_DA) and the British data set within EUVN_DA (see discussion below). Regarding the French nationwide data set, the RMS difference reduces from 7.6 cm (see Table 6) to 4.1 cm when considering additional tilt parameters; the tilt acts mainly in the north–south direction (about 0.25 m per 1,000 km distance) and is related to the older leveling network (IGN69), as almost no tilt exists in the comparisons with the new leveling data (NIREF) available for the French traverse. For the latter data set, the RMS is 2.6 cm for the centered differences and 2.5 cm after considering additional tilt parameters, while the corresponding RMS value based on the older IGN69 heights is 8.0 cm for the centered differences, which

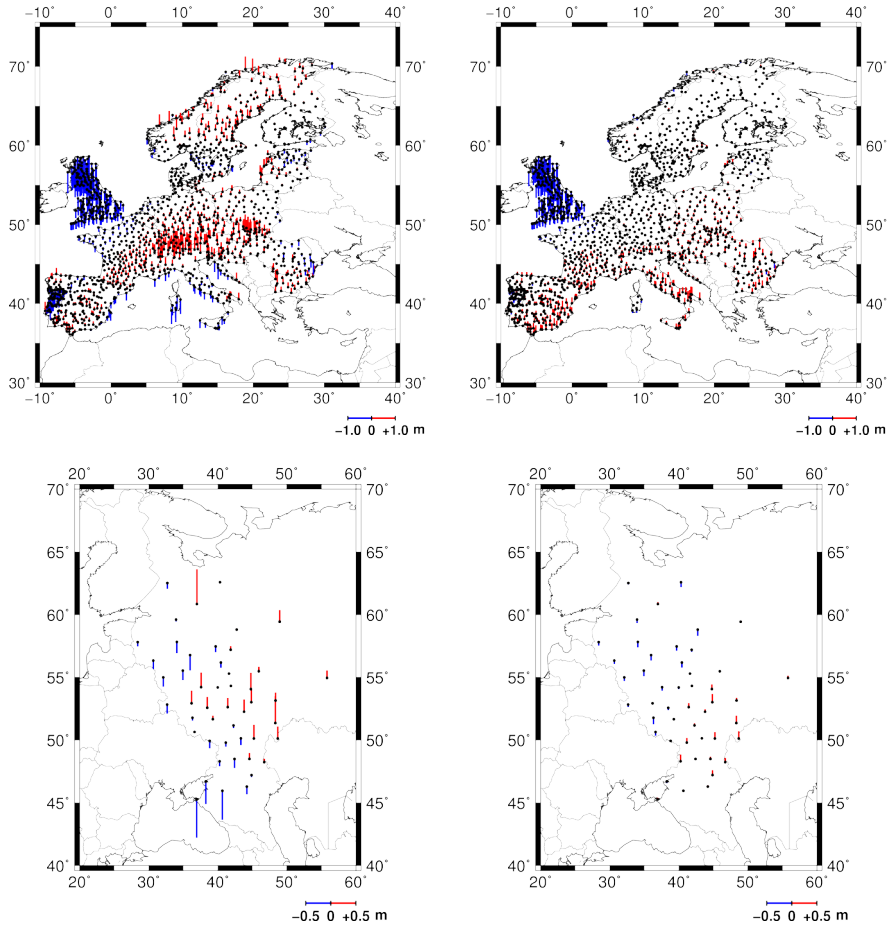

Fig. 17 Comparison of the EUVN_DA (*top*) and Russian (*bottom*) GPS and leveling data with the quasigeoid solutions EGG1997 (*left* part) and EGG2008 (*right* part); a constant bias is subtracted; stations (*dots*) and differences (positive: up in *red*; negative: down in *blue*) are depicted

clearly proves that the new French leveling is better than the old one (see also Sect. 2.4; Rebischung et al. 2008).

Of special interest are the results from the comparisons with the European EUVN_DA GPS/leveling data set, because it is based on common reference systems for GPS and leveling (see above). Table 7 and Fig. 17 (top) show that the EGG2008 model performs quite well over most parts of Europe, the main exception being Great Britain, but also over Italy and France (see previous paragraph) some systematic differences appear. Regarding Great Britain, the so-called second and third geodetic leveling differ by about 0.2 m in the north–south direction over

1,000 km distance (e.g., Kelsey 1972), and therefore the results from the third leveling were never used alone in practice; instead the results from the second leveling were held fixed and the third leveling was adjusted to it, leading to the "official ODN heights" from Ordnance Survey (Christie 1994). In addition, more recent studies suggest that the systematic error is mainly related to the third leveling (Hipkin et al. 2004; Ziebart et al. 2008), and as the EUVN_DA data set is most probably based exclusively on the third leveling, significant systematic differences show up (see Fig. 17); thus for Great Britain, the RMS of the centered differences with respect to EGG2008 is 11.9 cm, which reduces to 3.8 cm after considering additional tilt parameters. The situation over Italy has improved with respect to earlier results (e.g., Denker et al. 2009) due to a recently performed update (replacement) of the entire Italian data set (Kenyeres et al. 2010), but some systematic differences remain (see Fig. 17), requiring further investigations. For the entire EUVN_DA data set (excluding Great Britain and Italy), the RMS difference reduces from 16.1 cm for EGG1997 to 7.6 cm for EGG2008; this means an improvement of about 53% (Table 7). Furthermore, the comparisons on a country by country basis of the EUVN_DA data with EGG2008 give RMS values for the centered differences of less than 3 cm for Belgium, Denmark, Finland, Germany, Hungary, the Netherlands, Poland, Slovakia and Sweden, 3–6 cm for Austria, Croatia, the Czech Republic, Estonia, Lithuania, Norway and Switzerland, while the largest value is found for Romania (12.1 cm), which is certainly due to the low quality of the terrestrial data available for the EGG2008 development. Overall, the EUVN_DA comparison results are considered as quite satisfactory, in particular with regard to the very large area size (from the Iberian Peninsula to Northern Scandinavia, the Baltic States, Poland and Bulgaria) and the fairly small remaining systematic differences at the level of only about 1 dm (see also below).

Of significant importance is also the mean value between the EUVN_DA data (excluding Great Britain and Italy) and EGG2008 of +0.302 m, as it can be used to derive the potential value for the EVRF2007 zero level surface; formula (183) leads to

$$W_0^{\mathrm{EVRF2007}} = U_0 - \gamma_0 \, \zeta_0^{\mathrm{EVRF2007}} \,, \tag{185}$$

where U_0 is the normal potential of the GRS80 level ellipsoid. Another option is to work with potential quantities only (a more strict approach), resulting in

$$W_0^{\mathrm{EVRF2007}} = W_P + C = U_P + T_P + C \,, \tag{186}$$

followed by an averaging over all stations. Both procedures lead to the same result (within the specified significant digits) of

$$W_0^{\mathrm{EVRF2007}} = 62{,}636{,}857.89 \; \pm 0.02 \; \mathrm{m^2 s^{-2}} \,, \tag{187}$$

where the latter figure is the empirical standard deviation of the mean value. The above potential value differs from that published by Denker et al. (2005) based on the earlier EUVN GPS/leveling data set (Ihde et al. 2000), and upon closer exami-

nation it turned out that the tide correction for the GPS heights had a sign error in the 2005 computations; after correcting this error, the data sets used in Denker et al. (2005), i.e., EUVN GPS/leveling data, EGG2004 quasigeoid, lead to a zero potential of 62,636,857.94 ± 0.16 $m^2 s^{-2}$, while the EUVN data together with EGG2008 yield a value of 62,636,858.03 ± 0.12 $m^2 s^{-2}$, both being in good agreement with the result given in (187). Furthermore, a good agreement exists with the values given in Bursa et al. (2001) for Germany (62,636,857.51 ± 0.54 $m^2 s^{-2}$) and the Netherlands (62,636,857.35 ± 0.70 $m^2 s^{-2}$), both based on the NAP (however, no information exists about the tidal systems for GPS and leveling). Hence, the NAP zero level surface is about 2 dm below the level surface defined by the global W_0 value of IERS (2010); see (48). Accordingly, the potential of the zero level surfaces can be derived for all other (national) vertical datums involved in Table 6.

Furthermore, the mean values of the differences between the EUVN_DA and EGG2008 data are quite consistent on a country by country basis, ranging from +0.241 m to +0.377 m (excluding Great Britain and Italy). This suggests that systematic leveling errors over Europe are not very pronounced, besides the known problems in Great Britain, France and perhaps Italy (see above). This is also supported by Fig. 17 (right), showing only small long wavelength structures. In addition to this, the mean values listed in Tables 6 and 7 can also be employed to transform heights from one national or European height system to another one. For example, the largest mean value is found for Belgium (–2.065 m for EGG2008), which is due to the fact that the Belgian heights are referred to mean low water, while most other countries use MSL. Hence, in combination with the mean value for EVRF2007 of +0.302 m (EGG2008) it follows that the zero level surface of the Belgian heights is 2.363 m below the EVRF2007 zero level surface. This figure is in reasonable agreement with the results based exclusively on leveling, where the national heights are compared with the EVRF2007 (adjusted) leveling network, yielding a difference of 2.317 m (see http://www.crs-geo.eu); however, regarding the (small) difference between both figures, it should also be noticed that this is related to error contributions and time-variable effects from different epochs of all data sets involved, i.e., GPS, leveling, and gravimetric quasigeoid. The good agreement of the mean values related to EGG2008 for Germany (+0.297 m) and EUVN_DA (+0.302 m) is also remarkable, but both data sets rely on the Amsterdam tide gauge (NAP). On the other hand, the mean value for the Dutch data set is somewhat lower (+0.255 m), which is perhaps partly related to a subsidence of the area as well as different epochs of the involved data sets (see Ihde et al. 2008).

Finally, Tables 6 and 7 also include the comparison results with the complete EGM2008 model (n_{max} = 2,190). The results show that EGM2008 is performing very well in all the comparisons, in the case of Belgium and Russia even better than EGG2008. On the other hand, EGG2008 is performing a little better than EGM2008 in the other cases, with the largest improvements seen for the Netherlands and Austria, the latter being probably related to the higher resolution of EGG2008.

4.6 Summary and Outlook

Significant progress was made within the framework of the European gravity and geoid project regarding the collection and homogenization of high-resolution gravity and terrain data, which was then utilized in combination with the global geopotential model EGM2008 to develop the completely updated European Gravimetric (Quasi)Geoid EGG2008, covering the whole of Europe and the surrounding marine areas. The evaluation of this model by independent GPS and leveling data showed that the new GRACE based geopotential models as well as the upgraded terrestrial gravity and terrain data both lead to substantial improvements compared to the previous model EGG1997 (in total by 35–72%), and long wavelength errors, being the basic weakness of EGG1997, are virtually non-existent in the EGG2008 model. The RMS of the centered differences between national GPS/leveling data sets and EGG2008 range from about 1 cm to 5 cm for areas with a good data quality and coverage; the higher values are associated with Switzerland and Austria (high mountain regions), which is likely a consequence of both an insufficient gravity coverage and leveling quality in some local areas as well as theoretical shortcomings. On the other hand, the corresponding RMS differences exceed 10 cm for countries with a less favorable data quality (e.g., South-Eastern Europe). However, in this context it is also important to note that the differences from the GPS/leveling evaluation include error contributions and time-variable effects from different epochs of all data sets involved, i.e., GPS, leveling, and gravimetric quasigeoid. Taking this into account, the evaluation results indicate an accuracy potential of the gravimetric quasigeoid model EGG2008 in the order of 1–3 cm on a national basis, and 2–5 cm on continental scales, provided that high quality and resolution input data are available within the area of interest. These figures also conform to the internal error estimates of about 2–3 cm for the GRACE based calculations. In the end, the results obtained for large parts of Europe are about the optimum one can expect at present with up-to-date gravity, terrain, and GRACE data; further improvements are mainly anticipated from the GOCE and other future gravity field missions, as the terrestrial data can hardly be improved for the greater part of Europe, apart from a few exceptions (e.g., Eastern Europe).

Furthermore, a potential value for the EVRF2007 zero level surface was derived from the EGG2008 model as 62,636,857.89 ± 0.02 $m^2 s^{-2}$, and the connection between national vertical datums was investigated by using GPS/leveling data and the EGG2008 model. In the future, the control and replacement of the costly geometric leveling, a differential technique susceptible to systematic errors, as well as the so-called “geoid based vertical datum” (implemented soon in Canada and the U.S.A.) will be interesting study topics. Finally, regional gravity field modeling on the basis of terrestrial and satellite data will certainly retain its importance in the future, as short wavelength gravity field structures (e.g., of the geoid and quasigeoid) with a resolution of a few kilometers can never be recovered from satellite data alone due to the necessary orbit heights of a few hundred kilometers.

References

Ågren, J., Svensson, R. (2007) Postglacial land uplift model and system definition for the new Swedish height system RH 2000. Reports in geodesy and geographical information systems, Lantmateriet, Gävle

Andersen, E.G. (1976) The effect of the topography on solution of Stokes' problem. Unisurv S-14, Sydney

Andersen, E.G., Rizos, C., Mather, R.S. (1975) Atmospheric effects in physical geodesy. Unisurv G-23: 23-41, Sydney

Andersen, O.B., Knudsen, P., Berry, P.A.M. (2010) The DNSC08GRA global marine gravity field from double retracked satellite altimetry. J. Geod. 84: 191-199

Andersen, O.B., Knudsen, P., Trimmer, R. (2005) Improved high resolution altimetric gravity field mapping (KMS2002 global marine gravity field). In: Sansò, F. (ed.), A Window on the Future of Geodesy, IAG Symp. 128: 326-331, Springer-Verlag, Berlin, Heidelberg

Angermann, D., Seitz, M., Drewes, H. (2012) Global terrestrial reference systems and their realizations. Sciences of Geodesy – II, this volume, Springer-Verlag, Berlin, Heidelberg

Bäumker, M. (1984) Zur dreidimensionalen Ausgleichung von terrestrischen und Satellitenbeobachtungen. Wiss. Arb. d. Fachr. Verm.wesen d. Univ. Hannover, Nr. 130, Hannover

Behrend, D. (1999) Untersuchungen zur Schwerefeldbestimmung in den europäischen Randmeeren. Wiss. Arb. d. Fachr. Verm.wesen d. Univ. Hannover, Nr. 229, Hannover

Bian, S. (1997) Some cubature formulas for singular integrals in physical geodesy. J. Geod. 71: 443-453

BIPM (2006) Le Système international d'unités – The international system of units (SI). 8e édition, 2006, Bureau international des poids et measures, Sèvres, France

Bosch, W., Savcenko, R. (2010) On estimating the dynamic ocean topography – a profile based approach. In: Mertikas, S.P. (ed.), Gravity, Geoid and Earth Observation, IAG Symp. 135: 263-269, Springer-Verlag, Berlin, Heidelberg

Bürki, B., Müller, A., Kahle, H.-G. (2004) DIADEM: the new digital astronomical deflection measuring system for high-precision measurements of deflections of the vertical at ETH Zurich. Proceed. Gravity, Geoid and Space Missions, GGSM 2004, IAG Symp., Porto, Portugal, Aug. 30 – Sept. 3, 2004 (CD-ROM)

Bursa, M., Groten, E., Kenyon, S., Kouba, J., Radej, K., Vatrt, V., Voytiskova, M. (2002) Earth's dimension specified by geoidal potential. Stud. Geophys. Geod. 46: 1-8

Bursa, M., Kenyon, S., Kouba, J., Radej, K., Vatrt, V., Voytiskova, M. (2001) In: Drewes, H., Dodson, A., Fortes, L.P.S., Sanchez, L., Sandoval, P. (eds.), Vertical Reference Systems, IAG Symp. 124: 291-296, Springer-Verlag, Berlin, Heidelberg

Campbell, J. (1971) Eine Erweiterung der Theorie des astronomischen Nivellements bei Einbeziehung von Schweremessungen. Wiss. Arb. d. Lehrstühle f. Geodäsie, Photogrammetrie und Kartographie a. d. Techn. Univ. Hannover, Nr. 49, Hannover

Cazenave, A., Chen, J. (2010) Time-variable gravity from space and present-day mass redistribution in the Earth system. Earth and Planetary Science Letters 298: 263-274

Christie, R.R. (1994) A new geodetic heighting strategy for Great Britain. Survey Review 32: 328-343

Christodoulidis, D.C. (1979) Influence of the atmospheric masses on the gravitational field of the Earth. Bull. Géod. 53: 61-77

Condi, F., Wunsch, C. (2004) Gravity field variability, the geoid, and ocean dynamics. In: Sansò, F. (ed.), V Hotine-Marussi Symposium on Mathematical Geodesy, IAG Symp. 127: 285-292, Springer-Verlag, Berlin, Heidelberg

Demianov, G.V., Majorov, A.N. (2004) On the definition of a common world normal height system. In: Physical Geodesy, Scientific and Technical Reports on Geodesy, Photogrammetry and Cartography, Federal Office of Geodesy and Cartography (Roskartographia), ZNIIGAiK, Moscow, 168-182 (in Russian)

Denker, H. (1988) Hochauflösende regionale Schwerefeldbestimmung mit gravimetrischen und topographischen Daten. Wiss. Arb. d. Fachr. Verm.wesen d. Univ. Hannover, Nr. 156, Hannover

Denker, H. (1989) A new gravimetric quasigeoid for the Federal Republic of Germany. Deutsche Geodät. Komm., Reihe B, Nr. 291, München

Denker, H. (1998) Evaluation and improvement of the EGG97 quasigeoid model for Europe by GPS and leveling data. In: Vermeer, M., Ádám, J. (eds.), Second Continental Workshop on the Geoid in Europe, Proceed., Rep. Finnish Geod. Inst. 98:4: 53-61, Masala

Denker, H. (2001) On the effect of datum inconsistencies in gravity and position on European geoid computations. Poster, IAG 2001 Scientific Assembly, 2-7 Sept. 2001, Budapest

Denker, H. (2003) Computation of gravity gradients over Europe for calibration/validation of GOCE data. In: Tziavos, I.N. (ed.), Gravity and Geoid 2002, 3rd Meeting of the Internat. Gravity and Geoid Comm., 287-292, Ziti Editions, Thessaloniki

Denker, H. (2005) Evaluation of SRTM3 and GTOPO30 terrain data in Germany. In: Jekeli, C., Bastos, L., Fernandes, J. (eds.), Gravity, Geoid and Space Missions, IAG Symp. 129: 218-223, Springer-Verlag, Berlin, Heidelberg

Denker, H., Barriot, J.-P., Barzaghi, R., Fairhead, D., Forsberg, R., Ihde, J., Kenyeres, A., Marti, U., Sarrailh, M., Tziavos, I.N. (2009) The development of the European gravimetric geoid model EGG07. In: Sideris, M.G. (ed.), Observing Our Changing Earth, IAG Symp. 133: 177-186, Springer-Verlag, Berlin, Heidelberg

Denker, H., Barriot, J.-P., Barzaghi, R., Forsberg, R., Ihde, J., Kenyeres, A., Marti, U., Tziavos, I.N. (2005) Status of the European Gravity and Geoid Project EGGP. In: Jekeli, C., Bastos, L., Fernandes, J. (eds.), Gravity, Geoid and Space Missions, IAG Symp. 129: 125-130, Springer-Verlag, Berlin, Heidelberg

Denker, H., Roland, M. (2005) Compilation and evaluation of a consistent marine gravity data set surrounding Europe. In: F. Sansò (ed.), A Window on the Future of Geodesy, IAG Symp. 128: 248-253, Springer-Verlag, Berlin, Heidelberg

Denker, H., Torge, W. (1998) The European gravimetric quasigeoid EGG97 – An IAG supported continental enterprise. In: Forsberg, R., Feissel, M., Dietrich, R. (eds.), Geodesy on the Move – Gravity, Geoid, Geodynamics and Antarctica, IAG Symp. 119: 249-254, Springer-Verlag, Berlin, Heidelberg

Denker, H., Tziavos, I.N. (1999) Investigation of the Molodensky series terms for terrain reduced gravity field data. Boll. Geof. Teor. appl. 40: 195-203

Denker, H., Wenzel, H.-G. (1987) Local geoid determination and comparison with GPS results. Bull. Géod. 61: 349-366

Duquenne, H., Duquenne, F., Rebischung, P. (2007) New scientific levelling network NIREF. Data set and internal report, prepared for European gravity and geoid project (EGGP)

Ecker, E., Mittermayer, E. (1969) Gravity corrections for the influence of the atmosphere. Boll. Geof. Teor. appl. 11: 70-80

Eeg, J., Krarup, T. (1973) Integrated geodesy. The Danish Geodetic Institute, Internal Rep., No. 7, Copenhagen

Ekman, M. (1989a) The impact of geodynamic phenomena on systems for height and gravity. In: Andersen, O.B. (ed.): Modern techniques in geodesy and surveying, National Survey and Cadastre, KMS, Denmark, Publ. 4. Series Vol. 1: 109-167, Copenhagen, Denmark

Ekman, M. (1989b) Impacts of geodynamic phenomena on systems for height and gravity. Bull. Géod. 63: 281-296

Ekman, M. (1996) The permanent problem of the permanent tide: what to do with it in geodetic reference systems? Marées Terrestres, Bull. d'Inf. 125: 9508-9513, Bruxelles

Elhabiby, M., Sampietro, D., Sansò, F., Sideris, M.G. (2009) BVP, global models and residual terrain correction. In: Sideris, M.G. (ed.), Observing our Changing Earth, IAG Symp. 133: 211-217, Springer-Verlag, Berlin, Heidelberg

ESA (1999) Gravity field and steady-state ocean circulation mission. Reports for Mission Selection, The Four Candidate Earth Explorer Core Missions, ESA SP-1233(1)

Featherstone, W.E., Kirby, J.F., Hirt, C., Filmer, M.S., Claessens, S.J., Brown, N.J., Hu, G., Johnston, G.M. (2011) The AUSGeoid09 model of the Australian height datum. J. Geod. 85: 133-150

Flechtner F., Thomas, M., Dobslaw, H. (2010) Improved non-tidal atmospheric and oceanic dealiasing for GRACE and SLR satellites. In: Flechtner, F., Gruber, Th., Güntner, A., Mandea, M., Rothacher, M., Schöne, T., Wickert, J. (eds), System Earth via Geodetic-Geophysical Space Techniques, Advanced Technologies in Earth Sciences, 131-142, Springer-Verlag, Berlin, Heidelberg

Flury, J., Rummel, R. (2009) On the geoid-quasigeoid separation in mountain areas. J. Geod. 83: 829-847

Forsberg, R. (1984) A study of terrain reductions, density anomalies and geophysical inversion methods in gravity field modeling. Rep. Dept. Geodetic Science, No. 355, The Ohio State University, Columbus, Ohio, USA

Forsberg, R. (1987) A new covariance model for inertial gravimetry and gradiometry. J. Geophys. Research B 92: 1305-1310

Forsberg, R. (1993) Modelling of the fine-structure of the geoid: methods, data requirements and some results. Surveys in Geophys. 14: 403-418

Forsberg, R. (2010) Geoid determination in the mountains using ultra-high resolution spherical harmonic models – the Auvergne case. In: Contadakis, M.E., Kaltsikis, C., Spatalas, S., Tokmakidis, K., Tziavos, I.N. (eds), The Apple of the Knowledge, In Honor of Professor Emeritus Demetrius N. Arabelos, 101-111, Ziti Editions (ISBN: 978-960-243-674-5), Thessaloniki

Forsberg, R., Kenyon, S. (2004) Gravity and geoid in the Arctic region – the northern GOCE polar gap filled. Proceed. 2nd Internat. GOCE Workshop, Esrin, March 8-10, 2004, CD-ROM Proceed.

Forsberg, R., Tscherning, C.C. (1981) The use of height data in gravity field approximation. J. Geophys. Research B 86: 7843-7854

Forsberg, R., Tscherning, C.C. (1997) Topographic effects in gravity field modelling for BVP. In: Sansò, F., Rummel, R. (eds.), Geodetic boundary value problems in view of the one centimeter geoid, Lecture Notes in Earth Sciences 65: 241-272, Springer-Verlag, Berlin, Heidelberg

Förste, C., and 12 others (2008a) The GeoForschungsZentrum Potsdam/Groupe de Recherche de Gèodésie Spatiale satellite-only and combined gravity field models: EIGEN-GL04S1 and EIGEN-GL04C. J. Geod. 82: 331-346

Förste, C., and 12 others (2008b) EIGEN-GL05C – a new global combined high-resolution GRACE-based gravity field model of the GFZ-GRGS cooperation. General Assembly European Geosciences Union (Vienna, Austria 2008), Geophysical Research Abstracts, Vol. 10, Abstract No. EGU2008-A-06944

Gitlein, O., Timmen, L. (2006) Atmospheric mass flow reduction for terrestrial absolute gravimetry in the Fennoscandian land uplift network. In: Tregoning, P., Rizos, C. (eds), Dynamic Planet, IAG Symp. 130: 461-466, Springer-Verlag, Berlin, Heidelberg

Goad, C.C., Tscherning, C.C., Chin, M.M. (1984) Gravity empirical covariance values for the continental United States. J. Geophys. Research B 89: 7962-7968

Grafarend, E.W. (1978a) The definition of the telluroid. Bull. Géod. 52: 25-37

Grafarend, E.W. (1978b) Operational geodesy. In: Moritz, H., Sünkel, H. (eds.), Approximation Methods in Geodesy, Sammlung Wichmann, Neue Folge, Bd. 10, 235-284, H. Wichmann Verlag, Karlsruhe

Grafarend, E.W. (1988) The geometry of the Earth's surface and the corresponding function space of the terrestrial gravitational field. In: Festschrift Rudolf Sigl zum 60. Geburtstag, Deutsche Geod. Komm., Reihe B, Heft Nr. 287: 76-94, München

Grote, T. (1996) Regionale Quasigeoidmodellierung aus heterogenen Daten mit "cm"-Genauigkeit. Wiss. Arb. d. Fachr. Verm.wesen d. Univ. Hannover, Nr. 212, Hannover

Haagmans, R., de Min, E., von Gelderen, M. (1993) Fast evaluation of convolution integrals on the sphere using 1D FFT, and a comparison with existing methods for Stokes' integral. manuscripta geodaetica 18: 227-241

Haagmans, R., Prijatna, K., Omang, O. (2003). An alternative concept for validation of GOCE gradiometry results based on regional gravity. In: Tziavos, I.N. (ed.), Gravity and Geoid 2002, 3rd Meeting of the Internat. Gravity and Geoid Comm., 281-286, Ziti Editions, Thessaloniki

Heck, B. (1986) A numerical comparison of some telluroid mappings. Proceed. I Hotine-Marussi Symp. on Mathematical Geodesy (Roma, 3-6 June 1985), Vol. 1: 19-38, Milano

Heck, B. (1990) An evaluation of some systematic error sources affecting terrestrial gravity anomalies. Bull. Géod. 64: 88-108

Heck, B. (1991) On the linearized boundary value problems of physical geodesy. Rep. Dept. Geodetic Science and Surveying, No. 407, The Ohio State University, Columbus, Ohio, USA

Heck, B. (1997) Formulation and linearization of boundary value problems: from observables to a mathematical model. In: Sansò, F., Rummel, R. (eds.), Geodetic boundary value problems in view of the one centimeter geoid, Lecture Notes in Earth Sciences 65: 121-160, Springer-Verlag, Berlin, Heidelberg

Heck, B. (2003) Rechenverfahren und Auswertemodelle der Landesvermessung – Klassische und moderne Methoden. 3. Auflage, Wichmann Verlag, Heidelberg

Heck, B. (2004) Problems in the definition of vertical reference frames. In: Sansò, F. (ed.), V Hotine-Marussi Symposium on Mathematical Geodesy, IAG Symp. 127: 164-173, Springer-Verlag, Berlin, Heidelberg

Heck, B., Rummel, R. (1990) Strategies for solving the vertical datum problem using terrestrial and satellite geodetic data. In: Sünkel, H., Baker, T. (eds.), Sea Surface Topography and the Geoid, IAG Symp. 104: 116-128, Springer-Verlag, Berlin, Heidelberg

Heck, B., Seitz, K. (2007) A comparison of the tesseroid, prism and point-mass approaches for mass reductions in gravity field modeling. J. Geod. 81: 121–136

Hein, G.W. (1986) Integrated geodesy – state-of-the-art 1986 reference text. In: Sünkel, H. (ed.), Mathematical and Numerical Techniques in Physical Geodesy, Lecture Notes in Earth Sciences 7: 505-548, Springer-Verlag, Berlin, Heidelberg

Heiskanen, W.A., Moritz, H. (1967) Physical geodesy. W.H. Freeman and Company, San Francisco, London

Hipkin, R.G. (2004) Ellipsoidal geoid computation. J. Geod. 78: 167-179

Hipkin, R., Haines, K., Beggan, C., Bingley, R., Hernandez, F., Holt, J., Baker, T. (2004) The geoid EDIN2000 and mean sea surface topography around the British Isles. Geophys. J. Int. 157: 565-577

Hirt, C. (2004) Entwicklung und Erprobung eines digitalen Zenitkamerasystems für die hochpräzise Lotabweichungsbestimmung. Wiss. Arb. d. Fachr. Verm.wesen d. Univ. Hannover, Nr. 253, Hannover

Hirt, C., Feldmann-Westendorff, U., Denker, H., Flury, J., Jahn, C.-H., Lindau, A., Seeber, G., Voigt, C. (2008) Hochpräzise Bestimmung eines astrogeodätischen Quasigeoidprofils im Harz für die Validierung des Quasigeoidmodells GCG05. Zeitschrift f. Verm.wesen (zfv) 133: 108-119

Hirt, C., Flury, J. (2008) Astronomical-topographic levelling using high-precision astrogeodetic vertical deflections and digital terrain model data. J. Geod. 82: 231–248

Hirt, C., Seeber, G. (2008) Accuracy analysis of vertical deflection data observed with the Hannover digital zenith camera system TZK2-D. J. Geod. 82: 347-356

Hirt, C., Schmitz, M., Feldmann-Westendorff, U., Wübbena, G., Jahn, C.-H., Seeber, G. (2010) Mutual validation of GNSS height measurements from high-precision geometric-astronomical levelling. GPS Solutions 15: 149-159

Hotine M. (1969) Mathematical geodesy. ESSA Monograph 2, U.S. Department of Commerce, Washington, D.C.

IAG (1970) Geodetic Reference System 1967. Publ. Spéciale du Bull. Géod, Paris

IAG (1984) Resolutions of the XVIII General Assembly of the International Association of Geodesy, Hamburg, Germany, August 15-27, 1983. J. Geod. 58: 309-323

IERS (2010) IERS conventions (2010). G. Petit, B. Luzum (eds.), IERS Technical Note No. 36, Verlag des Bundesamtes für Kartographie und Geodäsie, Frankfurt am Main

Ihde J. (2009) Inter-commission project 1.2: Vertical reference frames. In: Drewes, H., Hornik, H. (eds.), Internat. Assoc. of Geodesy, Travaux, Vol. 36

Ihde, J., Adam, J., Gurtner, W., Harsson, B.G., Sacher, M., Schlüter, W., Wöppelmann, G. (2000) The height solution of the European Vertical Reference Network (EUVN). Veröff. Bayer. Komm. für die Internat. Erdmessung, Astronom. Geod. Arb., Nr. 61: 132-145, München

Ihde, J., Mäkinen, J., Sacher, M. (2008) Conventions for the definition and realization of a European Vertical Reference System (EVRS) – EVRS Conventions 2007. EVRS Conventions V5.1, Bundesamt für Kartographie und Geodäsie, Finnish Geodetic Institute, publication date 2008-12-17

Ihde, J., Sanchez, L. (2005) A unified global height reference system as a basis for IGGOS. Journal of Geodynamics 40: 400-413

Ihde, J., Wilmes, H., Müller, J., Denker, H., Voigt, C., Hosse, M. (2010) Validation of satellite gravity field models by regional terrestrial data sets. In: Flechtner, F., Gruber, Th., Güntner, A., Mandea, M., Rothacher, M., Schöne, T., Wickert, J. (eds), System Earth via Geodetic-Geophysical Space Techniques, Advanced Technologies in Earth Sciences, 277-296, Springer-Verlag, Berlin, Heidelberg

Jekeli, C. (1983) A numerical study of the divergence of the spherical harmonic series of the gravity and height anomalies at the Earth's surface. Bull. Géod. 57: 10-28

Jekeli, C. (2009) Potential theory and static gravity field of the Earth. In: Herring, T. (vol. ed.), Treatise on Geophysics, Vol. 3, Geodesy: 11-42, Elsevier, Amsterdam

Jekeli, C., Yang, H.J., Kwon, J.H. (2009) Evaluation of EGM08 – globally and locally in South Korea. In: External Quality Evaluation Reports of EGM08, Newton's Bull. 4: 38-49

JPL (2007) SRTM – The mission to map the world. Jet Propulsion Laboratory, California Inst. of Techn., http:// www2.jpl.nasa.gov/srtm/index.html.

Kaula, W.M. (1966) Theory of satellite geodesy. Blaisdell Publ. Comp., Waltham (Mass.), Toronto, London

Kellog, O.D. (1953) Foundations of potential theory. Dover Publ. Inc., New York

Kelsey, J. (1972) Geodetic aspects concerning possible subsidence in Southeastern England. Phil. Trans. R. Soc. Lond. 272: 141-149, doi:10.1098/rsta.1972.0040

Kenyeres, A., Sacher, M., Ihde, J., Denker, H., Marti, U. (2010) EUVN Densification Action – Final report. http://www.bkg.bund.de/nn_166762/geodIS/EVRS/EN/Projects/02EUVN-DA/01Introduction/introduction__node.html__nnn=true

Kern, M. (2004) A comparison of data weighting methods for the combination of satellite and local gravity data. In: Sansò, F. (ed.), V Hotine-Marussi Symposium on Mathematical Geodesy, IAG Symp. 127: 137-144, Springer-Verlag, Berlin, Heidelberg

Kovalevsky, J., Seidelmann, P.K. (2004) Fundamentals of astrometry. Cambridge University Press, Cambridge, UK

Krarup, T. (1969) A contribution to the mathematical foundation of physical geodesy. Geodætisk Institut, Meddelelse No. 44, Copenhagen

Kumar, M. (2005) When ellipsoidal heights will do the job, why look elsewhere? Surveying and Land Information Science 65: 91–94

Kurtenbach, E., Mayer-Gürr, T., Eicker, A. (2009) Deriving daily snapshots of the Earth's gravity field from GRACE L1B data using Kalman filtering. Geophys. Res. Letters 36, L17102, doi:10.1029/2009GL039564

Lemoine, F.G., and 14 others (1998) The development of the joint NASA GSFC and the National Imagery and Mapping Agency (NIMA) geopotential model EGM96. NASA/TP-1998-206861, Greenbelt, MD, U.S.A.

Li, Y.C., Sideris, M.G., Schwarz, K.-P. (1995) A numerical investigation on height anomaly prediction in mountainous areas. Bull. Géod. 69: 143-156

Liebsch G., Schirmer, U., Ihde, J., Denker, H., Müller, J. (2006) Quasigeoidbestimmung für Deutschland. DVW-Schriftenreihe 49: 127-146

MacMillan, W.D. (1958) Theoretical mechanics, Vol. 2, The theory of the potential. Dover Publ. Inc., New York

Mäkinen, J., Ihde, J. (2009) The permanent tide in height systems. In: Sideris, M.G. (ed.), Observing Our Changing Earth, IAG Symp. 133: 81-87, Springer-Verlag, Berlin, Heidelberg

Marti, U., Schlatter, A. (2001) The new height system in Switzerland. In: Drewes, H., Dodson, A., Fortes, L.P.S., Sanchez, L., Sandoval, P. (eds.), Vertical Reference Systems, IAG Symp. 124: 50-55, Springer-Verlag, Berlin, Heidelberg

Marussi, A. (1985) Intrinsic geodesy. Springer-Verlag, Berlin, Heidelberg

Mayer-Gürr, T. (2006) Gravitationsfeldbestimmung aus der Analyse kurzer Bahnbögen am Beispiel der Satellitenmissionen CHAMP und GRACE. Dissertation, University of Bonn

Mayer-Gürr, T., Kurtenbach, E., Eicker, A. (2010) ITG-Grace2010 gravity field model. URL: www.igg.uni-bonn.de/apmg/index.php

Meschkowski, H. (1962) Hilbertsche Räume mit Kernfunktionen. Springer-Verlag, Berlin, Göttingen, Heidelberg

Mohr, P.J., Taylor, B.N., Newell, D.B (2008) CODATA recommended values of the fundamental physical constants: 2006. Reviews of Modern Physics 80: 633-730

Molodenskii, M.S., Eremeev, V.F., Yurkina, M.I. (1962) Methods for study of the external gravitational field and figure of the Earth. Translation of the Russian Book, Israel Program for Scientific Translations, Jerusalem

Morelli, C., Pisani, M., Gantar, C. (1975) Geophysical anomalies and tectonics in the Western Mediterranean. Boll. Geof. Teor. appl., Vol. XVIII, No. 67, 211-249, Trieste

Moritz, H. (1962) Interpolation and prediction of gravity and their accuracy. Rep. Dept. Geodetic Science, No. 24, The Ohio State University, Columbus, Ohio, USA

Moritz, H. (1971) Kinematical geodesy II. Rep. Dept. Geodetic Science, No. 165, The Ohio State University, Columbus, Ohio, USA

Moritz, H. (1976) Integral formulas and collocation. manuscripta geodaetica 1: 1-40

Moritz, H. (1980) Advanced physical geodesy. Wichmann, Karlsruhe

Moritz, H. (2000) Geodetic Reference System 1980. J. Geod. 74: 128-133

Morse, P.M., Feshbach, H. (1953) Methods of theoretical physics. McGraw-Hill, New York

Müller, J., Soffel, M., Klioner, S.A. (2008) Geodesy and relativity. J. Geod. 82:133-145

NIMA (1997) Department of Defense World Geodetic System 1984 – Its definition and relationships with local geodetic datums. NIMA National Imagery and Mapping Agency, Technical Report, NIMA TR8350.2, 3rd Edition, 4 July 1997 (Amendment 1, 3 Jan. 2000; Amendment 2, 23 June 2004)

NIMA (2002) Addendum to NIMA TR 8350.2: Implementation of the World Geodetic System 1984 (WGS 84) Reference Frame G1150. http://earth-info.nga.mil/GandG/publications/tr8350.2/tr8350_2.html

Omang, O.C.D., Tscherning, C.C., Forsberg R. (2011) Generalizing the harmonic reduction procedure in residual topographic modeling. In: Sneeuw, N., Novák, P., Crespi, M., Sansò, F. (eds.), VII Hotine-Marussi Symposium on Mathematical Geodesy, IAG Symp. 137: 233-238, Springer-Verlag, Berlin, Heidelberg

Pail, R., Bruinsma, S., Migliaccio, F., Foerste, C., Goiginger, H., Schuh, W.-D., Hoeck, E., Reguzzoni, M., Brockmann, J.M., Abrikosov, O., Veicherts, M., Fecher, T., Mayrhofer, R., Krasbutter, I., Sansò, F., Tscherning, C.C. (2011) First GOCE gravity field models derived by three different approaches. J. Geod. 85: 819-843

Pavlis, N.K., Holmes, S.A., Kenyon, S.C., Factor, J.K. (2008) An Earth gravitational model to degree 2160: EGM2008. Presentation, 2008 General Assembly of the European Geosciences Union, Vienna, Austria, April 13-18, 2008

Poutanen, M., Vermeer, M., Mäkinen, J. (1996) The permanent tide in GPS positioning. J. Geod. 70: 499-504

Rapp, R.H. (1983a) The need and prospects for a world vertical datum. Proceed. IAG Symp. XVIII. IUGG General Assembly, Hamburg, FRG, 1983, Vol. 2, 432-445, Dept. of Geod. Science and Surveying, The Ohio State University, Columbus, Ohio, USA

Rapp, R.H. (1983b) Tidal gravity computations based on recommendations of the Standard Earth Tide Committee. Bull. d'Inf., Marées Terrestres 89: 5814-5819, Bruxelles

Rapp, R.H. (1995) A world vertical datum proposal. Allg. Verm. Nachr. 102: 297-304

Rapp, R.H. (1997) Use of potential coefficient models for geoid undulation determinations using a spherical harmonic representation of the height anomaly/geoid undulation difference. J. Geod. 71: 282-289

Rapp, R.H., Balasubramania, N. (1992) A conceptual formulation of a world height system. Rep. Dept. Geod. Science and Surveying, No. 421, The Ohio State University, Columbus, Ohio, USA

Rapp, R.H., Nerem, R.S., Shum, C.K., Klosko, S.M., Williamson, R.G. (1991) Consideration of permanent tidal deformation in the orbit determination and data analysis for the Topex/Poseidon mission. NASA Technical Memorandum 100775, Goddard Space Flight Center, Greenbelt, MD, U.S.A.

Rebischung, P., Duquenne, H., Duquenne, F. (2008) The new French zero-order levelling network – first global results and possible consequences for UELN. EUREF 2008 Symp., Brussels, Belgium, 18-21 June 2008

Rummel, R. (1988) Zur iterativen Lösung der geodätischen Randwertaufgabe. In: Festschrift Rudolf Sigl zum 60. Geburtstag, Deutsche Geod. Komm., Reihe B, Heft Nr. 287: 175-181, München

Rummel, R. (1995) The first degree harmonics of the Stokes problem – what are the practical implications? In: Festschrift E. Groten on the occasion of his 60th anniversary, 98-106, Munich

Rummel, R. (1997) Spherical spectral properties of the Earth's gravitational potential and its first and second derivatives. In: Sansò, F., Rummel, R. (eds.), Geodetic boundary value problems in view of the one centimeter geoid, Lecture Notes in Earth Sciences 65: 359-404, Springer-Verlag, Berlin, Heidelberg

Rummel, R., Rapp, R.H. (1976) The influence of the atmosphere on geoid and potential coefficient determinations from gravity data. J. Geophys. Res. 81: 5639-5642

Rummel, R., Teunissen, P. (1988) Height datum definition, height datum connection and the role of the geodetic boundary value problem. Bull. Géod. 62: 477-498

Rummel, R., van Gelderen, M. (1995) Meissl scheme – spectral characteristics of physical geodesy. manuscripta geodaetica 20: 379-385

Rummel, R., Weijong, Y., Stummer, C. (2011) GOCE gravitational gradiometry. J. Geod. 85: 777-790

Sanchez, L. (2008) Approach for the establishment of a global vertical reference level. In: Xu, P., Liu, J., Dermanis, A. (eds), VI Hotine-Marussi Symposium on Theoretical and Computational Geodesy, IAG Symposia 132: 119-125, Springer-Verlag, Berlin, Heidelberg

Sandwell, D.T., Smith, W.H.F. (2009) Global marine gravity from retracked Geosat and ERS-1 altimetry: Ridge Segmentation versus spreading rate. J. Geophys. Res. B 114, B01411, doi:10.1029/2008JB006008

Sansò, F. (1986) Statistical methods in physical geodesy. In: Sünkel, H. (ed.), Mathematical and Numerical Techniques in Physical Geodesy, Lecture Notes in Earth Sciences 7: 49-155, Springer-Verlag, Berlin, Heidelberg

Sansò, F. (1995) The long road from measurements to boundary value problems in physical geodesy. manuscripta geodaetica 20: 326-344

Sansò, F., Tscherning, C.C. (2003) Fast spherical collocation: theory and examples. J. Geod. 77: 101-112

Schwarz, K.P., Sideris, M.G., Forsberg, R. (1990) The use of FFT techniques in physical geodesy. Geophys. J. Int. 100: 485-514

Seitz, K. (1997) Ellipsoidische und topographische Effekte im geodätischen Randwertproblem. Deutsche Geod. Komm., Reihe C, Nr. 483, München

Sideris, M.G. (1987) Spectral methods for the numerical solution of Molodensky's problem. UCSE Reports, No. 20024, Dept. of Surveying Eng., The University of Calgary

Sideris, M.G. (1994) Regional geoid determination. In: Vanicek, P., Christou, N.T. (eds.), Geoid and its geophysical interpretations, 77-94, CRC Press, Inc., Boca Raton, FL, U.S.A.

Sideris, M.G. (2011a) Geoid determination, theory and principles. In: Gupta, H.K. (ed.), Encyclopedia of Solid Earth Geophysics, 356-362, Springer-Verlag, Berlin, Heidelberg

Sideris, M.G. (2011b) Geoid, computational method. In: Gupta, H.K. (ed.), Encyclopedia of Solid Earth Geophysics, 366-371, Springer-Verlag, Berlin, Heidelberg

Sigl, R. (1985) Introduction to potential theory. Abacus Press in association with H. Wichmann Verlag

Sjöberg, L. (1980) Least squares combination of satellite harmonics and integral formulas in physical geodesy. Gerlands Beitr. d. Geophysik 89: 371-377

Sjöberg, L. (1981) Least squares spectral combination of satellite and terrestrial data in physical geodesy. Annales de Géophysique 37: 25-30

Sjöberg L.E. (2003) A general model for modifying Stokes' formula and its least-squares solution. J. Geod. 77: 459−464

Sjöberg, L.E. (2010) A strict formula for geoid-to-quasigeoid separation. J. Geod. 84: 699-702

Sjöberg, L.E., Nahavandchi, H. (2000) The atmospheric geoid effects in Stokes' formula. Geophys. J. Int. 140: 95-100

Smith, D.A., Roman, D.R. (2001) GEOID99 and G99SSS: 1-arc-minute geoid models for the United States. J. Geod. 75: 469-490

Smith, D., Véronneau, M., Roman, D., Huang, J.L., Wang, Y.M., Sideris, M. (2010) Towards the unification of the vertical datums over the North American continent. IAG Comm. 1 Symp. 2010, Reference Frames for Applications in Geosciences (REFAG2010), Marne-La-Vallée, France, 4-8 Oct. 2010

Steinberg, G., Papo, H. (1998) Ellipsoidal heights: the future of vertical geodetic control. GPS World, Vol. 9, No. 2: 41-43

Strange, W.E. (1982) An evaluation of orthometric height accuracy using bore hole gravimetry. Bull. Géod. 56: 300-311

Sünkel, H. (1983) The geoid in Austria. Proceed. IAG Symp. XVIII. IUGG General Assembly, Hamburg, FRG, 1983, Vol. 1, 348-364, Dept. of Geod. Science and Surveying, The Ohio State University, Columbus, Ohio, USA

Tapley, B.D., Bettadpur, S., Ries, J.C., Thompson, P.F., Watkins, M. (2004a). GRACE measurements of mass variability in the Earth system. Science, 23 July 2004, Vol. 305, Issue 5683: 503-505

Tapley, B.D., Bettadpur, S., Watkins, M., Reigber, C. (2004b) The gravity recovery and climate experiment: mission overview and early results. Geophys. Res. Lett., Vol. 31, No. 9, L09607, doi:10.1029/2004GL019920

Tapley, B., Ries, J., Bettadpur, S., Chambers, D., Cheng, M., Condi, F., Poole, S. (2007) The GGM03 Mean Earth Gravity Model from GRACE. Eos Trans. AGU 88(52), Fall Meet. Suppl., Abstract G42A-03

Tenzer, R., Vaníček, P., Santos, M., Featherstone, W.E., Kuhn, M. (2005) The rigorous determination of orthometric heights. J. Geod. 79: 82–92

Timmen, L. (2010) Absolute and relative gravimetry. In: G. Xu (ed.): Sciences of Geodesy – I, Advances and Future Directions, 1-48, Springer-Verlag, Berlin, Heidelberg

Torge, W. (1977) Untersuchungen zur Höhen- und Geoidbestimmung im dreidimensionalen Testnetz Westharz. Zeitschrift f. Verm.wesen (zfv) 102: 173-186

Torge, W. (1982) Zur Geoidbestimmung im Meeresbereich. In: Geodaesia Universalis – Festschrift Karl Rinner zum 70. Geburtstag, Mitt. Geod. Inst. T.U. Graz, Folge 40: 346-355

Torge, W. (1989) Gravimetry. W. de Gruyter, Berlin, New York

Torge, W. (2001) Geodesy – 3rd Edition. W. de Gruyter, Berlin, New York

Torge, W., Denker, H. (1998) The European geoid – development over more than 100 years and present status. In: Vermeer, M., Ádám, J. (eds.), Second Continental Workshop on the Geoid in Europe, Proceed., Rep. Finnish Geod. Inst. 98:4: 47-52, Masala

Torge, W., Röder, R.H., Schnüll, M., Wenzel, H.-G., Faller, J.E. (1987) First results with the transportable absolute gravity meter JILAG-3. Bull. Géod. 61: 161-176

Torge, W., Weber, G., Wenzel, H.-G. (1982) Computation of a high resolution European geoid (EGG1). Proceed. 2nd Internat. Symp. on the Geoid in Europe and Mediterranean Area, Rome, 437-460, Istit. Geogr. Mil. Ital., Florence

Tscherning, C.C. (1976a) Computation of second-order derivatives of the normal potential based on the representation by a Legendre series. manuscripta geodaetica 1: 71-92

Tscherning, C.C. (1976b) On the chain-rule method for computing potential derivatives. manuscripta geodaetica 1: 125-141

Tscherning, C.C. (1985) Local approximation of the gravity potential by least squares collocation. In: Schwarz, K.P. (ed.), Proceed. Internat. Summer School on Local Gravity Field Approximation, Beijing, Aug. 21 – Sept. 4., 1984, The University of Calgary, Publ. 60003, 277-361

Tscherning, C.C. (1986) Functional methods for gravity field approximation. In: Sünkel, H. (ed.), Mathematical and Numerical Techniques in Physical Geodesy, Lecture Notes in Earth Sciences 7: 3-47, Springer-Verlag, Berlin, Heidelberg

Tscherning, C.C. (1994) Geoid determination by least-squares collocation using GRAVSOFT. In: Internat. School for the determination and use of the geoid, Lecture Notes, Milan, Oct. 10-15, 1994, 135-164

Tscherning, C.C. (2004) A discussion of the use of spherical approximation or no approximation in gravity field modeling with emphasis on unsolved problems in least-squares collocation. In: Sansò, F. (ed.), V Hotine-Marussi Symposium on Mathematical Geodesy, IAG Symp. 127: 184-188, Springer-Verlag, Berlin, Heidelberg

Tscherning, C.C., Rapp, R.H. (1974) Closed covariance expressions for gravity anomalies, geoid undulations, and deflections of the vertical implied by anomaly degree variance models. Rep. Dept. Geodetic Science, No. 208, The Ohio State University, Columbus, Ohio, USA

USGS (2007) Global 30 arc-second elevation data set GTOPO30. U.S. Geological Survey, Center for Earth Resources Observation and Science (EROS), http://edc.usgs.gov/products/elevation/gtopo30/gtopo30.html.

Vaníček, P. (1998) The height of reason (a letter to the editor). GPS World, Vol. 9, No. 4: 14

Véronneau, M., Duvai, R., Huang, J. (2006) A gravimetric geoid model as a vertical datum in Canada. Geomatica 60: 165-172

Véronneau M., Huang, J. (2007) The Canadian gravimetric geoid model 2005 (CGG2005). Report, Geodetic Survey Division, Earth Sciences Sector, Natural Resources Canada, Ottawa, Canada

Wahr, J.M. (2009) Time variable gravity from satellites. In: Herring, T. (vol. ed.), Treatise on Geophysics, Vol. 3, Geodesy: 213-237, Elsevier, Amsterdam

Wang, Y.M., Saleh, J., Li, X., Roman, D.R. (2011) The US Gravimetric Geoid of 2009 (USGG2009): model development and evaluation. J. Geod, doi:10.1007/s00190-011-0506-7

Weber, G. (1984) Hochauflösende Freiluftanomalien und gravimetrische Lotabweichungen für Europa. Wiss. Arb. d. Fachr. Verm.wesen d. Univ. Hannover, Nr. 135, Hannover

Wenzel, H.G. (1981) Zur Geoidbestimmung durch Kombination von Schwereanomalien und einem Kugelfunktionsmodell mit Hilfe von Integralformeln. Zeitschrift f. Verm.wesen (zfv) 106: 102-111

Wenzel, H.G. (1982) Geoid computation by least squares spectral combination using integral formulas. Proceed. General Meeting of the IAG, Tokyo, May 7-15, 1982, 438-453

Wenzel, H.-G. (1985) Hochauflösende Kugelfunktionsmodelle für das Gravitationspotential der Erde. Wiss. Arb. d. Fachr. Verm.wesen d. Univ. Hannover, Nr. 137, Hannover

Wenzel, H.-G. (1989) On the definition and numerical computation of free air gravity anomalies. Bull. d'Information 64: 23-40, Bureau Gravimetrique Internationale, Toulouse, France

Wichiencharoen, C. (1982) The indirect effects on the computation of geoid undulations. Rep. Dept. Geodetic Science, No. 336, The Ohio State University, Columbus, Ohio, USA

Wildermann, E. (1988) Untersuchungen zur lokalen Schwerefeldbestimmung aus heterogenen Daten dargestellt am Beispiel der Geotraverse venezolanische Anden. Wiss. Arb. d. Fachr. Verm.wesen d. Univ. Hannover, Nr. 155, Hannover

Wolf, H. (1974) Über die Einführung von Normalhöhen. Zeitschrift f. Verm.wesen (zfv) 99: 1-5

Wolf, K.I. (2007) Kombination globaler Potentialmodelle mit terrestrischen Schweredaten für die Berechnung der zweiten Ableitungen des Gravitationspotentials in Satellitenbahnhöhe. Wiss. Arb. d. Fachr. Geodäsie u. Geoinformatik d. Leibniz Univ. Hannover, Nr. 264, Hannover

Wolf, K.I. (2008) Evaluation regionaler Quasigeoidlösungen in synthetischer Umgebung. Zeitschrift f. Verm.wesen (zfv) 133: 52-63

Wunsch, C., Gaposchkin, E.M. (1980) On using satellite altimetry to determine the general circulation of the oceans with application to geoid improvement. Rev. Geophys. 18: 725-745

Zeman, A. (1987) Definition of the normal gravity field including the constant part of tides. Studia geoph. et geod. 31: 113-120

Ziebart, M.K., Iliffe, J.C., Forsberg, R., Strykowski, G. (2008) Convergence of the UK OSGM05 GRACE-based geoid and the UK fundamental benchmark network. J. Geophys. Res. B 113, B12401, doi:10.1029/2007JB004959

Zilkoski, D.B., Richards, J.H., Young, G.M. (1995) A summary of the results of the general adjustment of the North American Vertical Datum of 1988. Allg. Verm. Nachr. 102: 310-321